Accepted Manuscript

Research paper

Spectroscopic, electrochemical and DNA binding studies of some monomeric copper(II) complexes containing N_2S(thiolate)Cu core and N_4S(disulfide)Cu core

Manjuri K. Koley, Om Prakash Chouhan, Sumit Biswas, Joseph Fernandes, Arnab Banerjee, Anjan Chattopadhyay, Babu Varghese, Periakaruppan T. Manoharan, Aditya P. Koley

PII: S0020-1693(16)30784-8
DOI: http://dx.doi.org/10.1016/j.ica.2016.10.045
Reference: ICA 17338

To appear in: *Inorganica Chimica Acta*

Received Date: 6 June 2016
Revised Date: 25 October 2016
Accepted Date: 28 October 2016

Please cite this article as: M.K. Koley, O. Prakash Chouhan, S. Biswas, J. Fernandes, A. Banerjee, A. Chattopadhyay, B. Varghese, P.T. Manoharan, A.P. Koley, Spectroscopic, electrochemical and DNA binding studies of some monomeric copper(II) complexes containing N_2S(thiolate)Cu core and N_4S(disulfide)Cu core, *Inorganica Chimica Acta* (2016), doi: http://dx.doi.org/10.1016/j.ica.2016.10.045

This is a PDF file of an unedited manuscript that has been accepted for publication. As a service to our customers we are providing this early version of the manuscript. The manuscript will undergo copyediting, typesetting, and review of the resulting proof before it is published in its final form. Please note that during the production process errors may be discovered which could affect the content, and all legal disclaimers that apply to the journal pertain.

ACCEPTED MANUSCRIPT

Spectroscopic, electrochemical and DNA binding studies of some monomeric copper(II) complexes containing N_2S(thiolate)Cu core and N_4S(disulfide)Cu core

Manjuri K. Koley[a,*], Om Prakash Chouhan[b], Sumit Biswas[b], Joseph Fernandes[b], Arnab Banerjee[b], Anjan Chattopadhyay[c], Babu Varghese[d], Periakaruppan T. Manoharan[e,*] and Aditya P. Koley[c,*]

[a] Department of Chemical Engineering, Birla Institute of Technology and Science-Pilani, K.K. Birla Goa Campus, Goa 403726, India

[b] Department of Biological Sciences, Birla Institute of Technology and Science-Pilani, K.K. Birla Goa Campus, Goa 403 726, India

[c] Department of Chemistry, Birla Institute of Technology and Science-Pilani, K.K. Birla Goa Campus, Goa 403 726, India

[d] Sophisticated Analytical Instrument Facility, Indian Institute of Technology-Madras, Chennai 600 036, India

[e] Department of Chemistry, Indian Institute of Technology-Madras, Chennai 600 036, India

---

Abstract

We report the synthesis, characterization and spectroscopic results of the Cu(II) complexes [Cu(pabt)(OH_2)](ClO_4) (**1**), [Cu(pabt)(Imz)](ClO_4) (**2**), [Cu(pabt)(*N*-MeImz)](ClO_4) (**3**), [Cu(pabt)Cl] (**4**), [Cu(pma)Cl] (**5**), [Cu(pdta)Cl]Cl (**6**) and [Cu(*reduced*-pdta)Cl]Cl (**7**), (Hpabt = *N*-(2-mercaptophenyl)-2'-pyridylmethylenimine, Hpma = *N*-(2-pyridylmethyl)-2-mercaptoaniline, pdta = 2,2'-di(pyridyl-2-methyleneimine)diphenyl disulfide, *reduced*-pdta = 2,2'-di(pyridyl-2-methylamine)diphenyl disulfide, Imz = imidazole, N-MeImz = N-methylimidazole). Electronic spectra of all these compounds display strong LMCT bands in the visible region mainly associated with S $\rightarrow$ Cu(II), and consistent with TDDFT results. A four-line EPR pattern originating from the interaction of the unpaired electron with the central $^{63/65}$Cu nucleus (I = 3/2, natural abundances: ^{63}Cu, 69.17%; ^{65}Cu, 30.83%) with the isotropic coupling constant (A_{iso}) values of 80±1.5 G at RT for all these complexes suggests monomeric nature in solution. The redox behavior of these compounds show either nearly reversible or quasi-reversible Cu(II)/Cu(I) couple with redox potentials within the

ACCEPTED MANUSCRIPT

range −0.08 to −0.20 V versus Ag/AgCl. Some of these compounds show strong intercalative DNA binding and its complete cleavage. **1**-**3** exhibit remarkable cytotoxicity against C6 glioma cell line and human cervical cancer HeLa cell line. IC_{50} values of **2** and **3** for the cervical cancer HeLa cell line reveal that they exhibit higher cytotoxicity than many reported Cu(II) compounds.

Keywords: Cu(II) complex; EPR and electronic spectra; Cyclic voltammetry; DNA binding; Cytotoxicity

---

* Corresponding authors. Address: Department of Chemistry, Birla Institute of Technology and Science, Pilani-K. K. Birla Goa Campus, Goa 403 726, India. Fax: +91 832 255 7033.
Email: manjuri@goa.bits-pilani.ac.in (M. K. Koley); ptm@iitm.ac.in (P.T. Manoharan); koleyap@yahoo.co.in (A.P. Koley)

1. Introduction

Copper is one among the essential bio-relevant elements and it is present in the active sites of many metalloenzymes and metalloproteins [1-3] that are involved in electron transfer, oxygen transport and oxygenation reactions. Based on a number of spectroscopic [4-7] and metal substitution [8,9] studies three basic structural models CuN_3S, CuN_4S, and CuN_2S_2 have been proposed for a number of copper electron transfer proteins [4]. Such structures are not usually known in the coordination chemistry of copper. Due to the interest in the spectra of both “blue” and non-blue copper proteins [10, 11], a considerable number of studies involving the charge transfer spectra of copper(II) species with biological significance have been performed, particularly those species containing sulfur and imidazole ligands [12-20]. Recently, researchers are in search for copper(II) complexes that possess biologically accessible redox potentials and show high nucleobase affinity, because they are considered to be potential reagents for cleavage of DNA and may serve as new anticancer drugs. Thus, a considerable number of Cu(II) complexes have been investigated for DNA interaction and cleavage study [21-27] as well as antitumor agents [28-30]. Literature shows that mixed ligand complexes having heterocyclic base adducts like imidazole show higher binding constant as

ACCEPTED MANUSCRIPT

compared with parent complexes [31]. Our present study stems from our interest in designing, synthesizing and developing the chemistry of biocompatible Cu(II) complexes with selected N,S donor ligands which will possess suitable redox potentials, and will be capable of effectively binding and cleaving DNA. We have synthesized five stable four-coordinate Cu(II) complexes [Cu(pabt)(OH_2)](ClO_4) (**1**), [Cu(pabt)(Imz)](ClO_4) (**2**), [Cu(pabt)(*N*-MeImz)](ClO_4) (**3**), [Cu(pabt)Cl] (**4**), [Cu(pma)Cl] (**5**) [where, Hpabt = *N*-(2-mercaptophenyl)-2'-pyridylmethylenimine, Hpma = *N*-(2-pyridylmethyl)-2-mercaptoaniline, both of which act as tridentate NNS^- ligand [32-34]] and two six-coordinate complexes [Cu(pdta)Cl]Cl (**6**) and [Cu(*reduced*-pdta)Cl]Cl (**7**), [where, pdta = 2,2'-di(pyridyl-2-methyleneimine)diphenyl disulfide [35,36] and *reduced*-pdta = 2,2'-di(pyridyl-2-methylamine)diphenyl disulfide [37]. It is to be noted here that the synthesis and characterization for compound **4** was initially reported by Lindoy and Livingstone [34] and that for compounds **5** and **7** were initially reported by Kumbhat and coworkers [37]. These studies involved spectroscopic studies like IR and UV-Vis and conductivity results. Here, we present the synthesis, spectral (UV-visible, IR, and EPR) as well as electrochemical properties of seven compounds including those three reported. ^{1}H NMR spectra of compounds **2** and **3** provide valuable information about the structures of these two compounds in solution. Some of these complexes are found to bind to DNA effectively and cleaving it. Based on the DNA binding property, we have also studied the cytotoxicity and antibacterial activity of some of these compounds. We also explored the reactivity and catechol oxidase activity of a few selected compounds. Apart from these theoretical studies are performed for three compounds in order to get information about their geometries. The ground state geometries of the compounds **1**-**3** that are optimized at the B3LYP/LANL2DZ level of density functional theory (DFT) suggest that all of them possess distorted square planar geometry. We are also reporting the crystal structure of Cu(N-MeImz)$_4$(ClO_4)$_2$ (**8**) [38] which we have used in the synthesis of **3** as well as in the biological activity for comparison. To the best of our knowledge, crystal structure of Cu(N-MeImz)$_4$(ClO_4)$_2$ (**8**) is not reported in literature.

ACCEPTED MANUSCRIPT

2. Experimental

2.1. Materials

Pyridine-2-carboxaldehyde, *o*-aminobenzenethiol, imidazole, N-methyl imidazole, 3,5-di-*tert*-butyl catechol, $CuCl_2 \cdot 2H_2O$ and $Cu(ClO_4)_2 \cdot 6H_2O$ were obtained from Aldrich. Acetonitrile was obtained from Sigma, N,N-dimethylformamide (DMF, GR), absolute ethanol, methanol (GR), DMSO and dichloromethane (GR) were obtained from Merck and methanol (spectrasol) was obtained from BDH. Calf thymus (ct) DNA was purchased from Sigma-Aldrich (USA).

2.2. Preparation of 2-(2-Pyridyl)benzothiazoline. This was prepared following a reported method [32]. Yield 70%; mp 94 ^{o}C. *Anal*. Calc. for $C_{12}H_{10}N_2S$: C, 67.26; H, 4.70; N, 13.07. Found: C, 67.01; H, 4.68, N, 13.11%.

Care should be taken in the synthesis and recrystallization of this compound because it easily gets oxidized in solution at elevated temperature in presence of air and produces the corresponding 2-(2-pyridyl)benzothiazole.

2.3. Preparation of 2,2'-di(pyridyl-2-methyleneimine)diphenyl disulfide. 2,2'-dithiodianiline was prepared from *o*-aminobenzenethiol by following a procedure reported by Livingstone et al. [35]. Then 2, 2'-dithiodianiline (12.4 g, 0.05 mol) was dissolved in about 75 ml absolute ethanol by stirring at room temperature. To this 10.7 g (0.10 mol) of pyridine-2-carboxaldehyde was slowly added drop wise with constant stirring and stirring was continued for 1 h at RT when a light yellow compound separated. This was filtered, washed thoroughly with ethanol and air dried. This was recrystallized from ethanol. Yield 80%, mp 140 ^{o}C. *Anal*. Calc. for $C_{24}H_{18}N_4S_2$: C, 67.58; H, 4.25; N, 13.13. Found: C, 67.31; H, 4.21, N, 12.91%.

2.4. Preparation of the complexes

The complexes were synthesized as described below. All the synthesized complexes were recrystallized from a solution of the individual complex in acetonitrile-toluene (2 : 1) at −19 ^{o}C in

ACCEPTED MANUSCRIPT

dark to avoid any decomposition. However, suitable single crystals of any of these compounds were not grown despite of numerous attempts in different ways.

2.4.1. [Cu(pabt)(OH_2)](ClO_4) (**1**)**.** $Cu(ClO_4)_2·6H_2O$ (1.11 g, 0.003 mol) in cold methanol (15 mL, ~5 °C) was slowly added to a cold solution of 2-(2-Pyridyl)benzothiazoline (0.645 g, 0.003 mol) dissolved in 35 mL of methanol during 20 min with stirring below room temperature (~5 °C). A dark purple compound separated out from the purple solution. This was filtered, washed with methanol, and air-dried. Yield ~65%. *Anal*. Calc. for $C_{12}H_{11}N_2O_5SClCu$: C, 36.55; H, 2.81; N, 7.10. Found: C, 35.98, H, 2.75, N, 7.21%. ESI–MS in CH_3CN: *m/z* 277.1 $[Cu(pabt) + H]^+ = [(M–H_2O) + H]^+$; *m/z* 488.6 $[Cu(pabt)(2\text{-}(2\text{-pyridyl})benzothiazole)]^+$; *m/z* 489.6 $[Cu(pabt)(2\text{-}(2\text{-pyridyl})benzothiazole) + H]^+$; *m/z* 490.5 $[Cu(pabt)(2\text{-}(2\text{-pyridyl})benzothiazole) + 2H]^+$.

2.4.2. [Cu(pabt)(Imz)](ClO_4) (**2**)**.** Imidazole (0.136 g, 0.002 mol) in methanol (10 mL) was slowly added to a cold solution of $Cu(ClO_4)_2·6H_2O$ (0.741 g, 0.002 mol) in methanol (10 mL, ~ 5 ^oC) during 30 min with stirring below room temperature (~ 5 ^oC). Then this reaction mixture was slowly added to a cold solution of 2-(2-pyridyl)benzothiazoline (0.43 g, 0.002 mol) in methanol (30 mL, ~ 5 ^oC) during 30 min with stirring at ~ 5 ^oC. A dark purple, almost black, compound separated out from the purple solution. The solid was filtered, washed well with methanol and dried in vacuo. *Anal*. Calc. for $C_{15}H_{13}N_4O_4SClCu$: C, 40.55; H, 2.95; N, 12.61. Found: C, 41.01; H, 2.87; N, 13.01%. ESI–MS in CH_3CN: *m/z* 277.1 $[Cu(pabt) + H]^+ = [\{M–(Imz)\} + H]^+$; *m/z* 488.6 $[Cu(pabt)(2\text{-}(2\text{-pyridyl})benzothiazole)]^+$; *m/z* 489.4 $[Cu(pabt)(2\text{-}(2\text{-pyridyl})benzothiazole) + H]^+$; *m/z* 490.5 $[Cu(pabt)(2\text{-}(2\text{-pyridyl})benzothiazole) + 2H]^+$.

2.4.3. [Cu(pabt)(N-MeImz)](ClO_4) (**3**). $Cu(N\text{-}MeImz)_4(ClO_4)_2$ was synthesized following a published method [38] and we have characterized it by X-ray crystal structure (vide infra). Solid $Cu(N\text{-}MeImz)_4(ClO_4)_2$ (1.181 g, 0.002 mol) was added to a cold solution of 2-(2-pyridyl)-benzothiazoline (0.43 g, 0.002 mol) in methanol (50 mL) with stirring at ~ 5 ^oC. Then the solution was slowly brought to room temperature and stirring was continued for an hour. A dark purple,

ACCEPTED MANUSCRIPT

almost black, compound separated out from the violet solution. The solid was filtered, washed well with methanol followed by water and finally again with methanol, and dried in vacuo. *Anal.* Calc. for $C_{16}H_{15}N_4O_4SClCu$: C, 41.93; H, 3.30; N, 12.22. Found: C, 42.01; H, 3.34; N, 12.30%. ESI–MS in CH_3CN: *m/z* 276.1 $[Cu(pabt)]^+ = [\{M–(N\text{-}MeImz)\}^+]$; *m/z* 277.0 $[Cu(pabt) + H]^+ = \{M–(N\text{-}MeImz)\} + H]^+$; *m/z* 359.6 $[Cu(pabt)(N\text{-}MeImz) + H]^+ = [M + H]^+$; *m/z* 488.5 [Cu(pabt)(2-(2-pyridyl)benzothiazole)]$^+$; *m/z* 489.6 [Cu(pabt)(2-(2-pyridyl)benzothiazole) + H]$^+$; *m/z* 490.7 [Cu(pabt)(2-(2-pyridyl)benzothiazole) + 2H]$^+$.

2.4.4. [Cu(pabt)Cl] (**4**)**.** To a cold solution of 2-(2-pyridyl)benzothiazoline (0.43 g, 0.002 mol) in methanol (30 mL), a cold solution of $CuCl_2{\cdot}2H_2O$ (0.341 g, 0.002 mol) in methanol (25 mL, ~ 5 ^oC) was rapidly added with constant stirring. The solution turned violet and a red-purple compound separated. This was filtered and washed with methanol and air-dried. Yield ~80%. *Anal.* Calc. for $C_{12}H_9N_2SClCu$: C, 46.15; H, 2.90; N, 8.97. Found: C, 45.98, H, 2.87, N, 8.91%. ESI–MS in CH_3CN: *m/z* 276.1 $[Cu(pabt)]^+ = [(M–Cl)]^+$; *m/z* 277.1 $[Cu(pabt) + H]^+ = [(M–Cl) + H]^+$; *m/z* 315.9 $[Cu(pabt)Cl + 4H]^+ = [(M+4H)^+]$; *m/z* 488.6 [Cu(pabt)(2-(2-pyridyl)benzothiazole)]$^+$; *m/z* 489.5 [Cu(pabt)(2-(2-pyridyl)benzothiazole) + H]$^+$; *m/z* 551.7 $[\{Cu(2\text{-}(2\text{-pyridyl})benzothiazole)\}_2]^+$.

2.4.5. [Cu(pma)Cl] (**5**). This compound was prepared by modifying the method described by Corbin et al. [33]. A solution of $ZnCl_2$ (0.204 g, 0.0015 mol) in dry methanol (15 mL) was added to a solution of 2-(2-pyridyl)benzothiazoline (0.215 g, 0.001 mol) in dry methanol (35 mL) with constant stirring at room temperature. Then this solution was carefully treated with sodium borohydride (0.0378 g, 0.001 mol) over a period of 20 min and then H_2S gas was purged through this solution for 30 min to precipitate ZnS. This was filtered off and the filtrate containing the reduced ligand was collected and neutralized with bubbling hydrogen chloride gas. This solution was cooled to ~ 5 ^oC. Addition of $CuCl_2{\cdot}2H_2O$ (0.170 g, 0.001 mol) in methanol (10 mL) to this cold solution resulted in a red-violet solution and a dark, almost black compound separated. This was filtered and the dark

ACCEPTED MANUSCRIPT

compound was washed with methanol and air-dried. Yield ~60%. *Anal.* Calc. for $C_{12}H_{11}N_2SClCu$: C, 45.82; H, 3.53; N, 8.91. Found: C, 45.98, H, 3.58, N, 8.89%.

2.4.6. [Cu(pdta)Cl]Cl (**6**)**.** A solution of $CuCl_2 \cdot 2H_2O$ (0.341 g, 0.002 mol) in methanol (25 mL) was slowly added to a solution of 2,2'-di(pyridyl-2-methyleneimine)diphenyl disulfide (0.86 g, 0.002 mol) in methanol (50 mL) with constant stirring at room temperature. The solution turned red-violet and a red-purple compound separated. This was filtered and washed with methanol and air-dried. Yield ~85%. *Anal.* Calc. for $C_{24}H_{18}N_4S_2Cl_2Cu$: C, 51.38; H, 3.23; N, 9.99. Found: C, 51.98, H, 3.28, N, 9.91%. ESI–MS in CH_3CN: *m/z* 213.2 [(2-(2-pyridyl)benzothiazole) + H]$^+$; *m/z* 276.0 [Cu(2-(2-pyridyl)benzothiazole) + H]$^+$ or [Cu(pabt)]$^+$; *m/z* 277.1 [Cu(2-(2-pyridyl)benzothiazole) + 2H]$^+$ or [Cu(pabt) + H]$^+$; *m/z* 311.1 [Cu(2-(2-pyridyl)benzothiazole)Cl]$^+$; *m/z* 488.5 [Cu(pabt)(2-(2-pyridyl)benzothiazole)]$^+$; *m/z* 489.5 [Cu(pdta)]$^+$; *m/z* 490.6 [Cu(pdta) + H]$^+$; *m/z* 523.6 [Cu{(2-(2-pyridyl)benzothiazole}$_2$Cl]$^+$; *m/z* 525.5 [Cu(pdta)Cl]$^+$.

2.4.7. [Cu(*reduced*-pdta)Cl]Cl (**7**)**.** A solution of $ZnCl_2$ (0.204 g, 0.0015 mol) in dry methanol (15 mL) was added to a solution of 0.001 mol of 2,2'-di(pyridyl-2-methyleneimine)diphenyl disulfide (0.43 g, 0.001 mol) in dry methanol (35 mL) with constant stirring at room temperature. Then this solution was carefully treated with sodium borohydride (0.0378 g, 0.001 mol) over a period of 20 min and then H_2S gas was purged through this solution for 30 min to precipitate ZnS. This was filtered off and the filtrate was collected and neutralized with bubbling hydrogen chloride gas. Slow addition of $CuCl_2 \cdot 2H_2O$ (0.170 g, 0.001 mol) in methanol (10 mL) to this resulted in a red-violet solution and a dark, almost black compound separated. This was filtered and the purple filtrate was collected in a beaker and placed in a refrigerator for slow evaporation when a dark crystalline compound separated. This was collected by filtration and washed with methanol and air-dried. Yield ~50%. *Anal.* Calc. for $C_{24}H_{22}N_4S_2Cl_2Cu$: C, 51.02; H, 3.92; N, 9.91. Found: C, 50.98, H, 3.86, N, 9.88%.

ACCEPTED MANUSCRIPT

3. Methods for biological activity

3.1. Assay for antibacterial activity

The antibacterial activities of all the copper compounds were determined using disc diffusion method. The Gram negative bacterium *Escherichia coli* (*E.coli*) was used as the standard bacterial strain. A single colony from a fresh plate was transferred to 5 ml of Luria-Bertani (LB) broth and allowed to grow at 37°C with shaking at 120 rpm till the culture reached an OD_{600} of 0.8. This bacterial culture was swabbed on to LB agar media culture plates using sterile cotton swabs thrice to ensure that the entire plate surface is covered with bacterial cells. Inoculated plates were kept for 2 minutes in laminar air flow before the disc was applied. Sterile Whatman filter paper (number 3) discs of 5 mm diameter were prepared and sterilized at 121°C temperature and 15 psi before use. All the copper samples were dissolved in DMSO so as to achieve a final concentration of 100 µg/mL and sterilized individually by passing through a 0.22 micron membrane filter. The sterilized discs were then dipped in the sterilized sample solutions and allowed to air dry in laminar air flow for 2 minutes on a sterile surface. The air dried discs were applied to the LB agar culture plate surface (which was previously swabbed by bacterial culture) ensuring complete contact of the disc on agar surface. The plates were incubated at 37 °C overnight (approximately 16 hours) and the growth inhibition zones (clear zone) around each disc were measured.

3.2. DNA binding studies

Since DNA cleavage was observed (vide infra) for most of the compounds under study, we wanted to figure out the kind of binding to DNA. Thus, we have chosen **1** and **2** as representative compounds for the DNA binding studies. These studies were carried out for compounds **1** and **2** in aqueous medium by monitoring the overall electronic spectral change after addition of plasmid DNA (dissolved in Tris buffer, pH 7) as described below. A cold (~10 ^{o}C) aqueous solution (1.2 mL) of compound **2** [0.92×10^{-4} mol L^{-1}] was treated with 10 µL of cold DNA solution (140.5 ng/µL) in

ACCEPTED MANUSCRIPT

Tris buffer, allowed to stand to reach equilibrium and the electronic spectrum was recorded. This titration was repeated ten times, by adding 10 μL of cold DNA solution each time, until there is no further change observed in the electronic spectrum indicating the reaction reached a steady state after addition of a total of 100 μL of cold DNA solution amounting to 10.8 μg/mL DNA in the reaction mixture. In the case of compound **1**, 1 mL of cold (~10 ^{o}C) aqueous solution [1.51×10^{-4} mol L^{-1}] was directly treated with 83.4 μL of cold DNA solution and the electronic spectra were recorded with time. The spectrum became steady within 40 min and no further change was observed for another 25 min.

In addition, in order to get the binding constant for the compounds **1**-**3**, electronic spectra of the compounds with incremental amounts of calf thymus DNA (ct-DNA) have been recorded using a Jasco V-570 UV/VIS/NIR spectrophotometer. The absorption titration experiments were performed by keeping the complex concentration constant and by varying the concentration of ct-DNA from 0 to 40 μM in 10 mM Tris–HCl buffer (pH 7.43).

3.3. Nucleic acid degradation activity

Since DNA binding and its cleavage studies being one of the major objective for the present work, we have carried out DNA cleavage studies for all seven compounds as well as another reported compound $Cu(N\text{-}MeImz)_4(ClO_4)_2$ (**8**) as a reference. For DNA degradation assay, *E. coli* plasmid DNA purified by Qiagen plasmid isolation kit was subjected to treatment with each copper compound. The quantity of plasmid DNA was estimated to be 250 μg/μL. All the samples were dissolved in DMSO and sterilized as mentioned in the previous section. 5 μL (1250 μg) of the purified plasmid DNA was mixed with sample so that each reaction mixture contained 100 μg of the sample. The total reaction volume was 10 μL (made up with DNA loading dye). All the vials containing the reaction mixture were kept at room temperature for 12 h. The samples were run in a 1% agarose gel at 60 V for 2 h to achieve complete separation of nucleic acid bands.

ACCEPTED MANUSCRIPT

3.4. Cytotoxicity

3.4.1. Cell culture and treatment

The C6 glioma cell line and the cervical cancer HeLa cell line were maintained in DMEM (Dulbecco's Modified Eagle's Medium) supplemented with 10% fetal bovine serum (FBS). On achieving 80% confluency, the cells were seeded into 96 well plate with a density of 4×10^4 per well and treated with different concentrations of the compounds **1**-**3** dissolved in DMSO (10 µM, 20 µM, 50 µM, 100 µM) in triplicates, further incubating for two different incubation times, 24 h and 48 h, respectively. Each set of experiment was further repeated three times.

3.4.2. 3-(4,5-Dimethylthiazol-2-yl)-2,5-diphenyltetrazolium bromide (MTT) assay

To see the impact of the three compounds on biological system, MTT assay was performed. In this assay, cell viability was determined by the reduction of yellow MTT into purple formazan product by the enzymatic activity of mitochondrial dehydrogenase in the live cells based on the method of Mabley et al. [39]. C6 glioma cells and HeLa cells were plated on 96 well plates at a density of 4×10^4 per well and treated with **1**, **2**, and **3** as described earlier. After stipulated time period, media was removed and fresh media with MTT (final conc. 500 µg/µl) added. After 4h MTT solution was removed carefully and 100 µL of DMSO was added to solubilize the purple formazan crystals. Absorbance of the colored solution was measured at a test wavelength of 570 nm with a reference at wavelength of 620 nm. The absorbance obtained from treated cells was expressed as the percentage of absorbance obtained from untreated cells.

3.5. Detection of hydrogen peroxide in the catalytic reaction of catechol oxidase activity

The formation of H_2O_2 during the catalytic reaction of catechol oxidation by the compounds **1** and **2** was detected iodometrically by assaying I_3^- that was formed from the reaction of KI with the reaction mixture using a spectrophotometer since I_3^- has a characteristic absorption band at 353 nm ($\varepsilon = 26000\ M^{-1}cm^{-1}$) in water. The oxidation reaction of 3,5-DTBC by complex **1** or **2** in methanol

ACCEPTED MANUSCRIPT

was carried out as described in the kinetic experiment for catechol oxidase activity (vide infra). When the formation of 3,5-DTBQ reached a desired value at 401 nm after 1 h, the reaction mixture was acidified by adding an equal volume of cold H_2SO_4 (20×10^{-3} M) to quench the reaction. Then the quinone was extracted from the reaction mixture with CH_2Cl_2 until the organic layer was colorless. Then, 1 mL of a KI solution (10% aqueous) was added to the pink aqueous layer, divided into two parts, and spectra were recorded separately with both parts, one part without and the other part with a catalytic amount of ammonium molybdate (3% solution) to accelerate the formation of I_3^-. Blank experiment was performed under identical condition in the absence of the catalyst, but only very minor formation of I_3^- was observed as compared to that formed in presence of **1** and **2**.

3.6. Physical measurements

Elemental analyses (for C, H, and N) were performed on a Perkin-Elmer model 2400 series II CHNS/O analyzer. Mass spectra were recorded on a Varian Inc, USA Liquid Chromatograph Mass Spectrometer Model 410 Prostar Binary LC with 500 MS IT PDA Detectors operating in ESI mode. Infrared and far-infrared spectra were measured with a Jasco IR report-100 and a Shimadzu IR Affinity - 1 FT-IR and a Bruker IFS 66V FT-IR spectrometer using KBr and polyethylene pellet, respectively. Electronic absorption spectra were recorded on a CARY 5E UV-Vis-NIR spectrophotometer (Varian) and a Jasco V-570 UV/VIS/NIR spectrophotometer using a pair of matched quartz cell of path length of 1 cm. Diffuse reflectance spectral measurements were done with JASCO-ISN470 attachment with solid sample holder JASCO SSH-506. Electron paramagnetic resonance spectra were recorded on a Varian E-112 X/Q-band EPR spectrometer and a JEOL, Japan Model: JES - FA200 ESR spectrometer with X and Q band. Instrumental parameters: modulation frequency = 100 kHz, modulation amplitude = 1 G, microwave power = 20 mW. Diphenylpicrylhydrazyl (DPPH) was used as an internal field marker. Room temperature solution EPR spectra were recorded using an aqueous cell and frozen glass spectra were recorded in liquid

ACCEPTED MANUSCRIPT

nitrogen using a quartz dewer. Proton NMR spectra were recorded using a Bruker AVANCE III 500 MHz (AV 500) multi nuclei solution NMR Spectrometer. Conductivity measurement was done using a Mettler Toledo dual conductivity/pH meter model SevenMulti equipped with Inlab 730 and Inlab 413 electrodes. Electrochemical measurements were done with the help of a Bioanalytical system CV-27 electrochemical analyzer and a BAS model X-Y recorder at 298K under dinitrogen. A standard three electrode cell consisting of a platinum working electrode, a platinum auxiliary electrode and a Ag/AgCl reference electrode was used. Tetrabutylammonium hexafluorophosphate ($[N(n\text{-}Bu)_4]PF_6$) or tetrabutylammonium perchlorate ($[N(n\text{-}Bu)_4]ClO_4$) was used as supporting electrolyte.

3.7. Computational details

In our present work, computational studies have been performed at the density functional theory (DFT) [40] and time-dependent density functional theory (TD-DFT) [41] level using Gaussian 09 suite of program [42]. Becke's [43] three parameter exchange function (B3) with Lee-Yang-Parr correlation [44] function (LYP) have been employed using LANL2DZ basis sets for the geometry optimization calculations. The estimation of the peak positions of these complexes has been done at the Td-B3LYP/LANL2DZ level. Calculations with solvent (methanol) have been carried out using the Polarizable Continuum Model (PCM) [45, 46] in G09. The relevant molecular orbitals are analyzed through the visualization software Chemcraft.

3.8. X-ray crystallography for $Cu(N\text{-}MeImz)_4(ClO_4)_2$

Purple crystals were obtained from the slow evaporation of an aqueous solution of $Cu(N\text{-}MeImz)_4(ClO_4)_2$ [38] at room temperature. A crystal with approximate size of $0.35 \times 0.35 \times 0.30$ mm was mounted on a Bruker Axs Kappa Apex2 diffractometer equipped with graphite-monochromated [Mo Kα, $\lambda = 0.71073$ Å] radiation. The unit cell parameters were determined by the method of

ACCEPTED MANUSCRIPT

difference vectors using reflections scanned from three different zones of the reciprocal lattice. The intensity data were measured using ω and φ scan with frame width of 0.5°. The frames integration and data reduction were performed using Bruker SAINT-Plus (Version 7.06a) software [47]. The multi-scan absorption corrections were applied to the data using SADABS software. The crystal is indexed in monoclinic system with space group $P2_1/n$ and lattice parameters a = 8.0844(6) Å, b = 10.4731(6) Å, c = 14.3954(10) Å, α = 90.00°, β = 93.519(2)°, γ = 90.00°. SIR-92 program [48] was used for solving the structure. Structure was refined using SHELXL-97 program [49]. Successive difference fourier map showed the positions of all hydrogen atoms. However, the hydrogen positions were geometrically fixed and refined through riding model. The full matrix structure refinement was carried out through minimization of the function $\sum(w(F^2_o - F^2_c))^2$, where $w = [\sigma^2 (F^2_o) + (0.0667P)^2 + 0.7873P]^{-1}$ and $P = (F^2_o + 2F^2_c)/3$, F^2_o is the measured intensity (i.e., intensity observed) and F^2_c is the intensity calculated. The final residual factors were R = 0.0387 and wR = 0.1214. The largest difference map peak was 0.640 e/Å^3.

4. Results and discussion

We have studied the reactions of $Cu(ClO_4)_2 \cdot 6H_2O$ or $CuCl_2 \cdot 2H_2O$ and $Cu(N\text{-}MeImz)_4(ClO_4)_2$ with 2-(2-pyridyl)-benzothiazoline in methanol to prepare the complexes of the corresponding Schiff base N-(2-mercaptophenyl)-2'-pyridylmethylenimine with NNS^- coordination [32-34] and also the reactions of $CuCl_2 \cdot 2H_2O$ with another Schiff base 2,2'-di(pyridyl-2-methyleneimine)diphenyl disulfide (pdta) [35,36] and its reduced form 2,2'-di(pyridyl-2-methylamine)diphenyl disulfide [37] with NNSNN coordination [36], and also with N-(2-pyridylmethyl)-2-mercaptoaniline (Hpma) [32,33] derived from the reduction of *N*-(2-mercaptophenyl)-2'-pyridylmethylenimine (Hpabt) as shown in Fig. 1.

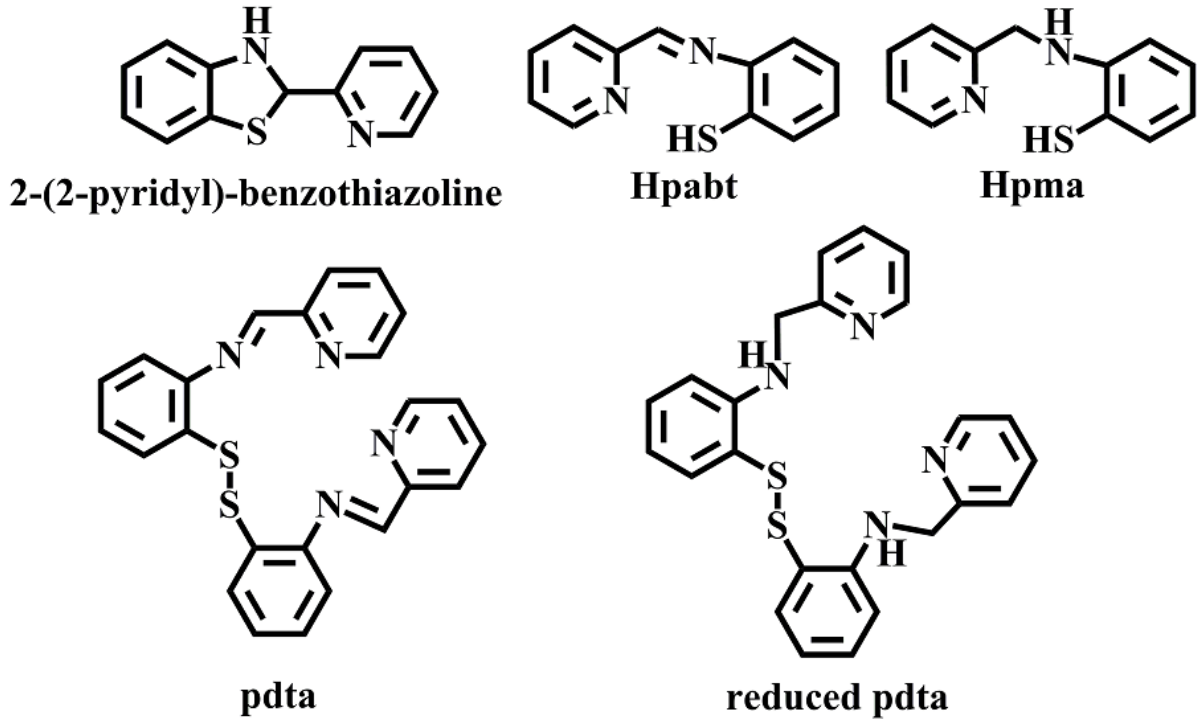

Fig.1. Structures of the ligands.

The complexes are readily soluble in methanol (blue purple solution), acetonitrile (red purple solution) and in DMF (dark purple to violet solution), but are insoluble in dichloromethane except the compounds [Cu(pabt)Cl] (**4**) and Cu(pma)Cl] (**5**) which are found to be moderately soluble in dichloromethane producing a bright blue solution in each case. Conductivity measurements with fresh solutions of the compounds **1** - **3** show these are 1 : 1 electrolyte while **4** and **5** are nonelectrolyte in nature. On the other hand, conductivity measurements for **6** and **7** in DMF show Λ = 76.6 Ohm^{-1} cm^2 mol^{-1} for **6** and Λ = 88.5 Ohm^{-1} cm^2 mol^{-1} for **7**, respectively, indicating that they are 1 : 1 electrolyte in this solvent [50]. However, on standing, the molar conductivity increases from 76.6 Ohm^{-1} cm^2 mol^{-1} to 162.48 Ohm^{-1} cm^2 mol^{-1} for **6** and from 88.5 Ohm^{-1} cm^2 mol^{-1} to 170.91 Ohm^{-1} cm^2 mol^{-1} for **7**. This strongly suggests that one of the two Cl^- ions is coordinated to the Cu^{2+} ion resulting octahedral complex in each case. On standing, the conductivity of these solutions changes with time and become steady after several hours when it shows 2 : 1 electrolyte [50] indicating that the coordinated Cl^- is gradually replaced by DMF. However, this change is not

ACCEPTED MANUSCRIPT

observed in acetonitrile for both **6** and **7**, and both of them are found to be 1 : 1 electrolyte in CH_3CN. But when the CH_3CN solution of **6** is reacted with solid imidazole (1 : 1 mmol ratio), the conductivity immediately increased and became steady within 20 min and the conductivity value calculated based on the initial concentration was found to be changed from 125 to 220 Ohm^{-1} cm^2 mol^{-1} for **6**. The isolated product (**6A**) (vide infra) confirms the substitution of the coordinated Cl^- ion by imidazole and making the final species 2 : 1 electrolyte in CH_3CN [50]. The ESI-MS spectra (in the positive-ion mode) for complexes **1**–**4** and for complex **6** have been recorded in acetonitrile and the results are presented in Fig. S1(Supplementary material). The complexes **1**–**4** showed a peak at *m/z* 277.1 corresponding to $[Cu(pabt) + H]^+$ while complex **6** displayed peaks at *m/z* 489.5 corresponding to $[Cu(pdta)]^+$, at *m/z* 490.6 corresponding to $[Cu(pdta) + H]^+$ and at *m/z* 525.5 corresponding to $[Cu(pdta)Cl]^+$. Based on the above observations, elemental analyses, conductivity results and X-band RT solution EPR results (vide infra) the proposed structures of **1-7** are shown in Fig. 2.

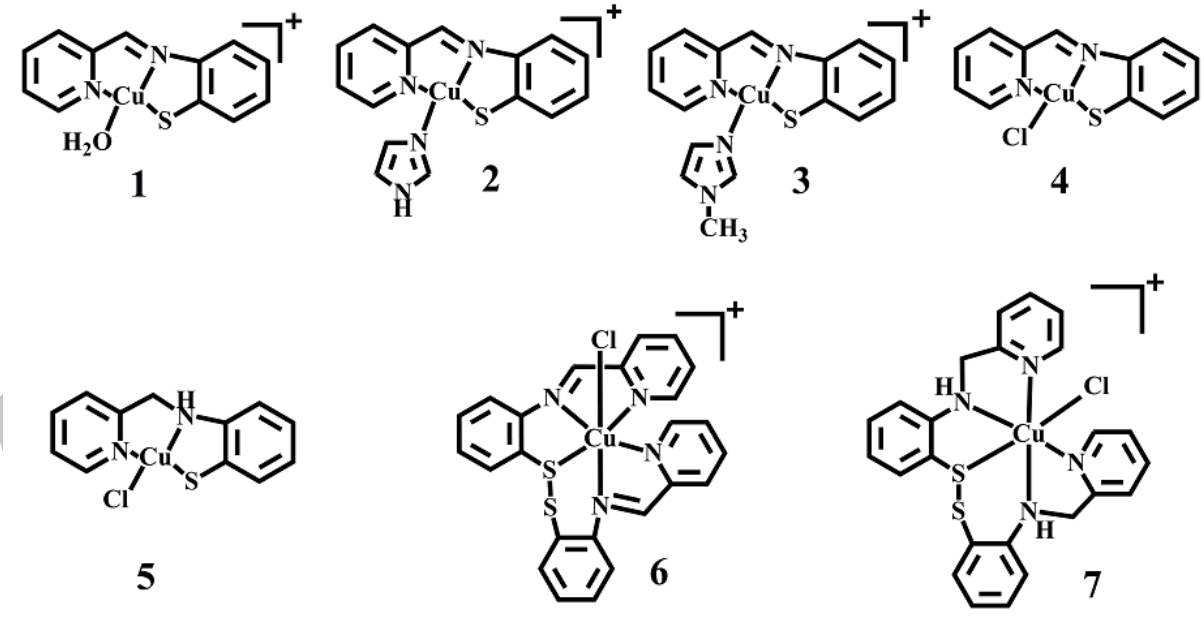

Fig. 2. Proposed structures of the compounds **1-7** in solution.

ACCEPTED MANUSCRIPT

4.1. ^{1}H NMR results

Though it is very difficult to get well resolved NMR spectra for paramagnetic mononuclear Cu(II) compounds due to unfavorable electronic relaxation time and only few mononuclear complexes are reported to have ^{1}H NMR spectra with considerable broadness [51-53], we were keen to get some information from ^{1}H NMR for at least a few of our compounds in the absence of any crystal structure since single crystals for any of the compounds under study could not be grown in spite of trying many different ways. So we have chosen compounds **2** and **3** which are very similar except the imidazole N–H proton in **2** is replaced by N–CH_3 group in **3**. The ^{1}H NMR spectra for these two compounds were recorded in d_6-DMSO and shown in Fig. 3. The spectra which show significant broadening [52,53] in both cases are found to be remarkably similar except that the broad peak at 11.552 ppm observed for **2** is absent in the spectrum of **3**, and the latter contains a peak at 4.261 ppm which is absent in the case of **2**. All other peaks appear to be very similar for both these compounds (Fig. 3). This broad peak at 11.552 ppm observed for **2** can be assigned to NH proton [54] which is not observed in **3**, on the other hand the signal at 4.261 ppm (corresponds to three protons) observed for **3** but not for **2** can be assigned to N-CH_3 protons [54]. The broad peak at 14.059 ppm observed for **2** or at 14.023 ppm observed in the spectrum of **3** is appearing for 2′–H of the imidazole group [55]. Though signals for all the protons did not show up in the ^{1}H NMR spectra of **2** and **3**, the number of signals observed has provided valuable information about the structures of these two compounds in solution.

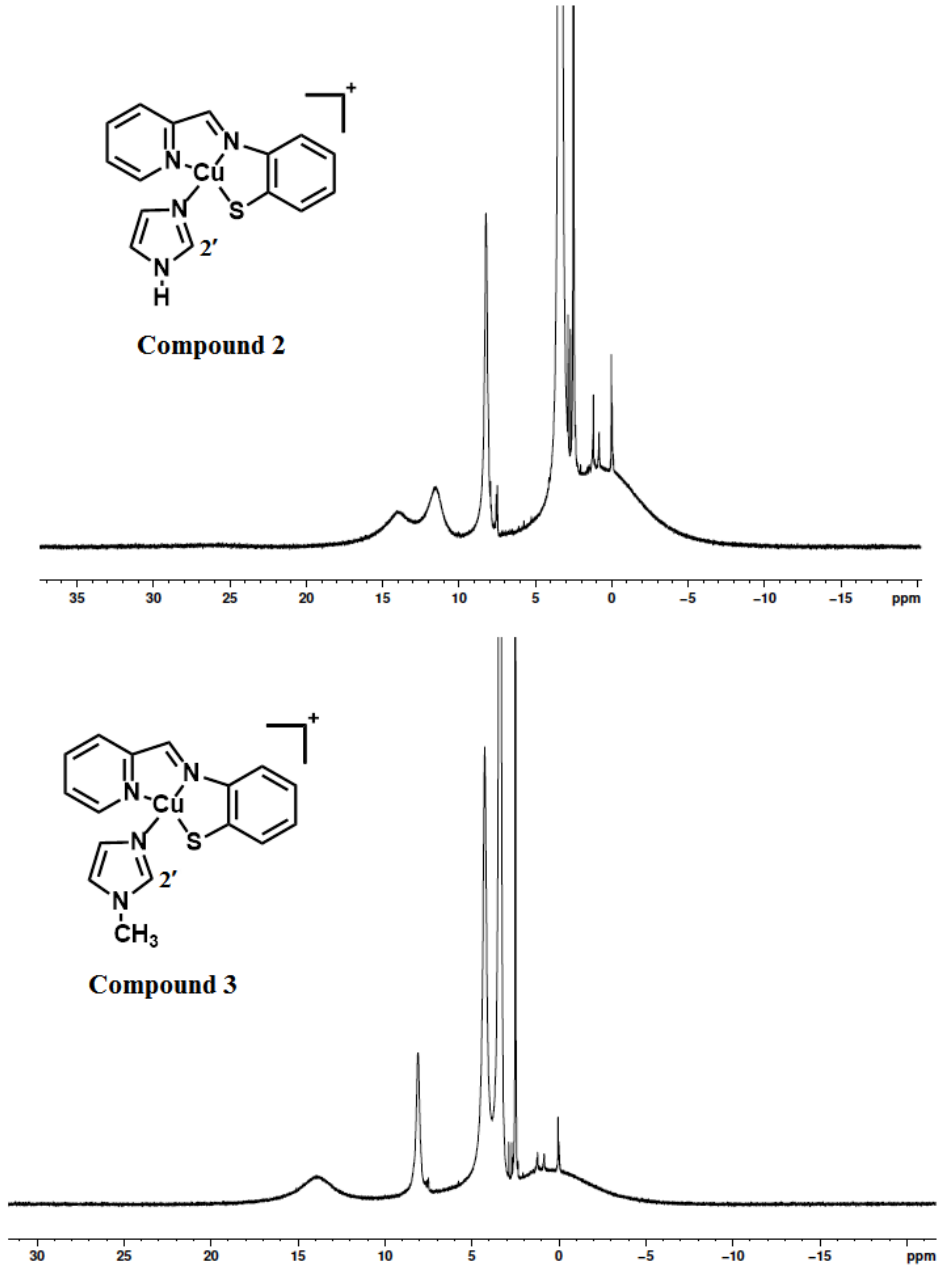

Fig. 3. ^{1}H NMR results of compounds **2** and **3** in d_6-DMSO at RT.

4.2. Electronic structures and spectral properties

Compounds **1**-**5** produce intense purple to violet color in methanol, acetonitrile and DMF while compounds **4** and **5** produce blue color in dichloromethane. All these solutions exhibit optical spectra at room temperature inclusive of an intense absorption in the UV region between 210 and 390 nm

ACCEPTED MANUSCRIPT

involving principally intraligand $\pi \rightarrow \pi^*$ transitions and another strong, relatively intense but broad band centered around 530 -573 nm in the visible region which is absent in the absorption spectrum of any of the free ligands is arising due to S→Cu(II) charge transfer transitions [10,11,16]. This band in the visible region involves both the ligand and the metal center and exhibits a significant solvatochromic shift [11, 56, 57], characteristic of a large dipole moment change between the ground and the excited state, and indicative of charge transfer (CT) character [56]. A blue shift with increasing solvent polarity is observed (Fig. 4, panels B, C), indicating a reduction in the dipole moment upon electronic excitation [11, 56]. Electronic spectra of **1**-**3** in methanol are found to be very similar (Fig. 4, panel A) and show a strong and broad band centered around 540 nm. Electronic spectra for **4** [34] and **5** [37] in CH_2Cl_2 are found to be very similar (Fig. 4, panel B) and exhibit a broad band in the visible region (λ_{max} at 573 nm). This λ_{max}, for example, is found to be shifted to 534 nm for **5** in methanol, and the blue color in CH_2Cl_2 is changed to purple in CH_3OH (and also in CH_3CN or DMF). The λ_{max} for **1** in CH_3OH is at 541 nm whereas the same in water is found to be at 478 nm causing a blue shift of 63 nm. Similarly, λ_{max} for **2** in CH_3OH is at 540 nm whereas in water it is found to be at 480 nm causing a blue shift of 60 nm (Fig. 4, panel C).

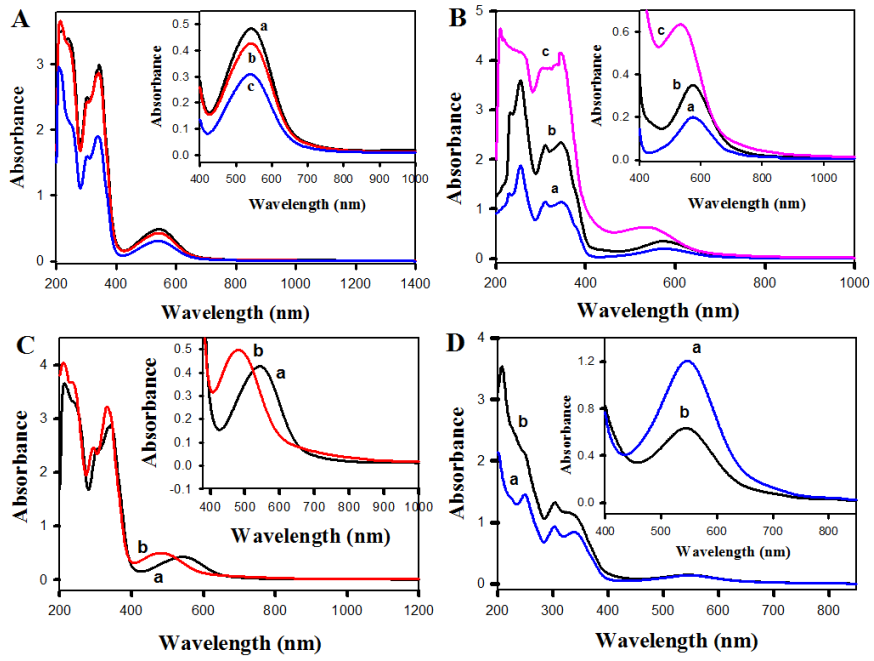

ACCEPTED MANUSCRIPT

Fig. 4. Electronic spectra of the compounds. Panel A. A quantitative comparison of the electronic spectra of **1**-**3** in methanol. Black curve *a* for **1** [1.89 $\times 10^{-4}$ mol L^{-1}], red curve *b* for **2** [2.17 $\times 10^{-4}$ mol L^{-1}] and blue curve *c* for **3** [1.84 $\times 10^{-4}$ mol L^{-1}], respectively. Panel B. Blue curve *a*. **4** in CH_2Cl_2 [6.1 $\times 10^{-4}$ mol L^{-1}]. black curve *b*: **5** in CH_2Cl_2 [2.1 $\times 10^{-4}$ mol L^{-1}], purple curve *c*: **5** in CH_3OH [3.2 $\times 10^{-4}$ mol L^{-1}]. Panel C. black curve *a*: **2** in CH_3OH [2.17 $\times 10^{-4}$ mol L^{-1}], red curve *b*: **2** in water [2.19 $\times 10^{-4}$ mol L^{-1}]. Panel D. Blue curve *a*. **6** in CH_3CN [0.8 $\times 10^{-4}$ mol L^{-1}]. black curve *b*: **7** in CH_3CN [0.6 $\times 10^{-4}$ mol L^{-1}]. Inset of panel D. Blue curve *a*. **6** in CH_3CN [7.0 $\times 10^{-4}$ mol L^{-1}]. black curve *b*: **7** in CH_3CN [2.6 $\times 10^{-4}$ mol L^{-1}].

To check the difference between the solution spectrum with that of the solid, we have recorded the diffused reflectance spectra with the powder samples of **1** and **2**. Both of them have strong and broad absorbance in the visible as well as in the UV region as shown in Fig. S2 (Supplementary material). It should be pointed out in this context that the overall spectral features for all these complexes are comparable in the visible region and these are very similar to that reported in literature [16] for a pseudo-tetrahedral Cu(II) complex with a dianionic tetradentate $N_2S_2^{2-}$ ligand. The ligand field bands for our complexes under study are not seen due to the broad tail of the LMCT band masking these bands. This can be resolved only by deconvolution [32] of the strong and broad band in the visible and near-IR region (Fig. S3 of Supplementary material) that clearly suggests a number of electronic transitions in this region.

Compound **6** is found to be highly soluble in acetonitrile producing a purple to violet solution (λ_{max} at 547 nm) while **7** which is moderately soluble in acetonitrile produces a red-purple solution (λ_{max} at 545 nm) and both these solutions exhibit very similar electronic spectra (Fig. 4, panel D). It is to be noted here that the electronic spectra exhibited by these six-coordinate compounds **6** and **7** in the

ACCEPTED MANUSCRIPT

visible region are found to be very similar to those obtained for **1**-**5** in the same solvent. This observation along with the intense purple color for compounds **6** and **7** in acetonitrile (also in methanol and DMF) strongly suggest equatorial coordination of the sulfur ligand (one of the two sulfur atoms of the disulfide) in these complexes also, resulting in a tetragonal elongated octahedral complex. It should be mentioned here that normally in such cases the axially coordinated ligands in general do not show any charge transfer (CT) absorption [11]. The hexacoordinated Cu(II) thiolato complexes with sulfur ligands in the equatorial positions reported by Bhardwaj and coworkers [16] exhibited an intense band centered around 600 nm that was resulted from the good overlap between the equatorially bound thiolate and the $d_{x^2-y^2}$ orbital on Cu(II) and was assigned as σ(thiolate) → Cu(II) LMCT transition [16]. The equatorial S coordination for the pentadentate ligand used in our study has been established in the crystal structure of chloro[bis[2-(2-pyridylmethyl)imino]phenyl]-disulfide]nickel(II)perchlorate reported by Warner et al. [36] where the ligand is found to act as a pentadentate NNSNN donor with an equatorial S (from the disulfide) coordination to Ni(II).

4.3. Computational results

We have carried out theoretical studies to get an understanding of the ground state geometries of the compounds **1**-**3** that are optimized at the B3LYP/LANL2DZ level of density functional theory (DFT) (Fig. 5, and Table S1 of Supplementary Materials). All of them possess distorted square planar geometry as revealed from the bond angles and dihedral angles (Table 1, and Fig. S4 of Supplementary material) and the extent of distortion is found to be more in the cases of **2** and **3** as compared to **1**. It is to be noted here that the RT solution EPR spectra for **1** and **2** in methanol also showed that these are more distorted toward tetrahedral in this solvent (vide infra). The calculated peak positions obtained from the TDDFT results are presented in Table 1. The experimentally observed positions of the peaks are almost reproduced by the TDDFT results (Table 1) with slight deviations. Interestingly, all these peaks are found to be dominated by configurations where the

ACCEPTED MANUSCRIPT

electrons from the inner beta orbitals are excited to the first unoccupied beta spin orbital which is antibonding in nature and has the characteristic of $d_{x^2-y^2}$ orbital on Cu with p_x/p_y orbitals on the sulfur and the nitrogens (Fig. 6). Among different inner beta orbitals from where this excitation originates, the one having strong bonding nature between the copper d orbital and the p orbital of sulfur has a good contribution in all the studied complexes. In other words, the Cu−S bond weakens due to the electronic transfer to the vacant beta spin orbital where the electronic cloud is delocalized on copper $d_{x^2-y^2}$ orbital and on p orbitals of sulfur, nitrogens and oxygen.

Table 1. Theoretically predicted peak positions and the oscillator strength of the electronic transitions corresponding to these peaks, and the bond angles and dihedral angles obtained from the optimized geometry of the compounds **1**-**3** (without and with solvent).

Complex	Peak position (nm)	Oscillator strength of the corresponding transition	Bond angles and dihedral angles (without solvent)	Bond angles and dihedral angles (in methanol)
1	516[a], 535[b]	0.025[a], 0.014[b]	N2-Cu-S,170^0; N1-Cu-O, 180^0; C7-N2-Cu-S, 180^0; N2-Cu-S-C5, 0^0; C7-N2-Cu-O, 0^0.	N2-Cu-S, 170^0; N1-Cu-O, 177^0; C7-N2-Cu-S, 180^0; N2-Cu-S-C5, 0^0; C7-N2-Cu-O, 0^0.
2	493[a], 503[b]	0.009[a], 0.023[b]	N2-Cu-S, 168^0; N1-Cu-N4, 176^0; C7-N2-Cu-S, 164^0; N2-Cu-S-C5, 14^0; C7-N2-Cu-N4, 5^0.	N2-Cu-S, 168^0; N1-Cu-N4, 180^0; C7-N2-Cu-S, 177^0; N2-Cu-S-C5, 2^0; C7-N2-Cu-N4, 0^0.
3	495[a], 505[b]	0.016[a], 0.026[b]	N2-Cu-S, 168^0; N1-Cu-N4, 176^0; C7-N2-Cu-S, 162^0; N2-Cu-S-C5, 15^0; C7-N2-Cu-N4, 6^0.	N2-Cu-S, 168^0; N1-Cu-N4, 177^0; C7-N2-Cu-S, 168^0; N2-Cu-S-C5, 11^0; C7-N2-Cu-N4, 4^0.

[a] without solvent, [b] in methanol

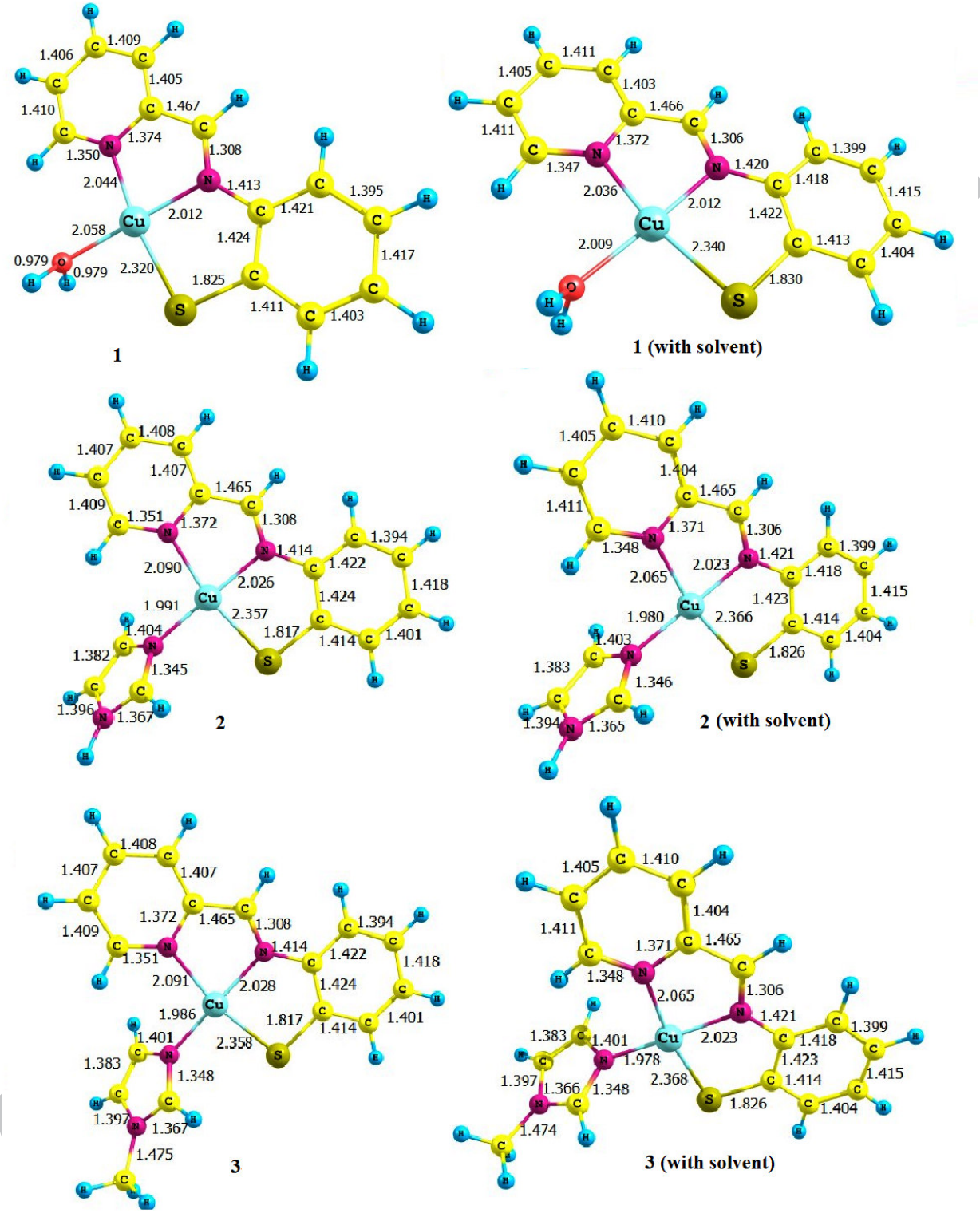

Fig. 5. Ground state optimized structures of the complexes **1**, **2**, and **3** without and with solvent, respectively. The numbers between the atoms are respective bond distances in Å.

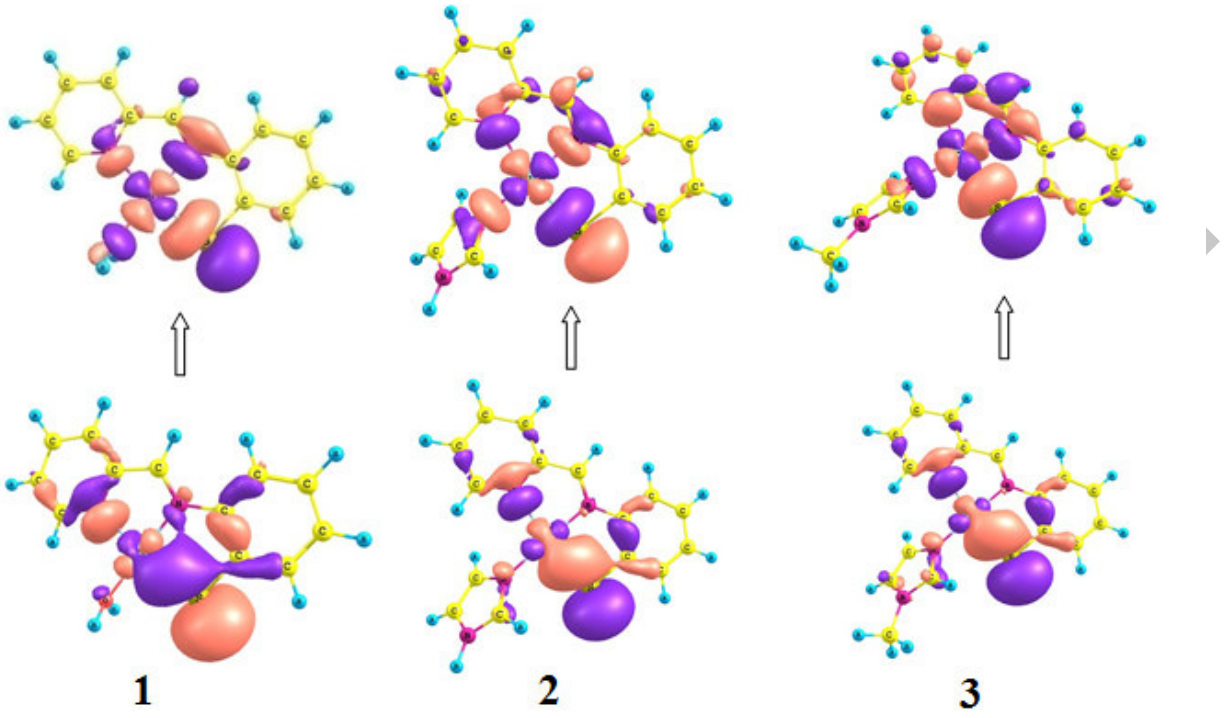

Fig. 6. Orbitals involved in the electronic excitations corresponding to the dominant configurations for compounds **1**, **2**, and **3**, respectively.

4.4. Reactivity of the complexes

For chemical reactivity we have chosen compounds **2** and **6** to react with imidazole, because **2**, if it reacts at all, will undergo only addition reaction to form either a 5-coordinate or a 6-coordinate product while compound **6** should undergo only Cl^- substitution reaction. Thus interpretation of the spectral data is expected to be simple and easy to derive kinetics parameters. Reactions of these two complexes in CH_3CN at RT with imidazole have been studied by monitoring the electronic spectral change in the visible region as shown in Fig. 7. Imidazole readily reacts with **2** as evident from the electronic spectral change. When 2-fold solid imidazole is added to the acetonitrile solution of **2** having the spectrum shown in Fig. 7, curve *a* of panel A, the intensity of the peak increases immediately as shown in curve *b*, and becomes steady within 5 min and no further change is observed up to 20 min (curve *c*). The λ_{max} is found to be shifted from 533 nm to 540 nm upon

reaction with imidazole. On the other hand, **6** reacts with imidazole in CH_3CN and the λ_{max} at 546 nm (curve *a*, Fig. 7 panel B) immediately blue shifts with increased intensity (curve *b*, Fig. 7 panel B) and then slowly increases and becomes steady within 20 min when the λ_{max} is found to be at 542 nm (and the absorbance is increased from c.a. 0.94 to 1.47) (curve *e*, Fig. 7 panel B).

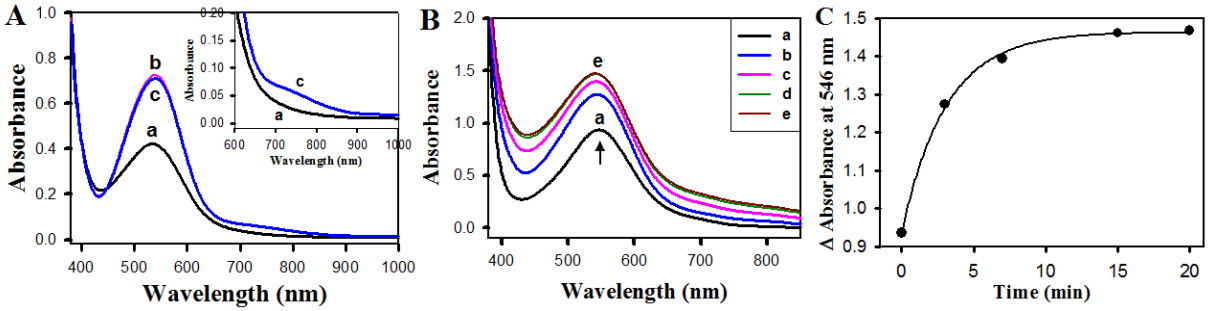

Fig. 7. Electronic spectral changes for the reactions of the compounds. Panel A. Reaction of **2** with imidazole. Black curve *a*. **2** in CH_3CN [2.17×10^{-4} mol L^{-1}], red curve *b*: within 5 min after addition of 2-fold excess of solid imidazole, and blue curve *c*: after 20 min. Panel B. Reaction of **6** with imidazole. Black curve *a*. **6** in CH_3CN [5.50×10^{-4} mol L^{-1}], blue curve *b*: immediately after adding 2-fold excess of solid imidazole, curve *d*: recorded after 15 min, and curve *e*: recorded after 20 min. Curves *d* and *e* are identical indicating the steady state reached within 15 min. Panel C. Plot of absorbance change at 546 nm with time for the spectral data presented in panel B. The solid line represents the fitting of the experimental points (circles) using the model $\Delta A_t = c + a(1 - e^{-k\,t})$.

Based on the electronic spectral change shown in Fig. 7 panel A for the reaction of **2** with imidazole, and the final product isolated from this reaction (vide infra), it is concluded that imidazole undergoes addition reaction forming a six-coordinate octahedral complex $[Cu(pabt)(Imz)_3](ClO_4)$ which has a strong absorbance at 540 nm and exhibit a weak broad ligand field band [16] in the 700-800 nm region (shown in inset of Fig. 7, panel A) apart from other charge transfer bands in the UV region. The λ_{max} at 533 nm which is assigned as $\sigma S(1) \rightarrow Cu(II)\ d_{x^2-y^2}$ [10,11 16, 58] is found to be shifted to 540 nm with increased intensity. The higher intensity of this band in the reaction product is most

ACCEPTED MANUSCRIPT

likely due to a better overlap between the Cu(II) d_x^2-$_y^2$ and the equatorially bound thiolate donor [16]. This reaction product was easily synthesized from the reaction of **2** in CH_3CN with imidazole (1 : 2) by stirring the solution at RT for 30 min, and the volume was then reduced in vacuum to get a solid. This was filtered and the dark compound was washed with methanol and air dried. The elemental analysis of the isolated product was found to be consistent with the formulation of $[Cu(pabt)(Imz)_3](ClO_4)$ (**2A**).

Unlike the reaction of **2** with imidazole that resulted in an abrupt change in the spectrum due to the formation of a six-coordinate complex owing to addition of the incoming ligand, **6** shows only a gradual change of its λ_{max} at 546 nm which is blue shifted to 542 nm with enhanced intensity (Fig. 7 curve e of panel B) upon completion of the reaction within 20 min due to the slow substitution of the Cl^- by the incoming imidazole ligand in the sixth coordination site, and this is supported by the increase in conductivity of **6** in CH_3CN after addition of solid imidazole (1 : 1 mmol) already mentioned resulting a 2 : 1 electrolyte. Isolation of this reaction product followed by purification was found to be consistent with the formulation $[Cu(pdta)(Imz)]Cl_2$ (**6A**). A plot of absorbance change at 546 nm with time for the spectral data presented in panel B of Fig. 7 clearly shows an exponential rise to maximum (Fig. 7, panel C) and this was fitted using the single exponential equation (1)

$$\Delta A_t = c + a(1 - e^{-kt}) \qquad (1)$$

This fitting yielded the kinetic parameters: $c = 0.938 \pm 0.013$, $a = 0.526 \pm 0.015$ and k (min^{-1}) = 0.324 ± 0.024 for this ligand substitution reaction.

4.5. DNA binding studies

DNA binding studies were carried out for compounds **1** and **2** in aqueous medium by monitoring the overall electronic spectral change (Fig. S5, Supplementary material) after addition of plasmid DNA dissolved in Tris buffer, pH 7. The final spectra (Fig. 8) clearly suggests that both the compounds

strongly bind with the DNA [24, 29, 30]. Compound **1** exhibits hypochromism of ~43% of the π→π* absorption band at 333 nm and compound **2** exhibits hypochromism of ~51% of the π→π* absorption band at 332 nm.

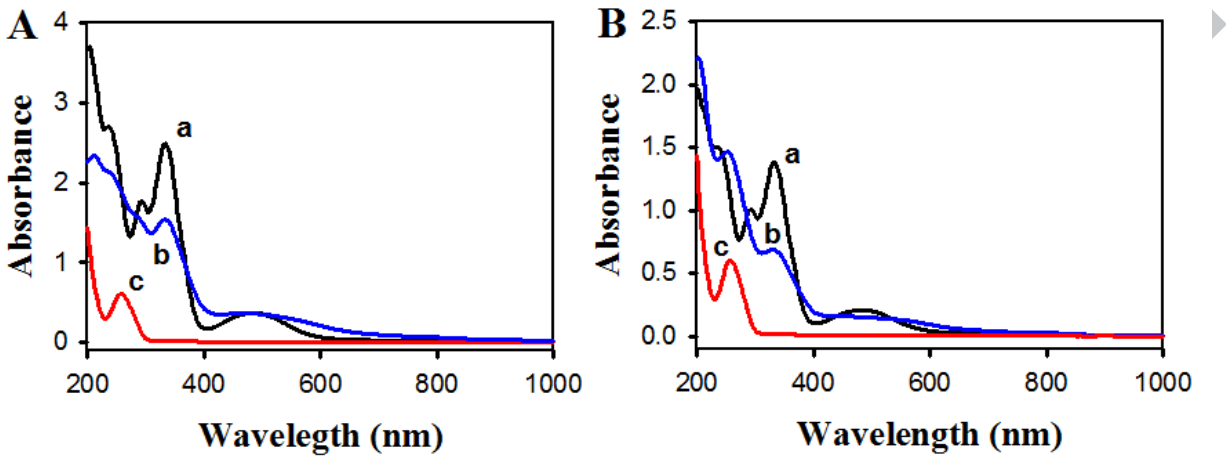

Fig. 8. Panel A. Electronic spectra (a) compound **1** in water [1.51×10^{-4} mol L^{-1}], (b) compound **1** in water [1.51×10^{-4} mol L^{-1}] + 10.8 µg/mL plasmid DNA, and (c) plasmid DNA in water [10.8 µg/mL]. Panel B. Electronic spectra (a) compound **2** in water [0.92×10^{-4} mol L^{-1}], (b) compound **2** in water [0.92×10^{-4} mol L^{-1}] + 10.8 µg/mL plasmid DNA, and (c) plasmid DNA in water [10.8 µg/mL].

In order to get the binding constant for the compounds **1**-**3**, absorption titration experiments were performed with incremental amounts of calf thymus DNA (ct-DNA) in 10 mM Tris–HCl buffer (pH 7.43) and by keeping the individual complex concentration constant. The binding of complexes to the ct-DNA exhibits hypochromism (Fig. S5, Supplementary material) with a minor red shift of the band at around 332 nm indicating intercalative binding, resulting in strong stacking between the DNA base and aromatic chromophore [59].

The binding constant K_b has been calculated from the kinetic data obtained using the following equation (2).

ACCEPTED MANUSCRIPT

$$\frac{[DNA]}{(\varepsilon_a - \varepsilon_f)} = \frac{[DNA]}{(\varepsilon_b - \varepsilon_f)} + \frac{1}{K_b(\varepsilon_b - \varepsilon_f)} \quad (2)$$

where, [DNA] is the concentration of ct-DNA used, and ε_a, ε_f and ε_b correspond to apparent extinction coefficients for the complex i.e., Abs/[complex] in the presence of DNA, in the absence of DNA and to fully bound DNA, respectively. A plot of $[DNA]/(\varepsilon_a - \varepsilon_f)$ versus [DNA] yields a slope = $1/(\varepsilon_b - \varepsilon_f)$, and the intercept = $1/K_b(\varepsilon_b - \varepsilon_f)$, respectively. The binding constant K_b is calculated from the ratio of the slope to the intercept.

The binding constant K_b is found to be 1.47×10^5 M^{-1} for **1**, 2.03×10^5 M^{-1} for **2**, and 2.09×10^5 M^{-1} for **3**, respectively. The K_b values are comparable to that reported for a classical intercalator such as ethidium bromide ($K_b = 1.40 \times 10^5$ M^{-1}) in 25 mM Tris-HCl buffer (pH 7.33) [60]. The higher K_b values for **2** and **3** as compared to **1** suggest that **2** and **3** possessing the imidazole or N-methyl imidazole group interact with DNA more strongly than complex **1**. This is consistent with the observation of complete cleavage of the DNA by **2** and **3**, but not **1** (vide infra). Similar observations of enhanced cleavage activity of copper(II) complexes showing stronger DNA-binding affinity resulting from a partially intercalating co-ligand dipyrido-[3,2-d:2′,3′-f]-quinoxaline (dpq) are reported in literature [61-63].

4.6. Catechol oxidase activity

We have chosen **1** and **2** as representative compounds, both being 4-coordinate, to explore the catechol oxidase activity, to see the influence of imidazole present in **2** as the fourth ligand in this activity as compared to the water molecule present as the fourth ligand in **1**. The catalytic activity of compounds **1** and **2** were performed by treating 1×10^{-4} mol L^{-1} complex solutions in methanol with 1×10^{-2} mol L^{-1} of 3,5-di-*tert*-butyl catechol (3,5-DTBC) as model substrate in methanol at RT in presence of air. Fig. 9 shows the spectral change for **1** and **2**, respectively. The reaction was

monitored for ~24 h after. Initially, in the absence of 3,5-DTBC, complexes **1** and **2** show very low absorbance at ~401 nm (bottom curve *i*). Upon addition of 3,5-DTBC the spectra recorded immediately shows increment of the absorbance at 401 nm. Since it is well established [64] that 3,5-di-*tert*-butyl benzoquinone (3,5-DTBQ) shows band maxima at 401 nm in pure methanol, the experiment unequivocally proves oxidation of 3,5-DTBC to 3,5-DTBQ catalyzed by the Cu(II) complexes. The chemical kinetics of 3,5-DTBC oxidation was determined by monitoring the increase of the absorbance at 401 nm for the formation of the product 3,5-DTBQ, and to get an idea about the number of intermediate species involved in this oxidation process, the plot of absorbance change at 401 nm with time (figure 9, panel C) was fitted using the model (3)

$$\Delta A_t = c + a_1(1 - e^{-k_1 t}) + a_2(1 - e^{-k_2 t}) \quad (3)$$

It is also evident from this plot that compound **2** was found to be more efficient in the catalytic oxidation of 3,5-DTBC than compound **1** under identical experimental conditions.

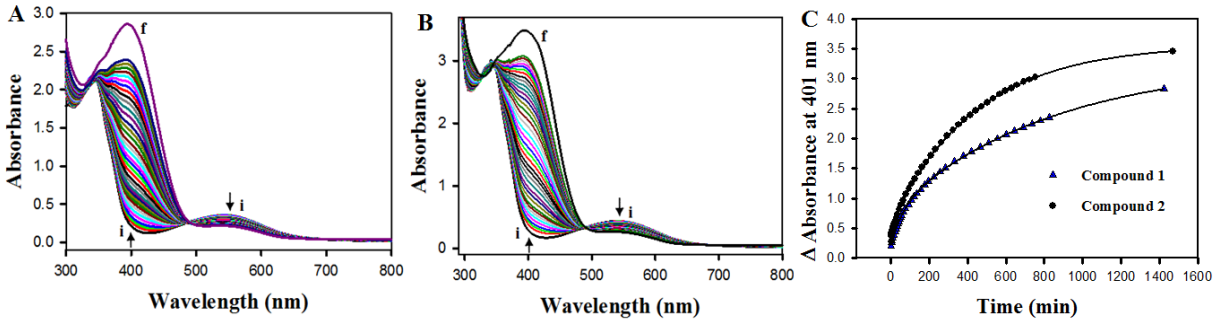

Fig. 9. The catalytic activity of compounds **1** and **2** were performed by treating 1×10^{-4} mol L^{-1} complex solutions with 1×10^{-2} mol L^{-1} of 3,5-di-*tert*-butyl catechol (3,5-DTBC) as model substrate in methanol at RT. Panel A and B show the electronic spectral change for the formation of 3,5-DTBQ from the catalytic oxidation of 3,5-DTBC with compounds **1** and **2**, respectively, in methanol at RT. Panel C shows the plot of absorbance change at 401 nm with time showing the relative rate of formation of 3,5-DTBQ. The solid line represents the fitting of the experimental points (circles) using the model $\Delta A_t = c + a_1(1 - e^{-k_1 t}) + a_2(1 - e^{-k_2 t})$.

ACCEPTED MANUSCRIPT

Table 2. Kinetic parameters for the reaction of compounds **1** and **2** with 3,5-DTBC in CH_3OH at RT. Data for the plot of absorbance change at λ_{max} = 401 nm with time for the formation of 3,5-DTBQ in both the cases were fitted using the equation (3).

	Complex **1**	Complex **2**
Constant *c*	0.233±0.004	0.322±0.007
a_1	0.564±0.014	0.284±0.011
k_1 (min^{-1})	0.015±0.001	0.037±0.003
a_2	2.477±0.021	2.958±0.011
k_2 (min^{-1})	0.0012±0.00003	0.0022±0.00003

It is to be noted here that there are recent reports of mononuclear Cu(II) [65] and Zn(II) [64] complexes apart from dinuclear complexes [66-69] that show catechol oxidase activity. During the catalytic oxidation of 3,5-DTBC by mononuclear Zn(II) complexes, Guha et al. [64] have detected spectroscopically two catalyst-substrate adducts intermediates for only the mononuclear Zn(II) catalysts but not for the dinuclear Zn(II) catalysts. Gajewska et al. [65] have reported the catechol oxidation reaction of $[Cu(bdtbpza)_2(tmeda)(H_2O)_2]$ (where, bdtbpza = bis(3,5-di-t-butylpyrazol-1-yl)acetate and tmeda = tetramethylethylenediamine) with 3,5-DTBC and have proposed a mechanism which includes an equilibrium between two intermediates, one of them being a radical species as suggested from the weak EPR signal at g = 1.9807 that was detected during the reaction of the said complex with 3,5-DTBC in CH_2Cl_2. Thus the observation of two exponent fit for the kinetic data in our cases (figure 9, panel C) of **1** and **2** with the reaction of 3,5-DTBC in methanol to form 3,5-DTBQ is not surprising and proceeds through two intermediates, one major and another minor, to form the final product 3,5-DTBQ. **2** is much efficient than **1** in the oxidation process as obvious from the kinetic curves (Fig. 9, panel C) as well as from the kinetic parameters presented in Table 2.

We have also carried out the kinetics experiment to determine the catalytic activity for these two compounds as described below.

The kinetics of the 3,5-DTBC oxidation catalyzed by the compounds **1** and **2** was studied by monitoring the increase in the product 3,5-DTBQ which has a characteristic absorption band maxima

ACCEPTED MANUSCRIPT

at 401 nm in methanol. The rate dependence on the substrate (3,5-DTBC) concentration was studied by keeping the individual complex concentration constant in methanol while varying the substrate concentration. For each experimental run the initial rate was determined and rate versus 3,5-DTBC concentration was plotted. Both the complexes showed saturation kinetics, and the Michaelis–Menten model was used to analyse the kinetic data. The Michaelis binding constant (K_M), maximum velocity (V_{max}) and the turnover number (k_{cat}) were calculated for these complexes using the Lineweaver–Burk plot of 1/V versus 1/[S] (Fig. S6, Supplementary material) using the following equation

$$1/V = \{K_M/V_{max}\}\{1/[S]\} + 1/V_{max} \qquad (4)$$

The values of the kinetic parameters are presented in Table 3. The values of V_{max} are $1.70 \times 10^{-}6$ for **1**, and 6.17×10^{-6} for **2**, K_M values are 1.13×10^{-4} for **1** and 9.77×10^{-4} for **2**, and k_{cat} values are 6.13×10^{2} for **1** and 11.11×10^{2} for **2**, respectively, clearly indicating that **2** is a better catalyst.

Table 3. The values of the kinetic parameters of catechol oxidase activity calculated using eq 4.

Complex	V_{max} (Ms^{-1})	K_M (M)	k_{cat} (h^{-1})
1	$1.70 \times 10^{-6} \pm 0.0208 \times 10^{-6}$	$1.13 \times 10^{-4} \pm 0.063 \times 10^{-4}$	6.13×10^{2}
2	$6.17 \times 10^{-6} \pm 0.214 \times 10^{-6}$	$9.77 \times 10^{-4} \pm 0.834 \times 10^{-4}$	11.11×10^{2}

The k_{cat} values for complexes **1** and **2** indicate that the presence of imidazole group in **2** has a significant impact on the catecholase activity. Also these k_{cat} values are higher than those reported for some dinuclear complexes [66]. However, these k_{cat} values are much lower than that reported very recently by Adak et al. [69] for the mononuclear species $[CuL^1H^{py}(3,5\text{-DTBCH})]$ formed from the reaction of 3,5-$DTBCH_2$ and a binuclear Cu(II) complex of formula $[Cu(L^1H^{py})Cl]_2(ClO_4)_2$, [$L^1H_2$ is a tridentate ligand formed by condensation of 2-aminomethyl pyridine and pyridoxal], but higher than that reported by Gajewska et al. [65] for their mononuclear complex. A major difference in the proposed mechanism for these two reported cases is that the dioxygen directly coordinates to

ACCEPTED MANUSCRIPT

the Cu(I) species proposed by Adak et al. [69] based on their theoretical study, while dioxygen is proposed to attack the semiquinone coordinated to Cu(I) in the latter case. However, in the absence of exact information about the nature of the intermediates in our present study, we propose the following tentative mechanism for the catalytic cycle.

Based on the spectroscopic data and the reactivity of compound **2**, it appears that the catechol molecule directly coordinates to the four-coordinate catalyst (**1** or **2**), forming an intermediate complex–substrate adduct which in turn may equilibrate between Cu(II)-(3,5-DTBC) and the semiquinone (SQ) intermediate Cu(I)-(3,5-DTBSQ) as proposed by Gajewska et al. [65]. This Cu(I)-(3,5-DTBSQ) species reacts with dioxygen resulting an oxygenated species that oxidizes the Cu(I) center to regenerate the Cu(II) catalyst and 3,5-DTBQ and hydrogen peroxide are released. It is to be noted here that H_2O_2 has been detected iodometrically as described in the experimental section.

4.7. Infrared and far-infrared spectra

The infrared spectra of the compounds **1**-**7** in the region 4000-400 cm^{-1} are recorded using KBr pellet. The compound **1** exhibits a broad band in the 3400 cm^{-1} region clearly indicating the presence of the water molecule in this compound. This band is completely absent in case of **4** (Fig. S7, Supplementary material). The strong band at 3190 cm^{-1} observed due to the N–H stretching for 2-(2-pyridyl)benzothiazoline is found to be absent in the IR spectra of **1–4** indicating the formation of the corresponding Schiff base complexes in these cases [32]. No S–H band is observed in the region 2500–2600 cm^{-1} for all of these complexes. A very strong and broad band at 1095 cm^{-1} originating from ν_3 of ionic perchlorate for **1** - **3** confirms the presence ClO_4^- in these three compounds [70]. This band is absent, as expected, in the IR spectra of **4-7**. The far-infrared spectra of the compounds **1**, **2** and **4** are shown in supplementary Fig. S8 and the important far-IR bands (all in cm^{-1}) with their assignments [70] are given in Table S2 of the Supplementary material.

ACCEPTED MANUSCRIPT

4.8. EPR results

The powder EPR spectra for the compounds **1**-**7** were recorded at room temperature at X-band frequency and are shown in Fig. 10. The g values are found to be: $g_{\parallel}$ = 2.190 and $g_{\perp}$ = 2.057 for **1,** and g = 2.057 for **2**, $g_{\parallel}$ = 2.160 and $g_{\perp}$ = 2.069 for **3,** while the $g_{\parallel}$ = 2.158 and $g_{\perp}$ = 2.041 for **4**; $g_{\parallel}$ = 2.128 and $g_{\perp}$ = 2.012 for **5**, $g_{\parallel}$ = 2.169 and $g_{\perp}$ = 2.055 for **6,** g = 2.057 for **7.** The compound **7** has an isotropic signal because of its almost octahedral coordination while compound **2** and **3** look somewhat isotropic because of unresolved parallel and perpendicular components. All of them have a g_{av} of ~2.05−2.10 revealing their almost similar ligand field character. The solution EPR spectra for **1**, **2**, **3**, **5**, **6** and **7** were recorded in acetonitrile while that for **4** and **6** were recorded in DMF. These are shown in Fig. 11. All these solutions exhibit similar EPR spectra ($A_{iso} \cong 80$ G) consisting of four lines describing the interaction of the unpaired electron with the central $^{63/65}$Cu nucleus (I = 3/2, natural abundances of 69.17% and 30.83%, for ^{63}Cu and ^{65}Cu, respectively). It is to be noted that all complexes show isotropic hyperfine coupling from copper without any resolution from ^{63}Cu and ^{65}Cu due to large but differential line width, ΔH. Hence, the much smaller hyperfine couplings from either ^{14}N or ^{35,37}Cl is not resolved even under isotropic situation. The respective g_{iso} values are: 2.1051 for **1**, 2.1108 for **2**, 2.0913 for **3**, 2.0947 for **4**, 2.0803 for **5**, 2.0826 for **6** and 2.0830 for **7**. The solutions of compounds **1** and **2** in methanol also exhibit four-line EPR spectra (Figs. 11E, F) but the A_{iso} value is found to be ~67 G in each case. However, the room temperature solution EPR spectrum of the compound **4** in dichloromethane shown in Fig. S9 (Supplementary material) is found to be very different from that in DMF. The frozen glass spectra of the compounds **1** and **2** were recorded in methanol whereas that for **4** was recorded in DMF as well as in CH_2Cl_2: THF (1:1) glass at LNT. These are shown in Fig. 12 and Fig. S9 (Supplementary material).

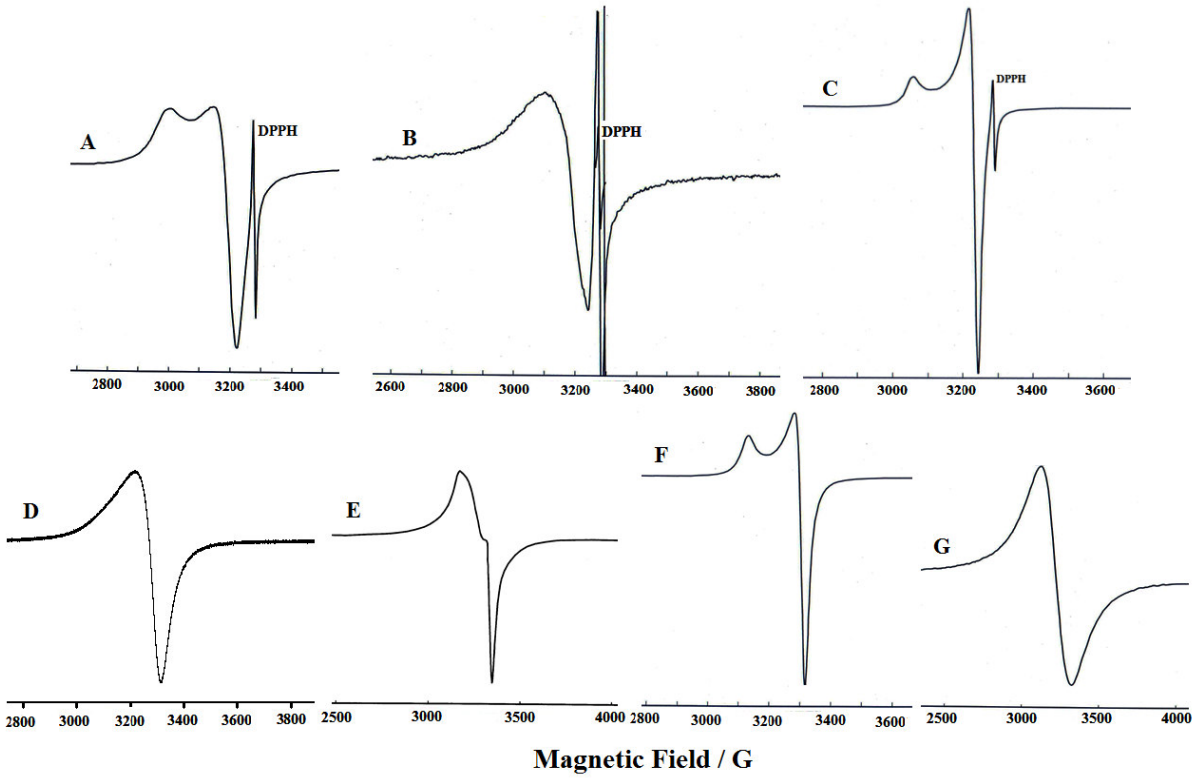

Fig. 10. X-band powder EPR spectra for **1-7** at RT. (A) **1** with DPPH; (B) **2** with DPPH; (C) **4** with DPPH; (D) **3** without DPPH, (E) **5** without DPPH, (F) **6** without DPPH, and (G) **7** without DPPH.

The intense EPR signal displayed by powder samples indicates that they are paramagnetic. This observation along with the stoichiometric results of the compounds **1**-**7** indicate that the metal ion is in +2 oxidation state with a d^9 configuration. The appearance of intense four-line pattern is arising due to the interaction of the unpaired electron with the copper nucleus with $I = 3/2$. Also the occurrence of a four-line multiplet from the acetonitrile or methanol solution of **1**, **2** and **3**, and from DMF solution of **4** clearly indicates that these are monomeric species in these solutions. It is important to note here that the A_{iso} value (80 G) of the compounds in acetonitrile or in DMF is much higher than the A_{iso} value (67 G) of compounds **1** and **2** in methanol. This clearly indicates that the later two compounds **1** and **2** which are predominantly tetrahedral in methanol undergo structural change towards square planar in acetonitrile. This is consistent with the observed electronic spectral results for **2** in methanol where the transitions are red shifted as compared to those obtained in

ACCEPTED MANUSCRIPT

acetonitrile (figure not shown). The optimized structures obtained from the DFT results for **1**-**3** in presence of methanol also indicate distortion from square planar geometry. The solution EPR spectrum of **4** in dichloromethane (Fig. S9) indicates that there are two weakly interacting species present. This is also evident from the frozen glass EPR spectrum (Fig. S9) of **4** in CH_2Cl_2 : THF (1 : 1) at 77 K. This is most likely originating from the partial dissociation of the coordinated Cl^- in CH_2Cl_2 or CH_2Cl_2 : THF solutions. This is consistent with the observation of Lindoy and Livingstone [34] who reported from the conductivity study that this compound undergoes slight dissociation in nitromethane. However, in DMF **4** undergoes complete dissociation resulting a 1 : 1 electrolyte as indicated from the molar conductivity value (73.5 Ohm^{-1} cm^2 mol^{-1}) and this solution exhibits a 4-line EPR spectrum (Fig. 11) at RT suggesting a single monomeric species in DMF. The isotropic *g* value for **5** in CH_3CN is 2.0803 while that for **7** in CH_3CN is 2.0830, respectively. The differing spectral width and hence the resolution of the 4-line splitting are due to the differing tumbling motion of the molecules and their iconicity.

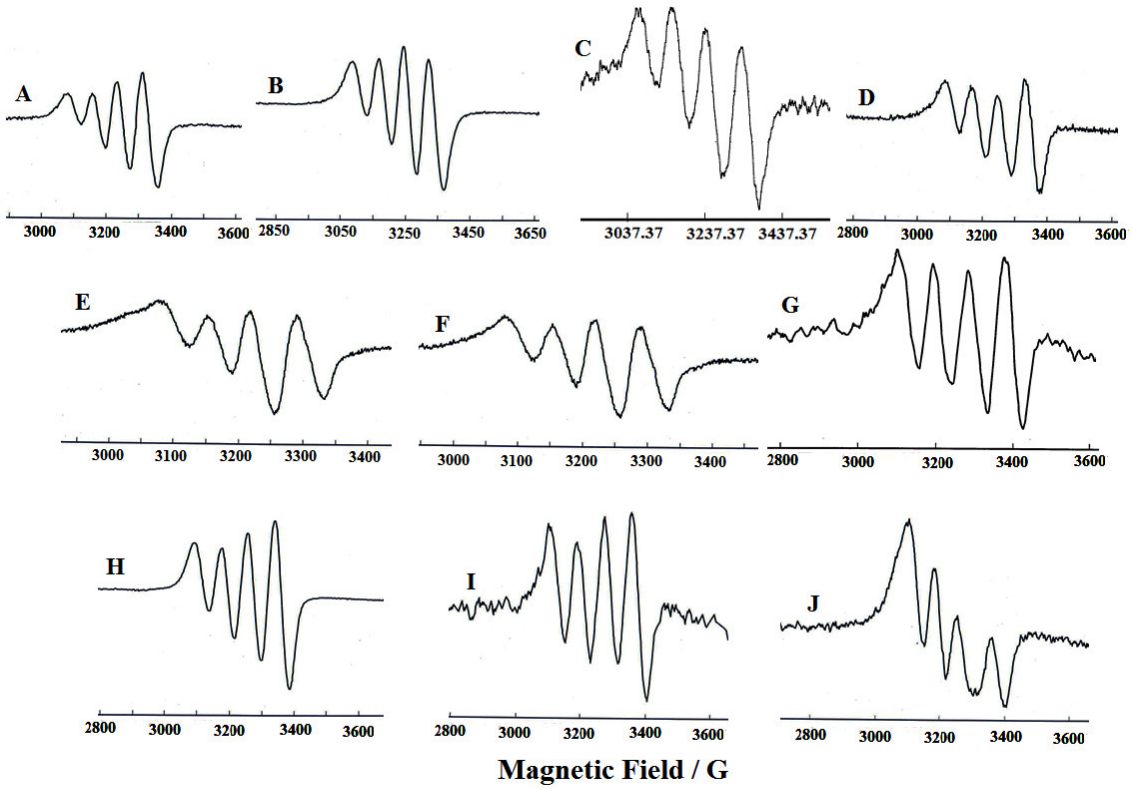

Fig. 11. X-band solution EPR spectra of **1**-**7** at RT. (A) **1** in CH_3CN:CH_2Cl_2 (2 : 1), (B) **2** in CH_3CN:CH_2Cl_2 (2 : 1); (C) **3** in CH_3CN, (D) **4** in DMF; (E) **1** in CH_3OH; (F) **2** in CH_3OH; (G) **5** in CH_3CN; (H) **6** in DMF; (I) **6** in CH_3CN; and (J) **7** in CH_3CN.

The frozen-glass EPR spectra of **1** and **2** in methanol clearly show the parallel and perpendicular features with the $g_{\parallel} = 2.3218$ and $g_{\perp} = 2.0690$ for **1** and $g_{\parallel} = 2.2775$ and $g_{\perp} = 2.0522$ for **2** while the $g_{\parallel} = 2.1516$ and $g_{\perp} = 2.0378$ for **4** in CH_2Cl_2 at 77 K (figure not shown). It may be pointed out here that these g values for the imidazole compound **2**, which satisfies the basic CuN_3S structural model are close to those of blue copper ($g_{\parallel} \approx 2.25$ and $g_{\perp} \approx 2.05$) [10,19]. The increased $g_{\parallel}$ value in solution is due to the relaxation of rigid molecular structure of solid to become planar with four ligands. $A_{\parallel}$ from copper in frozen solutions vary from 150 to 160 G indicating that the geometry of the complexes vary from distorted tetrahedron to deviated planar geometry for ligand coordination. Unfortunately only in cases of the frozen solutions of A and C (Fig. 12), $A_{\parallel}$ from copper is resolved, restricting us to derive the information on geometry of other complexes.

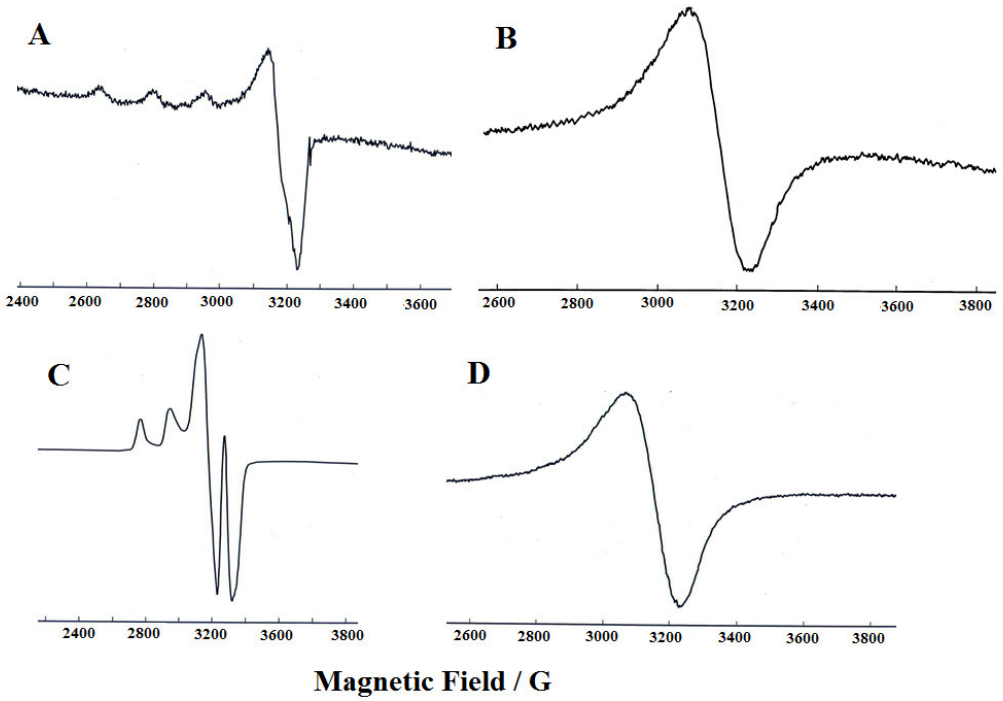

Fig. 12. Frozen glass EPR spectra of the compounds at LNT without DPPH. (A) **2** in CH_3OH. (B) **5** in CH_3CN. (C) **6** in DMF, and (D) **7** in CH_3CN.

4.9. Results on biological activity

4.9.1. Antibacterial activity

Post 16 hours of incubation, when there was visible lawn formation of *Escherichia coli* in the control plate, the plate with the sample discs were checked for zones of inhibition around the discs. All the samples showed some antibacterial activity against *E. coli* as indicated by the clear growth inhibition zones seen around each disc containing the copper compound (Fig. 13). Measurement of the size of the growth inhibition zones showed that the activity was maximum for **2** (9 mm), followed by **1** (8 mm) and **4** (7 mm). **5**, **6** and **7** (6 mm) had marginal activity when compared to the previous three. This was against the control disc with DMSO which showed a negligible zone of inhibition. The antibacterial activity of **3** was found to be very similar to that of **2** while $Cu(N\text{-}MeImz)_4(ClO_4)_2$ showed a negligible zone of inhibition, similar to that of DMSO only (figure not shown).

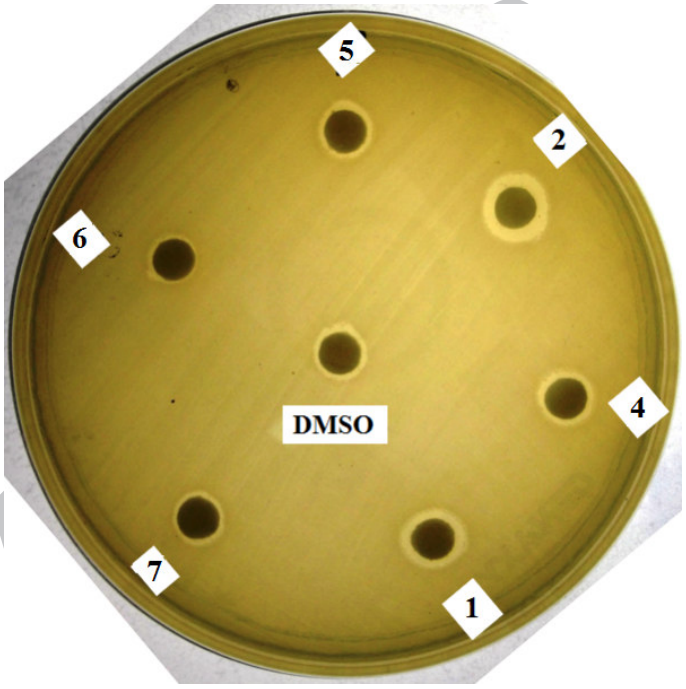

Fig. 13. Plate with *Escherichia coli* lawn showing the effect of sample discs (labels are for compounds **1**, **2**, **4**-**6**). The control disc with just DMSO is in the center.

4.9.2. Nucleic acid degradation activity

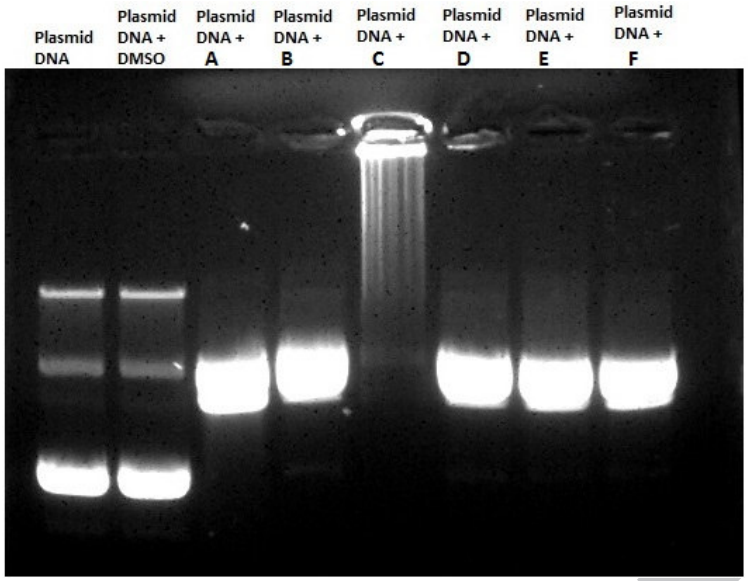

Fig. 14. 1% agarose gel depicting effects of treatment of 5 µL plasmid DNA with copper compounds. The loading volume is 10 µL in each lane. A = compound **1**, B = compound **4**, C = compound **2**, D = compound **7**, E = compound **6**, and F = compound **5**. Final concentration: [1.69×10^{-4} mol L^{-1}] for **1**, [1.50×10^{-4} mol L^{-1}] for **2**, [2.13×10^{-4} mol L^{-1}] for **4**, [2.13×10^{-4} mol L^{-1}] for **5**, [1.18×10^{-4} mol L^{-1}] for **6**, [1.18×10^{-4} mol L^{-1}] for **7**, and [0.1 mol L^{-1}] for DMSO.

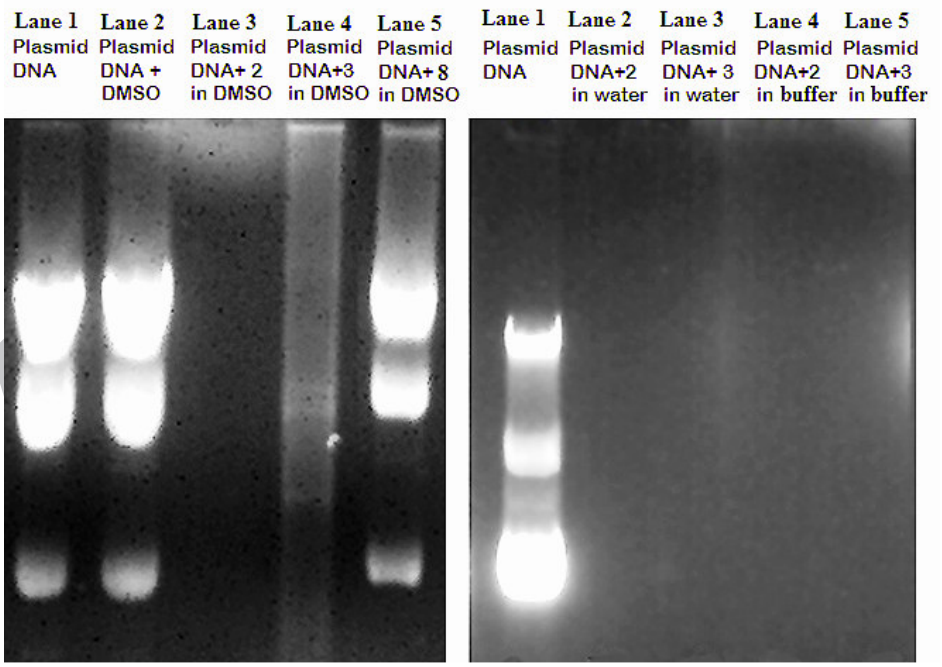

ACCEPTED MANUSCRIPT

Fig. 15. Effect on DNA. 1% agarose gel depicting effects of treatment of 5 μL plasmid DNA with copper compounds. Left panel. Lane 1: Control Plasmid DNA, lane 2: Plasmid DNA + DMSO, lane 3: Plasmid DNA + **2** in DMSO, lane 4: Plasmid DNA + **3** in DMSO, lane 5: Plasmid DNA + $Cu(NMe\text{-}Imz)_4(ClO_4)_2$ in DMSO, respectively. Right panel. Lane 1: Control Plasmid DNA, lane 2: Plasmid DNA + **2** in water, lane 3: Plasmid DNA + **3** in water, lane 4: Plasmid DNA + **2** in sodium phosphate buffer (pH 7.00), lane 5 : Plasmid DNA + **3** in sodium phosphate buffer (pH 7.00), respectively. Final concentration: [1.69×10^{-4} mol L^{-1}] for **1**, [1.50×10^{-4} mol L^{-1}] for **2**, [1.45×10^{-4} mol L^{-1}] for **3**, [1.13×10^{-4} mol L^{-1}] for $Cu(NMe\text{-}Imz)_4(ClO_4)_2$ and [0.1 mol L^{-1}] for DMSO.

The separated bands in the agarose gel were observed and recorded in a UV gel imager. The control (purified plasmid DNA alone) showed three distinct bands – circular, linear and supercoiled DNA from the top to the bottom (Fig. 14). The lane having plasmid DNA with DMSO showed the same pattern as well. In the lanes containing plasmid DNA treated with copper compounds, the supercoiled band was not visible pointing to the binding of DNA by these compounds and subsequent degradation. The effect is most pronounced in the case of C (compound **2**), where the entire lane is smeared, a pattern similar to the activity of DNase on plasmid DNA. The two results cumulatively indicate that C (compound **2**) has a pronounced effect on DNA and leads to degradation, which may also be the reason behind the enhanced antibacterial activity of this compound **2**. Also we carried out the same experiments for the compounds **2**, **3**, and $Cu(N\text{-}MeImz)_4(ClO_4)_2$ (**8**) in DMSO and also for **2** and **3** in water and in sodium phosphate buffer (pH 7.00), respectively (Fig. 15). Compounds **2** and **3** showed very similar results in all three solvents and the DNA is completely wiped out for both the compounds whereas $Cu(N\text{-}MeImz)_4(ClO_4)_2$ (**8**) showed no effect at all as evident from the pattern (Fig. 15 left panel, lane 5) that was found to be same as that for control (Fig. 15 lanes 1 and 2). Thus, both **2** and **3** are found to be more potent in DNA cleavage compared to other compounds under study though all of them bind to DNA. Thus the presence of the imidazole ligand along with the NNS chelate makes the Cu(II) compounds very efficient in wiping out the DNA. Similar observations were made by Rajendiran et al. [61] who have

ACCEPTED MANUSCRIPT

shown in their studies of mixed-ligand Cu(II)-phenolate compounds that the presence of coligand enhanced DNA and protein binding, DNA cleavage as well as anticancer activity.

4.9.3. Cytotoxicity

Since the present complexes strongly bind and cleave DNA in the absence of a reductant, and since DNA cleavage is considered to be an important factor for a drug to act as an anticancer agent [71,72], we decided to investigate the cytotoxicity of some of the complexes dissolved in DMSO. The effect of the compounds **1**, **2** and **3** were tested on the C6 glioma cell line and cervical cancer HeLa cell line. MTT assay was performed to study the cytotoxicity of these compounds thereby analyzing the cell viability. Only the viable cells having active enzyme could reduce the MTT to its colored product formazan crystals. For the HeLa cell line, all the compounds (**1**, **2** and **3**) caused significant decrease in the viability at concentration of 10, 20, 50 and 100 μM at both 24 and 48 h incubation times in comparison to the control (Fig. 16). **2** and **3** caused more number of cell death in 24 h incubation time than **1**, however, these compounds proved more potent at their higher concentrations at both 24 h and 48 h incubation times. For the C6 glioma cell lines, compounds **1** and **2** showed similar patterns in lowering cell viability as it had shown in HeLa cells lines; however, the compound **3** at 10 μM for 48 h incubation time showed no significant decrease in cell viability in comparison to the control (Fig. 16).

ACCEPTED MANUSCRIPT

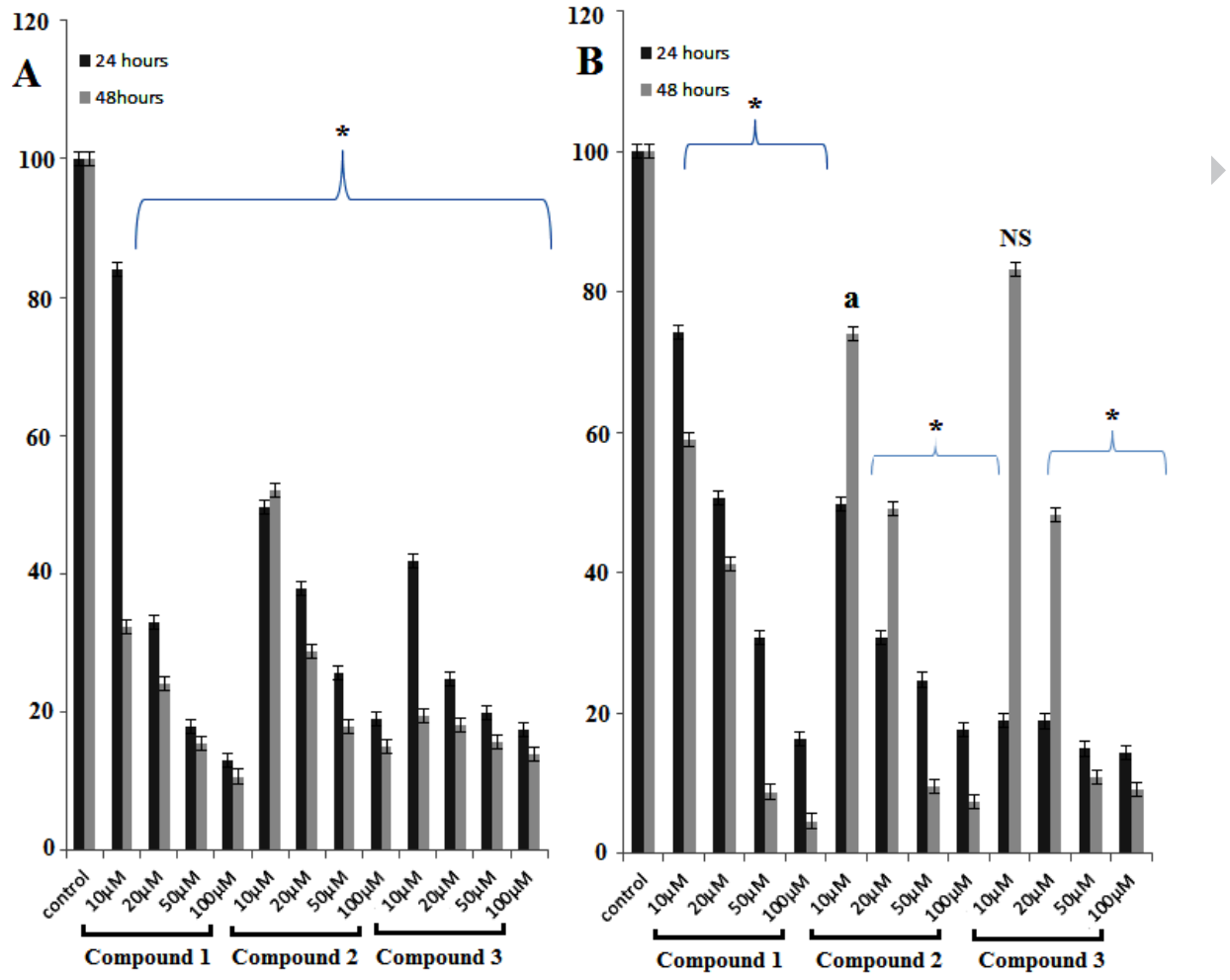

Fig. 16. Effect of metal complexes **1**, **2**, and **3** on the cell viability of cultured HeLa cells (A) and C6 glioma cells (B) using the 3-[4,5-dimethylthiazol-2-yl]2,5-diphenyl-tetraazolium bromide (MTT) assay. The two different cell lines were treated with different doses (10, 20, 50 and 100 μM) of the compounds **1**, **2**, and **3** for 24 h and 48 h incubation times. Results are expressed as percentage of viable cells as means of three experiments. *Mean values of the groups are significantly ($p < 0.0001$) decreased from the control of compounds **1**, **2**, and **3**, respectively at both time points 24h and 48h ; [a] Mean values of the groups are significantly ($p < 0.01$) decreased from the control of compound **2** at dose 10 μM and time point 48 h. [NS] Non significant.

ACCEPTED MANUSCRIPT

Analyses of these results show that for the HeLa cell line, all the three compounds (**1**, **2** and **3**) showed significant ($p < 0.0001$) decrease in cell viability for all the concentrations used (10, 20, 50, and 100 µM), at both the incubation times (24 h and 48 h), respectively. For the C6 glioma cell line, the compounds **1** and **2** showed significant ($p < 0.0001$) decrease in cell viability at all concentrations at both the time points. Also the compound **3** showed significant ($p < 0.0001$) decrease in cell viability at doses 20, 50 and 100 µM, respectively, at both the incubation times, but for the dose 10 µM there was significant decrease in cell viability only at 24 h but not at 48 h incubation time.

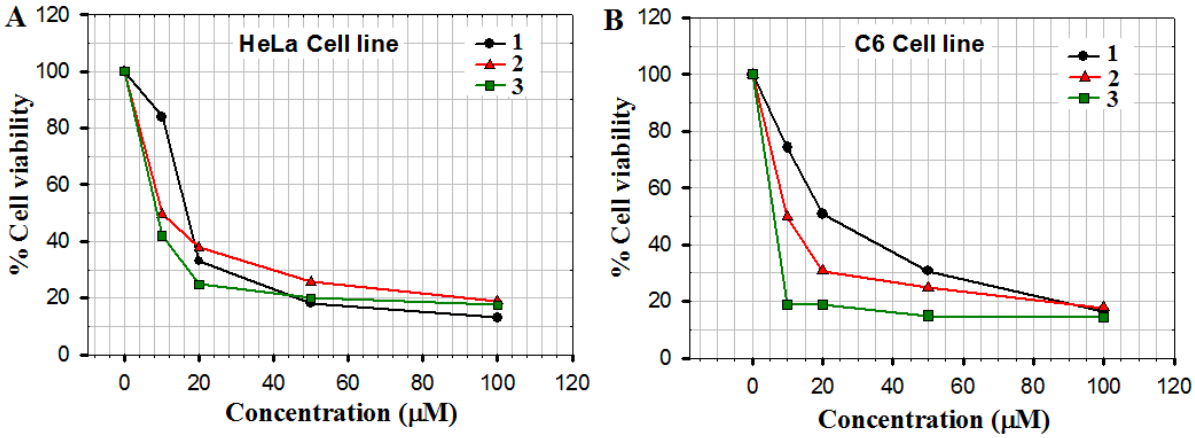

Fig. 17. Plot of cell viability versus concentrations of the compounds **1**, **2**, and **3**. Panel A. HeLa cell line. Panel B. C6 glioma cell line.

From Fig. 17, IC_{50} values for the compounds **1**, **2**, **3**, respectively are obtained for both the cell lines. It is found that IC_{50} values of **1**, **2** and **3** are 20.0, 10.0, and 6.2 µM, respectively for the C6 glioma cell line and for 24 h incubation time. On the other hand, IC_{50} values of **1**, **2** and **3** are 16.8, 10.0, and 8.7 µM, respectively for the HeLa cell line and also for 24 h incubation time. Thus the IC_{50} values for **2** and **3**, containing imidazole and N-methyl imidazole group, respectively, as the coligand, are very close and both of them exhibit much higher cytotoxicity than **1** that contains an water molecule as the coligand. Also it is noted that IC_{50} values for these compounds are much lower than those reported for some copper compounds of thiosemicarbazones on HeLa cells by Saswati et al. [73]

ACCEPTED MANUSCRIPT

who have also assessed Cisplatin, Gefitinib, Gemcitabine, 5-Florouracil, and Vinorelbine on HeLa cells under similar experimental conditions and reported their IC_{50} values of 13 μM, 20 μM, 35 μM, 40 μM and 48 μM, respectively. Thus the IC_{50} values of compounds **1**-**3** under study are remarkably similar to or better than these well-known anticancer drugs and deserve further studies in this area.

4.10. Electrochemical results

The electrochemical behaviour of compounds **1, 2** and **3** have been studied in CH_3CN containing 0.1 M $[N(n\text{-}Bu)_4]ClO_4$ while that for **5** and **6** have been studied in CH_3CN containing 0.1 M $[N(n\text{-}Bu)_4]PF_6$ at a platinum working electrode using cyclic voltammetry (CV) in dinitrogen atmosphere. For an initial negative scan compound **1** shows (Fig. 18) three successive reductions at –0.2277, –0.6718, and –0.9318 V, respectively. These last two waves at –0.6718 and –0.9318 V are found to be coupled to a broad anodic peak around –0.5418 V (Fig. 18). Then two more anodic responses are observed at +0.0535 and +1.0285 V, respectively. The reduction at –0.2277 V is found to be coupled to the weak oxidation wave at +0.0535 V (figure not shown) suggesting a quasi-reversible process ($\Delta E_p \cong 174$ mV), most likely associated with Cu(II)/Cu(I) redox couple. This large ΔE_p value (174 mV) indicates that the reduced species is not stable enough to undergo reoxidation forming back the same initial Cu(II) species under the experimental condition. It is to be mentioned here that for a reversible redox couple, ΔE_p should be ~60 mV with well-defined anodic and cathodic peaks of equal height indicating that the gross stereochemistry in both oxidation states is same and involves one-electron transfer. The remaining responses (Fig. 18) are associated with ligand centered oxidation and reduction.

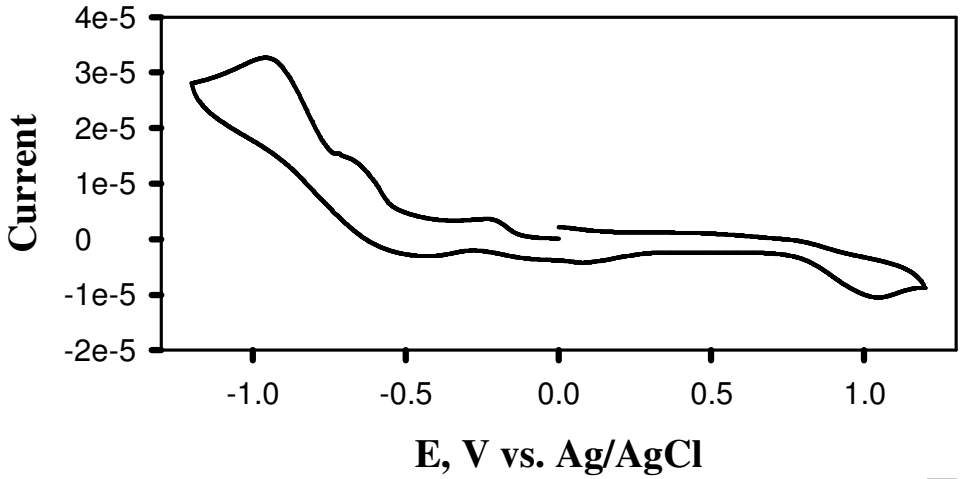

Fig. 18. Cyclic voltammogram of **1** (1.5×10^{-3} mol L^{-1}) in CH_3CN containing 0.1 M $[N(n\text{-}Bu)_4]ClO_4$ at a scan rate of 100 mV s^{-1}.

Compound **2**, on the other hand, displays a reduction wave at –0.1705 V which is found to be coupled to the oxidation wave at –0.1060 V, indicating a nearly reversible process ($E_{½}$ = –0.138 V, ΔE_p = 64.5 mV) (Fig. 19, panel A) associated with Cu(II)/Cu(I) redox couple. Apart from this, compound **2** also shows an oxidation wave around +0.6782 V which is coupled to a reductive response at +0.5382 V (Fig. 19, panel B) indicating a quasi-reversible redox process (ΔE_p = 140 mV), associated with ligand centered oxidation and reduction.

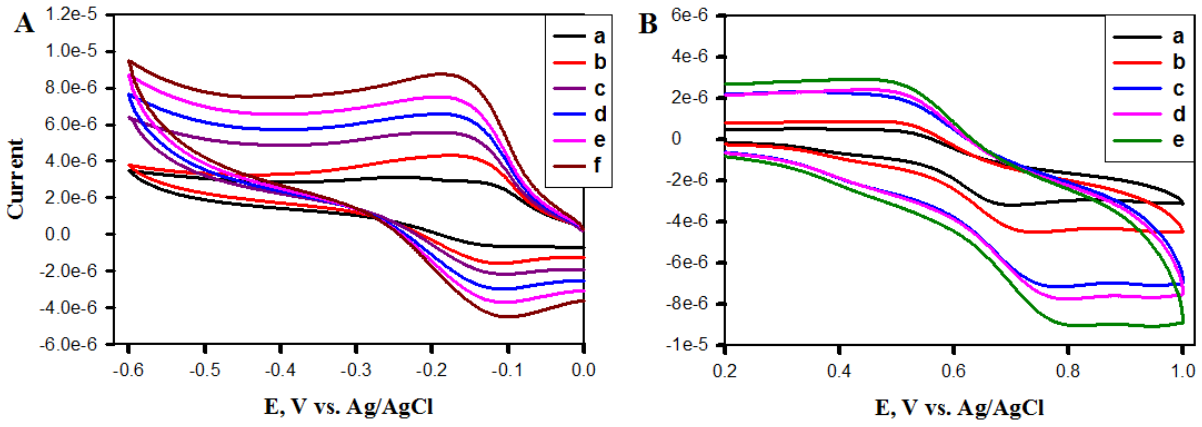

Fig. 19. Cyclic voltammogram of **2** (1.15×10^{-3} mol L^{-1}) in CH_3CN containing 0.1 M $[N(n\text{-}Bu)_4]ClO_4$: Panel A. reduction at different scan rates: (a) 50, (b) 100, (c) 200, (d) 300, (e) 400, and

(f) 500 mV s^{-1}, respectively. Panel B. oxidation at different scan rates: (a) 50, (b) 100, (c) 250, (d) 300, and (e) 400 mV s^{-1}, respectively.

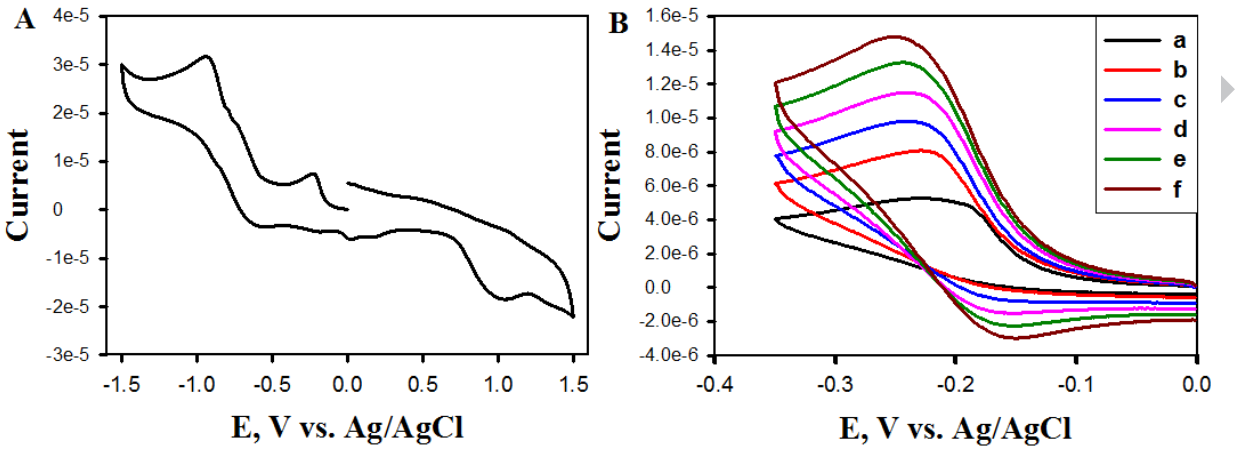

Fig. 20. Panel A. Cyclic voltammogram of **3** (1.25×10^{-3} mol L^{-1}) in CH_3CN containing 0.1 M $[N(n\text{-}Bu)_4]ClO_4$ at a scan rate of 100 mV s^{-1}. Panel B. Reduction of **3** (1.25×10^{-3} mol L^{-1}) in CH_3CN containing 0.1 M $[N(n\text{-}Bu)_4]ClO_4$ at different scan rates: (a) 50, (b) 100, (c) 200, (d) 300, (e) 400, and (f) 500 mV s^{-1}.

Compound **3** undergoes two successive reductions at –0.226 and –0.940 V, reversal of scan yields two broad oxidative responses around –0.613 and +1.047 V. The reductive response at –0.226 V is found to be coupled to a oxidative response at –0.138 V indicating a nearly-reversible process ($E_{½}$ = –0.182 V, ΔE_p = 88.0 mV) (Fig. 20) most likely associated with Cu(II)/Cu(I) redox couple. So the remaining responses are associated with ligand centered oxidation and reduction.

The redox behavior of compounds **6** and **7** are shown in Fig. 21. Compound **6** undergoes two successive reductions at –0.225 and –1.002 V, respectively. Reversal of this scan resulted in oxidation waves at –0.6876, –0.1128, +0.1248 and +0.6876 V. This oxidation wave at +0.6876 V is found to be coupled to the reduction wave at +0.525 V, suggesting a quasi-reversible process (Fig. 21 panel A). The reduction at –0.225 V is found to be coupled with an oxidation wave at –0.145 V, suggesting a nearly reversible process (ΔE_p = 80 mV) (Fig. 22 panel A).

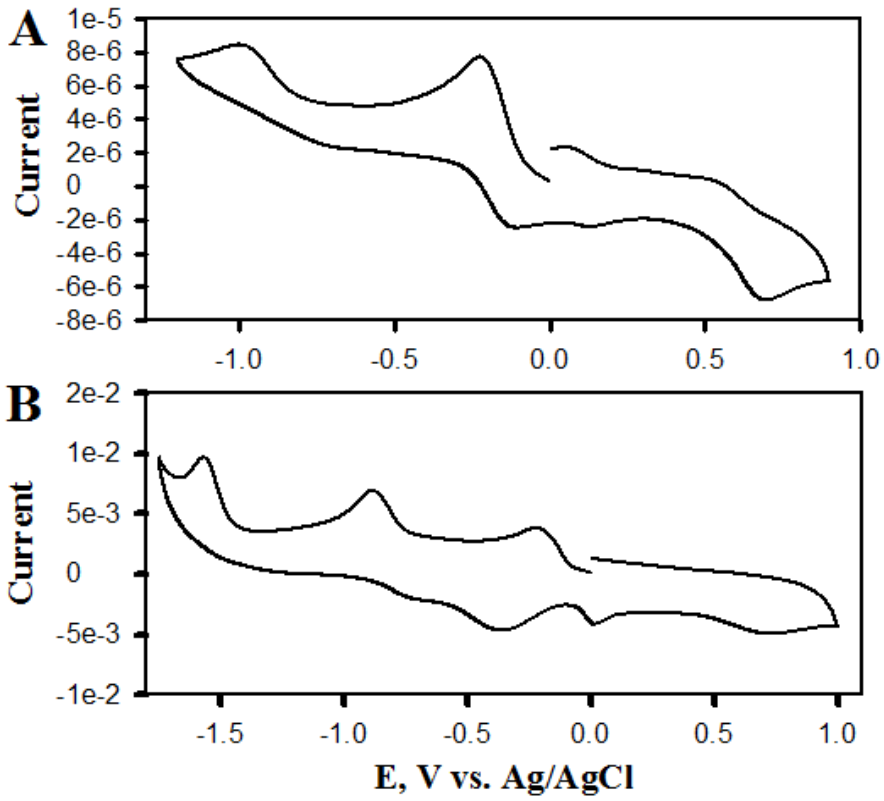

Fig. 21. Cyclic voltammograms of **6** (2.05×10^{-3} mol L^{-1}) (panel A) and **7** (1.25×10^{-3} mol L^{-1}) (panel B) in CH_3CN containing 0.1 M $[N(n\text{-}Bu)_4]PF_6$ at a scan rate of 100 mV s^{-1}.

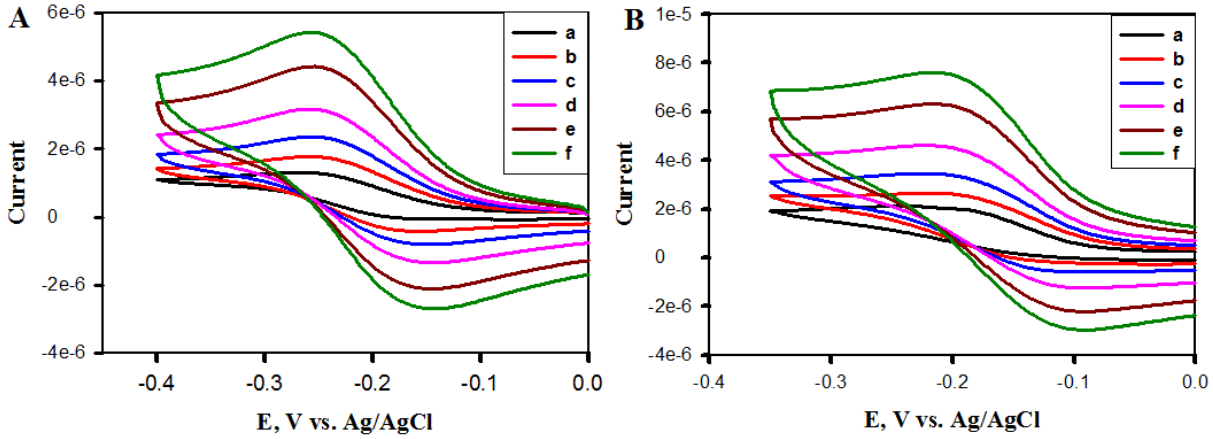

Fig. 22. Cyclic voltammograms of **6** (2.05×10^{-3} mol L^{-1}) (panel A) and **7** (1.25×10^{-3} mol L^{-1}) (panel B) in CH_3CN containing 0.1 M $[N(n\text{-}Bu)_4]PF_6$. Panel A. Reduction of **6** at different scan rates: (a) 20, (b) 50, (c) 100, (d) 200, (e) 400, and (f) 600 mV s^{-1}, respectively. Panel B. Reduction of **7** at different scan rates: (a) 20, (b) 50, (c) 100, (d) 200, (e) 400, and (f) 600 mV s^{-1}, respectively.

ACCEPTED MANUSCRIPT

Compound **7** undergoes three successive reductions at −0.205, −0.8818 and −1.5709 V, respectively. Reversal of the scan yields oxidation responses at −0.7368, −0.362, +0.0125 and +0.7375 V, respectively (Fig. 21 panel B). However, this compound undergoes reduction at −0.1967 V which is coupled to an anodic wave at −0.1084 V, indicating a nearly-reversible process (ΔE_p = 88 mV) (Fig. 22 panel B). Thus it appears that in the complexes **2**, **3**, **6**, and **7** which involve either a reversible or nearly reversible Cu(II)/Cu(I) redox couple retain almost same geometry in both these oxidation states because the redox potentials of Cu(II)/Cu(I) systems depend on the relative thermodynamic stabilities of the two oxidation states in a given ligand environment [74]. Yoko and Addison have discussed in their work the spectroscopic and redox properties of some pseudo-tetrahedral Cu(II) complexes with some Schiff base ligands which could vary in their stereochemistry and capable of undergoing tetrahedral distortion and have demonstrated their relationship with copper proteins [74]. It may be mentioned here that blue copper proteins which are considered to be prototype electron transfer (ET) proteins, use the Cu(II)/Cu(I) redox couple to perform this critical biological function [75]. If the structures of the complexes are already distorted toward tetrahedral instead of square planar Cu(II) geometry, or can adopt a tetrahedral structure easily then upon metal center reduction, the generated Cu(I) species which will prefer to have a tetrahedral ligand environment will need minimum structural change, and then the Cu(II)/Cu(I) couple is expected to be nearly reversible or quasi-reversible depending on the degree of distortion. This is most likely the cause for the observation of nearly-reversible or quasi-reversible Cu(II)/Cu(I) couple in the cases of four-coordinate complexes **1**-**3**. This is supported by the optimized ground state structure obtained for the reduced form (Cu^+) of **2**, shown in Fig. 23 which is found to be tetrahedral.

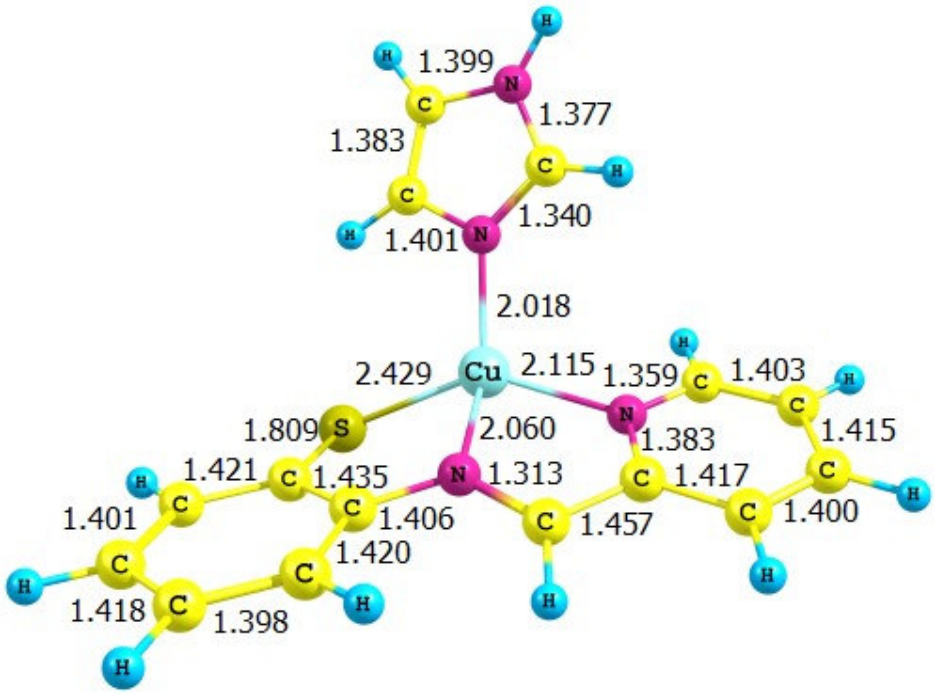

Fig. 23. Optimised structure for the one-electron reduced Cu^{+} species of **2**.

*4.11. Crystal structure of Cu(N-MeImz)$_4$(ClO$_4$)$_2$ (**8**)*

The structure of the compound has been determined by X-ray crystallography. Fig. 24 shows the ORTEP representation of the molecule with 40% probability ellipsoids [76]. The geometry around the Cu(II) metal ion is square planar. The two Cu–N(2) bond lengths are found to be the same (N(2)-Cu(1), 1.981(2)) while the two Cu–N(3) bond lengths are also found to be same (N(3)-Cu(1), 2.026(2)). The bond angles confirm that the four N-methyl imidazole ligands in the equatorial plane form a square planar geometry. However, the two ClO_4^- ions occupy the apical positions making it an elongated octahedral as shown in figure 24. The copper atom stays at an inversion center (0.5, 0, 0) and has a distant coordination with O(1) of perchlorate anion with a distance of Cu(1) –O(1) = 2.734(5) Å. Cu(1) connects to inversion equivalent of O(1) also through same distance.

The packing of the molecules is shown in Fig. S10 of the Supplementary material. This compound gives well resolved X-band powder EPR spectrum at RT (shown in Fig. S11 of the Supplementary

material). Though the ClO_4^- ions are coordinated in the axial positions in the solid, these easily ionise in the aqueous solution as evident from its conductance value (Λ = 205.5 Ohm^{-1} cm^2 mol^{-1}) [50].

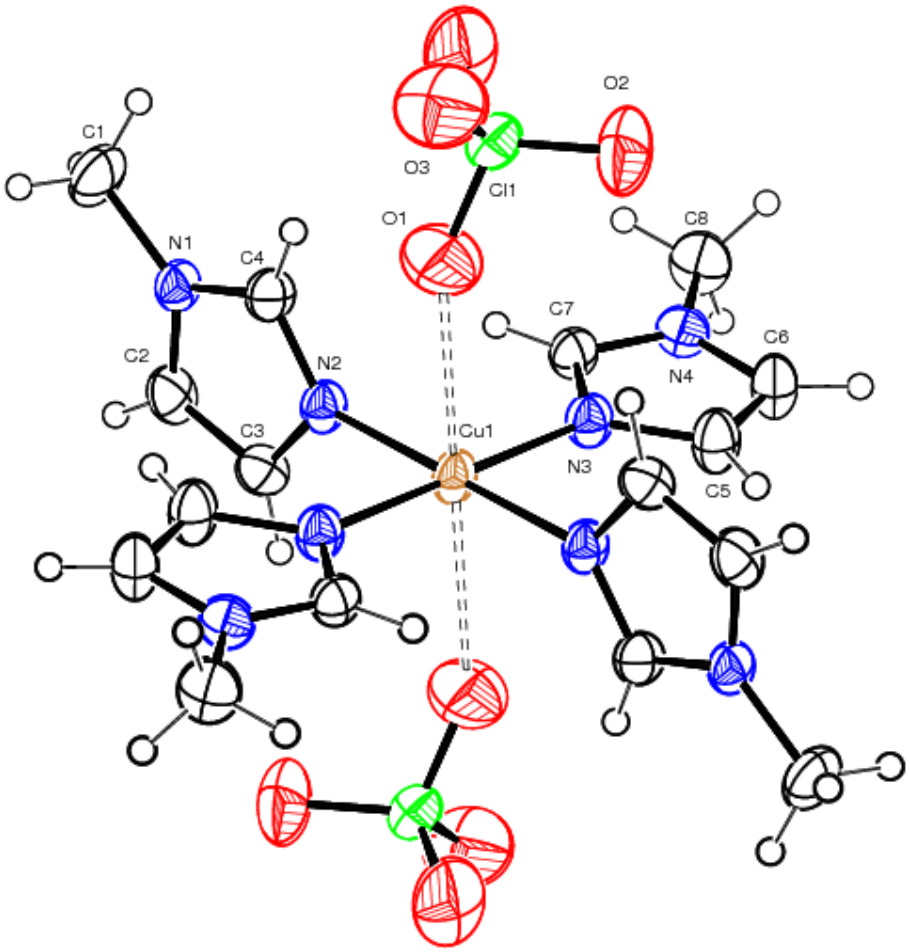

Fig. 24. ORTEP diagram of compound $Cu(NMe\text{-}Imz)_4(ClO_4)_2$. Selected bond lengths (Å) and angles (°): N(2)-Cu(1), 1.981(2) Å; N(3)-Cu(1), 2.026(2) Å; Cu(1)-N(2′), 1.981(2) Å; Cu(1)-N(3′), 2.026(2) Å; Cu(1) –O(1), 2.734(5) Å; N(2′)-Cu(1)-N(2), 180.0°; N(3)-Cu(1)-N(3′), 180.0°; N(2′)-Cu(1)-N(3), 90.00(9)°; N(2)-Cu(1)-N(3), 90.00(9)°; N(2′)-Cu(1)-N(3′), 90.00(9)°; N(2)-Cu(1)-N(3′), 90.00(9)°.

It may be noted here that the structure of the $[Cu(N\text{-}MeImz)_6]^{2+}$ cation was found to be tetragonally elongated octahedron [77] and the four Cu–N distances in the equatorial plane are reported to be Cu–N(1) = 2.009 Å and Cu–N(2) = 2.004 Å. The Cu–N distance for a mixed ligand Cu(II) complex with pseudo octahedral geometry is reported to be 1.938(4) Å with the N-methyl imidazole ligand in the

ACCEPTED MANUSCRIPT

equatorial plane [78]. For a five coordinate Cu(II) complex containing two N-methyl imidazole ligands, $Cu[L_2(N\text{-}MeImz)_2]\cdot H_2O$, where HL = 4amino-N-(thiazol-2-yl)benzenesulfonamide, the Cu–N (N-methyl imidazole) bond distances are found to be 2.000(9) and 1.983(9) Å, respectively [79]. Very recently, the crystal structure of $[Cu(N\text{-}MeImz)_4]Br_2$ is reported by Wang et al. [80] where the Cu^{2+} is coordinated by N atoms of the four N-methylimidazole ligands with slightly distorted square planar environment for the isolated $[Cu(N\text{-}MeImz)_4]^{2+}$ cation with Cu-N bond lengths of 2.007 and 2.026 Å, respectively and it contains two bromide anions.

5. Conclusions

The synthesized Cu(II) compounds containing N_2SCu core and N_4SCu core exhibit strong electronic spectra in the visible region due to S → Cu(II) charge transfer transition as well as display four-line EPR multiplet suggesting mononuclear in solution. DFT results for **1**-**3** are found to be in line with the observed electronic spectral results in the visible region. Cyclic voltammetric studies of the compounds clearly show a nearly-reversible or quasi-reversible Cu(II)/Cu(I) couple with redox potentials that fall within the range −0.08 to −0.20 V versus Ag/AgCl apart from the other ligand centered oxidations and reductions. Two of these compounds (**1** and **2**) tested for catechol oxidase activity with 3,5-DTBC as the model substrate (in methanol at RT in presence of air) were found to have good catalytic activity to produce the product 3,5-DTBQ. Also it is found that these compounds interact with DNA through intercalation, and the binding constant K_b is found to be $1.47 \times 10^5\ M^{-1}$ for **1**, $2.03 \times 10^5\ M^{-1}$ for **2**, and $2.09 \times 10^5\ M^{-1}$ for **3**, respectively. The higher K_b values observed for **2** and **3** as compared to **1** suggest that **2** and **3** interact with DNA more strongly than complex **1**. This is consistent with the nucleic acid degradation activity for these compounds which shows that DNA is completely wiped out in the cases of **2** and **3** containing imidazole group as the coligand.

The compounds **1**-**3** exhibit remarkable cytotoxicity against C6 glioma cell line and human cervical cancer HeLa cell line. The IC_{50} values of **2** and **3** for the cervical cancer HeLa cell line and for 24 h

ACCEPTED MANUSCRIPT

incubation time reveal that they exhibit higher cytotoxicity than many reported Cu(II) compounds and appear to be more potent than some anticancer drugs tested for the HeLa cell line.

Acknowledgements

M.K. thanks the Department of Inorganic Chemistry, Indian Association for the Cultivation of Science, Kolkata for help with the elemental analysis. We thank the SAIF, IIT-Madras for EPR, NMR, XRD, IR and far-IR facilities; and SAIF, IIT-Bombay for recording EPR of compound **3** using JEOL, Japan Model: JES - FA200 ESR spectrometer and ESI MS for the compounds with Varian Inc, USA Liquid Chromatograph Mass Spectrometer Model 410 Prostar Binary LC with 500 MS IT PDA Detectors. M.K. and A.P.K. thank Dr. Amrita Chatterjee, Department of Chemistry, BITS-Pilani K. K. Birla Goa Campus for valuable discussion for mass spectral results. A.P.K. thanks Dr. C. Baby, SAIF, IIT-Madras for help with the NMR studies and Mr. Rangaraj Prasath, Mr. Srimanta Haldar and Dr. P. Bhavana, Department of Chemistry, BITS-Pilani K. K. Birla Goa Campus for help with the electrochemical studies. P.T.M. thanks the DST, Govt. of India for a research Scheme (SR/S1/IC-53 /2012) and also the INSA for its Senior Scientistship. We thank the reviewers for their constructive suggestions to improve this manuscript.

Appendix A. Supplementary material

Fig. S1. Electrospray ionization mass spectra (ESI-MS) of the complexes **1**- **4** and **6** in acetonitrile. Fig. S2. Absorbance of the solid powder samples of compounds **1** (bottom black curve) and **2** (top red curve) as obtained from the diffuse reflectance spectral measurements. Fig. S3. Electronic spectra of the compounds in the visible and near-IR region along with their deconvolution. Fig. S4. Ground state optimized structures of the complexes **1**-**3** used for calculating bond angles and dihedral angles presented in Table 1. Fig. S5. DNA binding study for **1** and **2** using electronic spectra. Fig. S6. Dependence of the initial rate of oxidation reaction of 3,5-DTBC on the concentration of the substrate 3,5-DTBC catalyzed by complexes and the Lineweaver–Burk plots. Fig. S7. IR spectra of **1**

ACCEPTED MANUSCRIPT

and **4** in KBr. Fig. S8. Far infrared spectra for **1**, **2** and **4** in panels A-C, respectively. Fig. S9. EPR spectra of compound **4** at X-band without DPPH: (A) RT solution in CH_2Cl_2; (B) Frozen glass at LNT in CH_2Cl_2:THF (1 : 1). Fig. S10. Packing of the molecules of $Cu(N\text{-}MeImz)_4(ClO_4)_2$ in the unit cell. Fig. S11. X-band powder EPR spectrum of $Cu(N\text{-}MeImz)_4(ClO_4)_2$ at RT. Table S1. XYZ coordinates of the ground state optimized geometries of complexes **1**, **2**, and **3** (with & without solvent). Table S2. Far-infrared spectral band assignments for compounds **1**, **2** and **4**. Crystallographic data for the structural analysis for $Cu(N\text{-}MeImz)_4(ClO_4)_2$ have been deposited with the Cambridge Crystallographic Data Center, CCDC number 1437349 . These data can be obtained free of charge via http://www.ccdc.cam.ac.uk/conts/retrieving.html, or from the Cambridge Crystallographic Data Centre, 12 Union Road, Cambridge CB2 1EZ, UK; Fax: (+044) 1223-336-033; or E-mail: deposit@ccdc.cam.ac.uk.

References

[1] L. Que, W. B. Tolman, Nature 455 (2008) 333.

[2] M. Fontecave, J. L. Pierre, Coord. Chem. Rev. 170 (1998) 125.

[3] E.I. Solomon, U.M. Sundaram, T.E. Machonkin, Chem. Rev. 96 (1996) 2563.

[4] J. A. Fee, Struc. Bond. 23 (1975) 1.

[5] H.A.O. Hill, J.C. Leer, B.E. Smith, C.B. Storm, Biochem. Biophys. Res. Commun. 70 (1976) 331.

[6] J.L. Markley, E.L. Ulrich, S.P. Berg, D.W. Krogmann, *Biochemistry,* 14 (1975) 4428.

[7] J.A. Wurzbach, P.J. Grunthaner, D.M. Dooley, H.B. Gray, F.J. Grunthaner, R.R. Gay, E.I. Solomon, J. Am. Chem. Soc. 99 (1977) 1257.

[8] D.R. McMillin, R.C. Rosenberg, H.B. Gray, Proc. Natl. Acad. Sci. USA 71 (1974) 4760.

[9] E.I. Solomon, J. Rawlings, D.R. McMillin, P.J. Stephens, H.B. Gray, J. Am. Chem. Soc. 98 (1976) 8046.

ACCEPTED MANUSCRIPT

[10] E. I. Solomon, J. W. Hare, D. M. Dooley, J. H. Dawson, P. J. Stephens, H. B. Gray J. Am. Chem. Soc. 102 (1980) 168.

[11] A.B.P. Lever. Inorganic Electronic Spectroscopy, 2nd Edn, Elsevier, New York (1984).

[12] N. Aoi, G-e. Matsubayashi, T. Tanaka, J. Chem. Soc. Dalton Trans. 1059 (1983).

[13] J.L. Hughey, T.G. Fawcett, S.M. Rudich, R.A. Lalancette, J.A. Potenza, H.J. Schugar, J. Am. Chem. Soc. 101 (1979) 2617.

[14] M. Downes, J. Whelan, B. Bosnich, Inorg. Chem. 20 (1981) 1081.

[15] T. Yamabe, K. Hori, T. Minato, K. Fukui, Y. Sugiura, Inorg. Chem. 21 (1982) 2040.

[16] S. Mandal, G. Das, R. Singh, R. Shukla, P.K. Bharadwaj, Coord. Chem. Rev. 160 (1997) 191; and references therein.

[17] J.S. Thompson, T.J. Marks, J.A. Ibers, Proc. Natl. Acad. Sci. USA 74 (1977) 3114.

[18] J.S. Thompson, T.J. Marks, J.A. Ibers, J. Am. Chem. Soc. 101 (1979) 4180.

[19] P.L. Holland, W.B. Tolman *J. Am. Chem. Soc*., 122 (2000) 6331.

[20] K. D. Karlin, Science 261 (1993) 701.

[21] G. Barone, A. Terenzi, A. Lauria, A. M. Almerico,J.M. Leal, N. Busto, B. García, Coord. Chem. Rev. 257 (2013) 2848, and references therein.

[22] A. Draksharapu, A.J. Boersma, M. Leising, A. Meetsma, W.R. Browne, Gerard Roelfes, Dalton Trans. 44 (2015) 3647.

[23] J.G. Da Silva, A.A. Recio Despaigne, S.R.W. Louro, C.C. Bandeira, E.M. Souza-Fagundes, H. Beraldo, European J. of Med. Chem. 65 (2013) 415.

[24] A.D. Tiwari, A.K. Mishra, S.B. Mishra, B.B. Mamba, B. Maji, S. Bhattacharya, Spectrochim. Acta Part A 79 (2011) 1050.

[25] C. Marzano, M. Pellei, F. Tisato, C. Santini, Anti-Cancer Agents in Med. Chem. 9 (2009) 185, and references therein.

ACCEPTED MANUSCRIPT

[26] Cheng-Yong Zhou, J. Zhao, Yan-Bo Wu, Cai-Xia Yin, P. Yang, J. Inorg. Biochem. 101 (2007) 10.

[27] J. Liu, T. Zhang, T. Lu, L. Qu, H. Zhou, Q. Zhang, L. Ji, J. Inorg. Biochem. 91 (2002) 269.

[28] F. Tisato, C. Marzano, M. Porchia, M. Pellei and C. Santini, Med. Res. Rev. 30 (2010) 708.

[29] V.M. Manikandamathavan, B.Unni Nair, European J. Medicinal Chemistry 68 (2013) 244.

[30] S.K. Mal, M. Mitra, G. Kaur, V.M. Manikandamathavan, M.S. Kiran, A. Roy Choudhury, B. Unni Nair, R. Ghosh, RSC Adv. 4 (2014) 61337.

[31] M.S. Surendra Babu, K. H. Reddy, P. G. Krishna, Polyhedron 26 (2007) 572.

[32] A. P. Koley, R. Nirmala, L. S. Prasad, S. Ghosh, and P. T. Manoharan, Inorg. Chem. 31 (1992) 1764.

[33] J.L. Corbin, D.E. Work, Can. J. Chem. 52 (1974) 1054.

[34] L.F. Lindoy, S.E. Livingstone, Inorg. Chim. Acta 2 (1968) 166.

[35] S.E. Livingstone, J.D. Nolan, Aust. J. Chem. 26 (1973) 961.

[36] L.G. Warner, T. Ottersen, K. Seff, Inorg. Chem. **13** (1974) 2529.

[37] H. Dhillon, U. Singh, Pooja, S. Kumbhat, Indian J. Chem. 47A (2008) 1508.

[38] J. Reedljk, Inorg. Chim. Acta 3 (1969) 517.

[39] J.G. Mabley, W.L. Suarez-Pinzon, G. Hasko, A.L. Salzman, A. Rabinovitch, E. Kun, C. Br. Szabo, J. Pharmacol. 133 (2001) 909.

[40] R.R. Parr, R.G. Yang, Density functional theory of atoms and molecules, Oxford University Press: New York, 1989.

[41] R. Bauerschmitt, R. Alrichs, Chem. Phys. Lett. 256 (1996) 454.

[42] M.J. Frisch, G.W. Trucks, H.B. Schlegel, G.E. Scuseria, M.A. Robb, J.R. Cheeseman, G. Scalmani, V. Barone, B. Mennucci, G.A. Petersson, H. Nakatsuji, M. Caricato, X. Li, H.P. Hratchian, A.F. Izmaylov, J. Bloino, G. Zheng, J.L. Sonnenberg, M. Hada, M. Ehara, K. Toyota,

ACCEPTED MANUSCRIPT

R. Fukuda, J. Hasegawa, M. Ishida, T. Nakajima, Y. Honda, O. Kitao, H. Nakai, T. Vreven, J.J.A. Montgomery, J.E. Peralta, F. Ogliaro, M. Bearpark, J.J. Heyd, E. Brothers, K.N. Kudin, V.N. Staroverov, R. Kobayashi, J. Normand, K. Raghavachari, A. Rendell, J.C. Burant, S.S. Iyengar, J. Tomasi, M. Cossi, N. Rega, N.J. Millam, M. Klene, J.E. Knox, J.B. Cross, V. Bakken, C. Adamo, J. Jaramillo, R. Gomperts, R.E. Stratmann, O. Yazyev, A.J. Austin, R. Cammi, C. Pomelli, J.W. Ochterski, R.L. Martin, K. Morokuma, V.G. Zakrzewski, G.A. Voth, P. Salvador, J.J. Dannenberg, S. Dapprich, A.D. Daniels, O¨ Farkas, J.B. Foresman, J.V. Ortiz, J. Cioslowski, D.J. Fox (2009) Gaussian 09. Gaussian, Inc., Wallingford CT.

[43] A.D. Becke, J. Phys. Chem. 98 (1993) 5648.

[44] C. Lee, W. Yang, R.G. Parr, Phys. Rev. B 37 (1988) 785.

[45] J. Tomasi, B. Mennucci, R. Cammi, Chem. Rev. 105 (2005) 2999.

[46] G. Scalmani, M. J. Frisch, B. Mennucci, J. Tomasi, R. Cammi, V. Barone, J. Chem. Phys. 124 (2006) 1.

[47] Bruker-Nonius (2004). APEX-II and SAINT-Plus (Version 7.06a), Bruker AXS Inc., Madison, Wisconsin, USA.

[48] A. Altormare, G. Gascarano, C. Giacovazzo, A. Guagliardi. J. Appl. Cryst.. 26 (1993) 343.

[49] G.M. Sheldrick. (1997). SHELXL97. University of Göttingen, Germany.

[50] W.J. Geary, Coord. Chem. Rev. 7 (1971) 81.

[51] G.N. Law Mar, W. Horrocks, R.H. Holm (Eds.), NMR of Paramagnetic Molecules, Academic Press, New York, 1973; (b) I. Bertini, C. Luchinat, NMR of paramagnetic molecules in biological system, Benjamin & Cummings, Mento Park, CA, 1986.

[52] P.K. Mandal, P.T. Manoharan, Inorg. Chem. 34 (1995) 270; (b) R.C. Holz, J.M. Brink, *Inorg. Chem.*, **33** 4609 (1994).

ACCEPTED MANUSCRIPT

[53] P.S. Subramanian, E. Suresh, R.S. Shukla, Inorg. Chim. Acta 358 (2005) 2651.

[54] Feng-Jung Wu, D. M. Kurtz, Jr., J. Am. Chem. Soc. 111 (1989) 6563.

[55] M. Maekawa, S. Kitagawa, M. Munakata, H. Masuda, Inorg. Chem. 28 (1989) 1904.

[56] S. Di Bella, I. Fragala, I. Ledoux, M.A. Diaz-Garcia, T.J. Marks. J. Am. Chem. Soc. 119 (1997) 9550.

[57] M. K. Koley, S. C. Sivasubramanian, B. Varghese, P. T. Manoharan, A. P. Koley, J. Coord. Chem. 65 (2012) 3623.

[58] K.W. Penfield, A.A. Gewirth, E.I. Solomon, J. Am. Chem. Soc. 107 (1985) 4519.

[59] F. Gao, H. Chao, F. Zhou, Y.-X. Yuan, B. Peng, L.-N. Ji, J. Inorg. Biochem. 100 (2006) 1487.

[60] W. D. Wilson, L. Ratmeyer, M. Zhao, L. Strekowski, D. Boykin, Biochemistry 32 (1993) 4098.

[61] V. Rajendiran, R. Karthik, M. Palaniandavar, H. Stoeckli-Evans, V.S. Periasamy, M. A. Akbarsha, B.S. Srinag, H. Krishnamurthy, Inorg. Chem. 46 (2007) 8208.

[62] A. M. Thomas, M. Nethaji, S. Mahadevan, A. R. Chakravarty, J. Inorg. Biochem. 94 (2003) 171.

[63] B. K. Santra, P. A. N. Reddy, G. Neelakanta, S. Mahadevan, M. Nethaji, A. R. Chakravarty, J. Inorg. Biochem. 89 (2002) 191.

[64] A. Guha, T. Chattopadhyay, N.D. Paul, M. Mukherjee, S. Goswami, T.K. Mondal, E. Zangrando, D. Das, Inorg. Chem. 51 (2012) 8750, and references therein.

[65] M.J. Gajewska, Wei-Min Ching, Yuh-Sheng Wen, Chen-Hsiung Hung, Dalton Trans. 43 (2014) 14726.

[66] P. Chakraborty, J. Adhikary, B. Ghosh, R. Sanyal, S.K. Chattopadhyay, A. Bauzá, A. Frontera, E. Zangrando, D. Das, Inorg. Chem. 53 (2014) 8257.

[67] P. Gentschev, N. Moller, B. Krebs, Inorg. Chim. Acta 300–302 (2000) 442.

ACCEPTED MANUSCRIPT

ACCEPTED MANUSCRIPT

[68] D. Dey, G. Kaur, A. Ranjani, L. Gayathri, P. Chakraborty, J. Adhikary, J. Pasan, D. Dhanasekaran, A.R. Choudhury, M. A. Akbarsha, N. Kole, B. Biswas, Eur. J. Inorg. Chem. (2014) 3350.

[69] P. Adak, B. Ghosh, A. Bauza, A. Frontera, A. J. Blake, C. M. Corbella, C. Das-Mukhopadhyay, S. K. Chattopadhyay, RSC Adv., 2016, Accepted Manuscript, DOI: 10.1039/C6RA14059A.

[70] K. Nakamoto. Infrared and Raman Spectra of Inorganic and Coordination Compounds, Part B, Applications in Coordination, Organometallic, and Bioinorganic Chemistry, 5th ed., pp. 6, 24, 26, 83, 206,352-355.; Wiley, New York (1997).

[71] L. A. Basile, A. L. Raphael, J. K. Barton, *J. Am. Chem. Soc.*, 109 (1987) 7550;

[72] S. Ramakrishnan, E. Suresh, A. Riyasdeen, V. S. Periasamy, M. A. Akbarsha, M. Palaniandavar, Dalton Trans. 40 (2011) 3245.

[73] Saswati, A. Chakraborty, S.P. Dash, A.K. Panda, R. Acharyya, A. Biswas, S. Mukhopadhyay, S. K. Bhutia, A. Crochet, Y.P. Patil, M. Nethaji, R. Dinda, Dalton Trans. 44 (2015) 6140.

[74] H. Yoko, A.W. Addison, Inorg. Chem. 16 (1977) 1341.

[75] E.I. Solomon, L.B. LaCroix, D.W. Randall, Pure & Appl. Chem. 70 (1998) 799.

[76] L.J. Frrugia. J. Appl. Cryst., 30 (1997) 565.

[77] A. L. Abuhijleh, C. Woods, Inorg. Chem. Comm. 5 (2002) 269.

[78] A.C. Camposa, A.G.S. Zafra, J.M.G. Perez, J.N. Gutierrez, E. Chinea, A. Mederos, Inorg. Chim. Acta 241 (1996) 39.

[79] J. Casanova, G. Alzuet, J. Borras, O. Carugo, J. Chern. Soc. Dalton Trans. (1996) 2239.

[80] H. Wang, B. Lu, J. Zhao, Q. Cai, J. Chem. Sci. 127 (2015) 1261.

ACCEPTED MANUSCRIPT

Appendix A. Supplementary material

Fig. S1. ESI–MS for **1-4** and **6**.

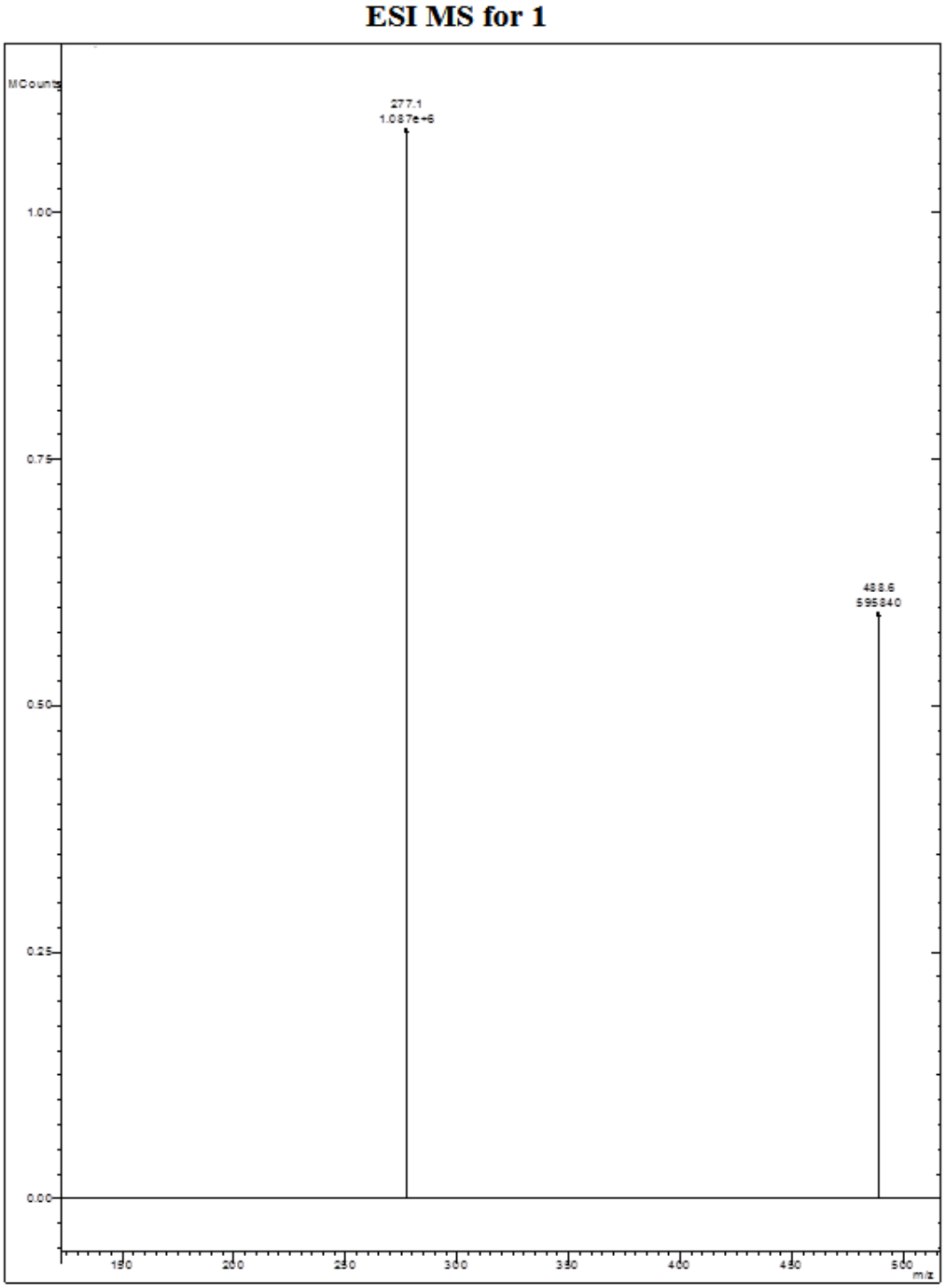

ESI MS for 1

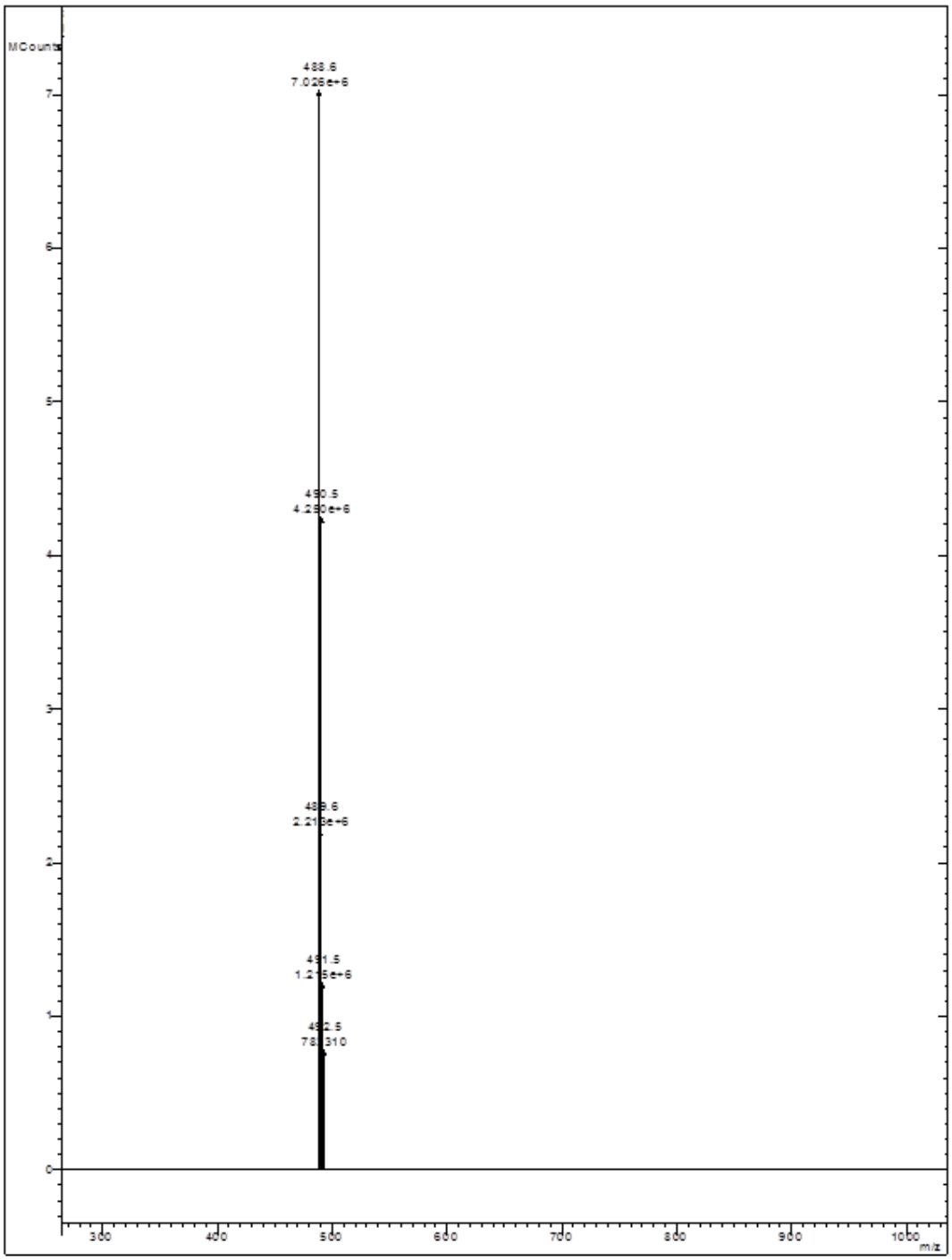
MCounts
488.6
7.026e+6
490.5
4.290e+6
489.6
2.218e+6
491.5
1.215e+6
492.5
781310
7
6
5
4
3
2
1
0
300
400
500
600
700
800
900
1000
m/z

ESI MS for 2

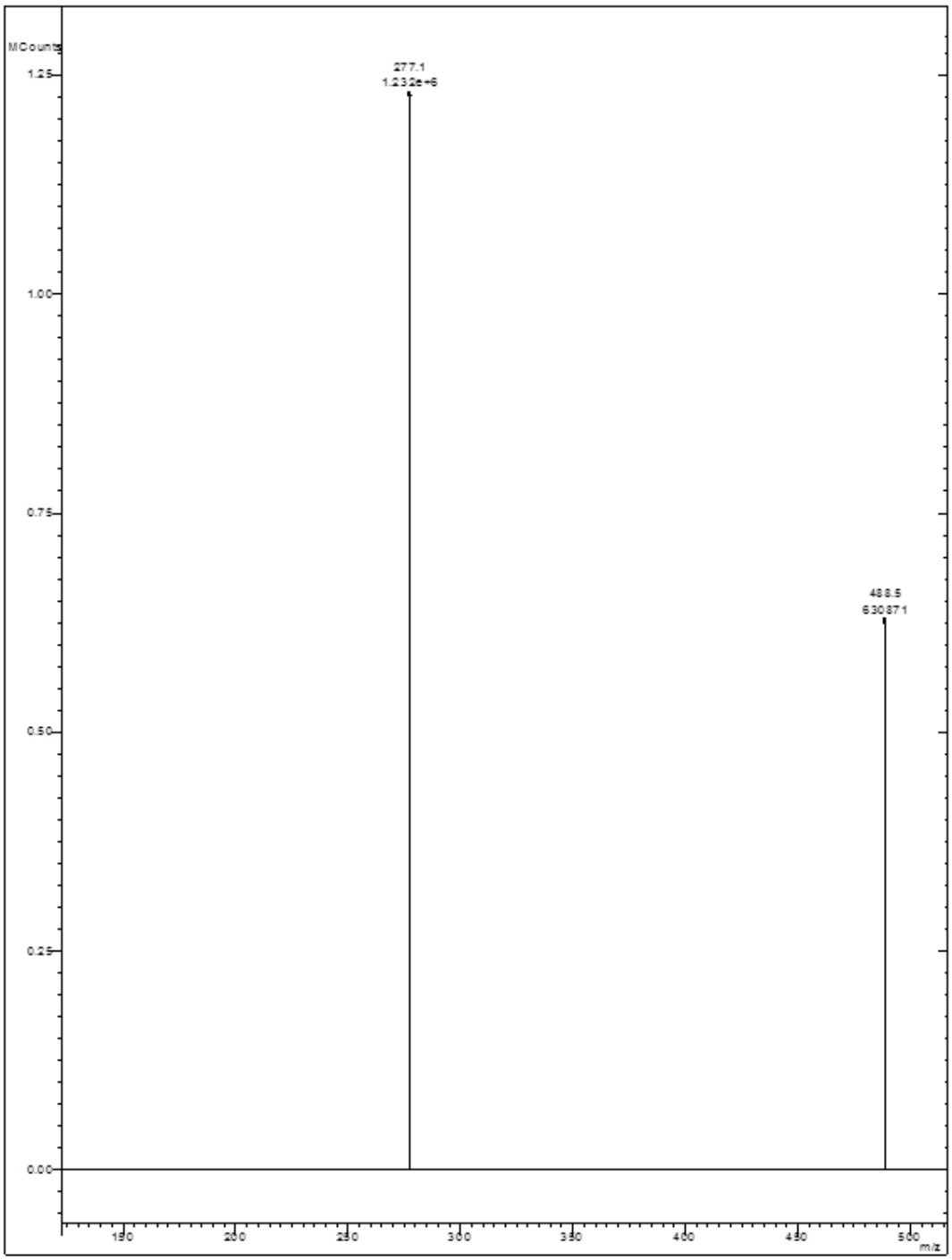
MCounts
1.25
1.00
0.75
0.50
0.25
0.00
277.1
1.232e+6
488.5
630871
150
200
250
300
350
400
450
500
m/z

ESI MS for 2

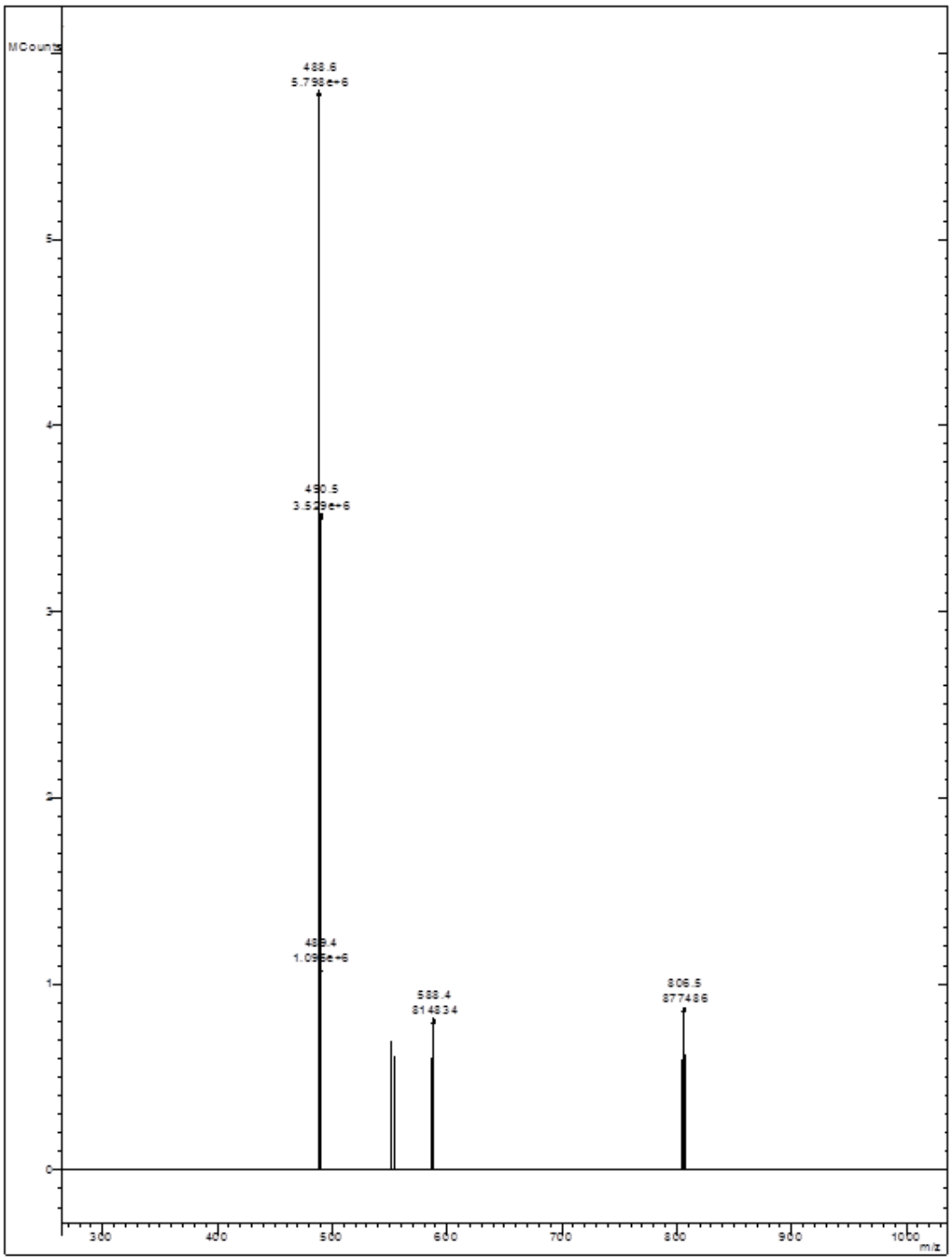
MCounts
488.6
5.798e+6
490.5
3.529e+6
489.4
1.096e+6
588.4
814834
806.5
877486
300
400
500
600
700
800
900
1000
m/z

ESI MS for 3

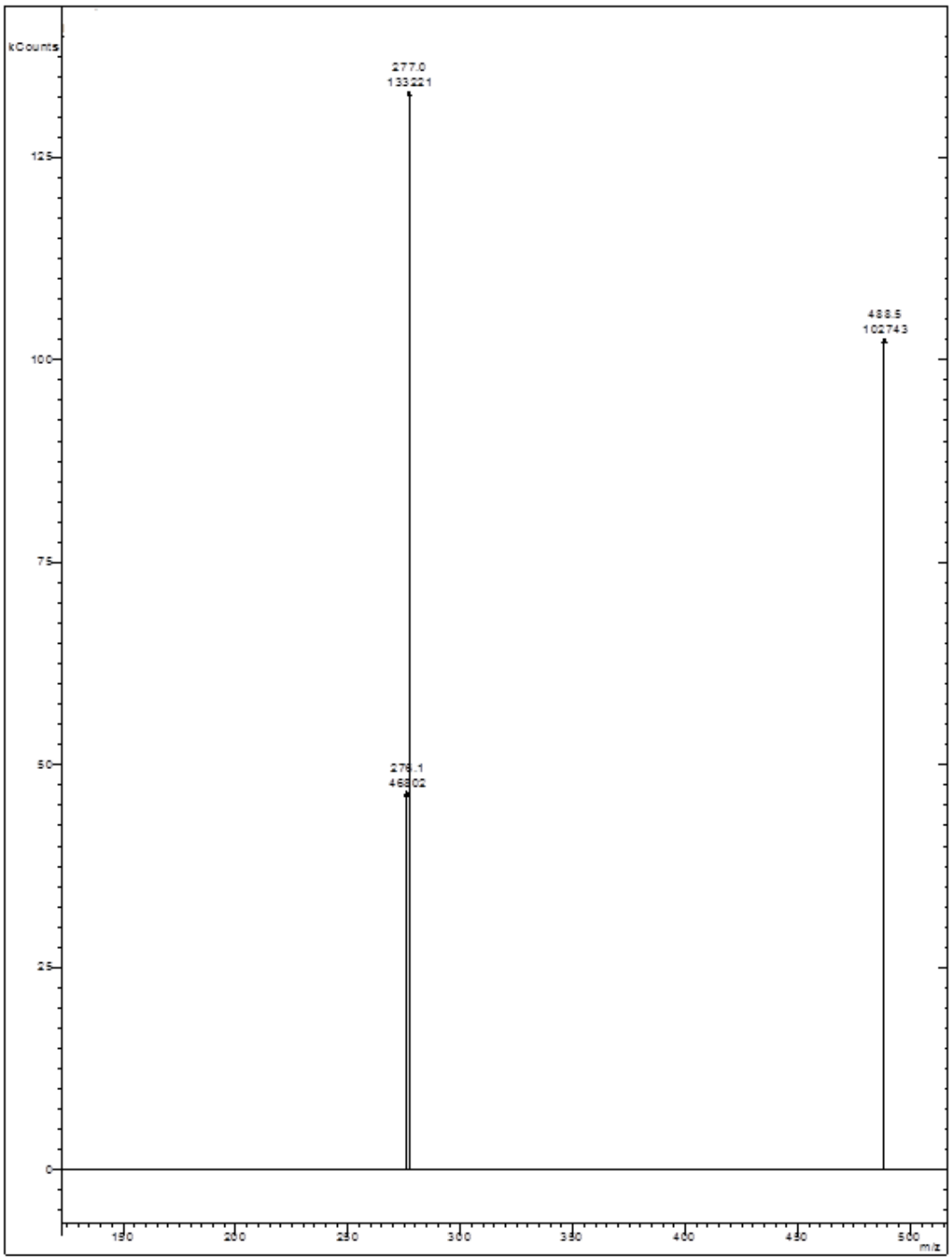
kCounts
277.0
133221
488.5
102743
278.1
46802
125
100
75
50
25
0
150
200
250
300
350
400
450
500
m/z

ESI MS for 3

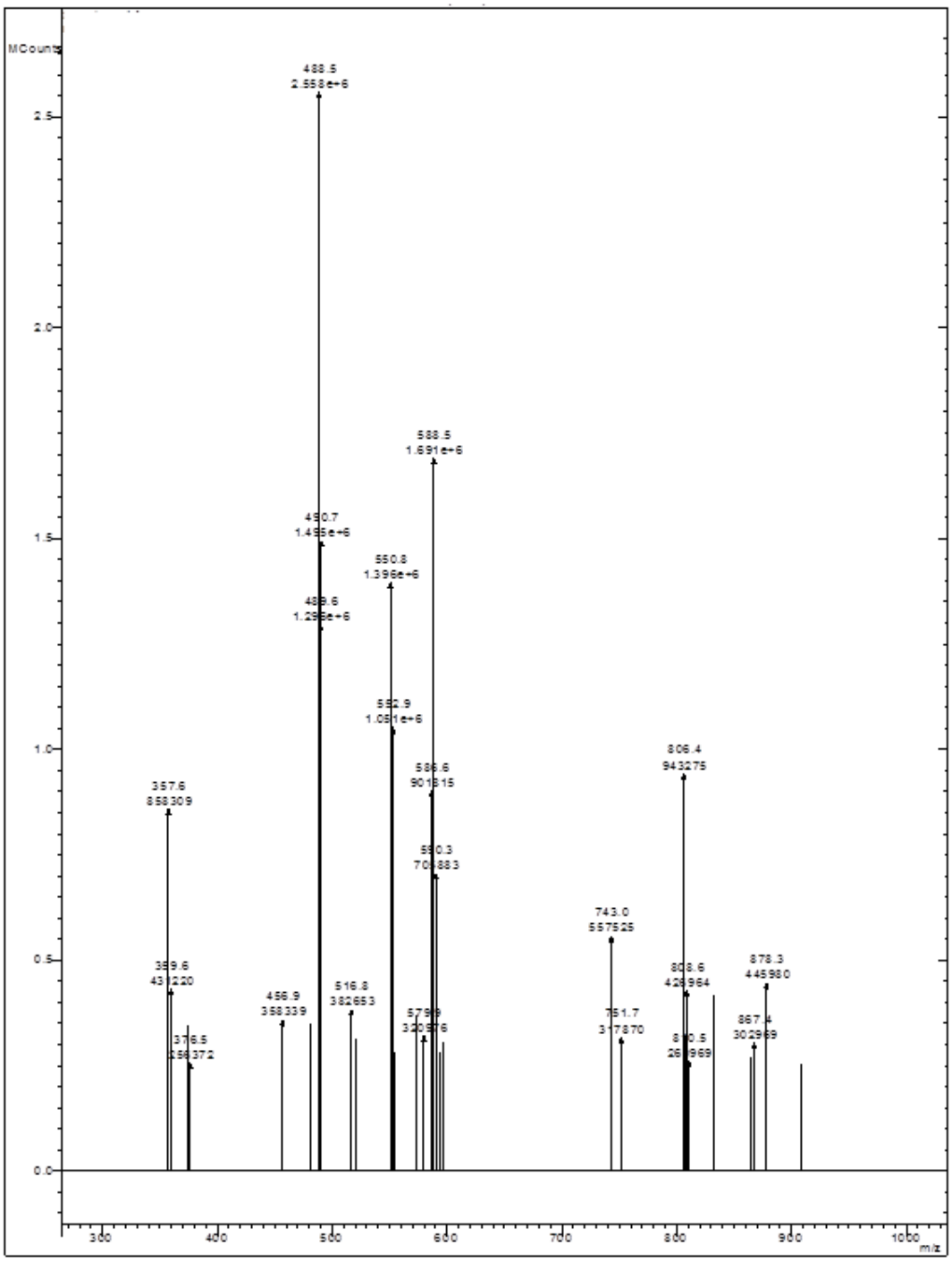
MCounts
488.5
2.558e+6
588.5
1.691e+6
490.7
1.495e+6
550.8
1.396e+6
489.6
1.296e+6
592.9
1.051e+6
806.4
943275
586.6
901815
590.3
701883
357.6
858309
743.0
557525
399.6
431220
808.6
428964
878.3
445980
456.9
358339
516.8
382653
751.7
317870
867.4
302969
376.5
256372
300
400
500
600
700
800
900
1000
m/z

ESI MS for 4

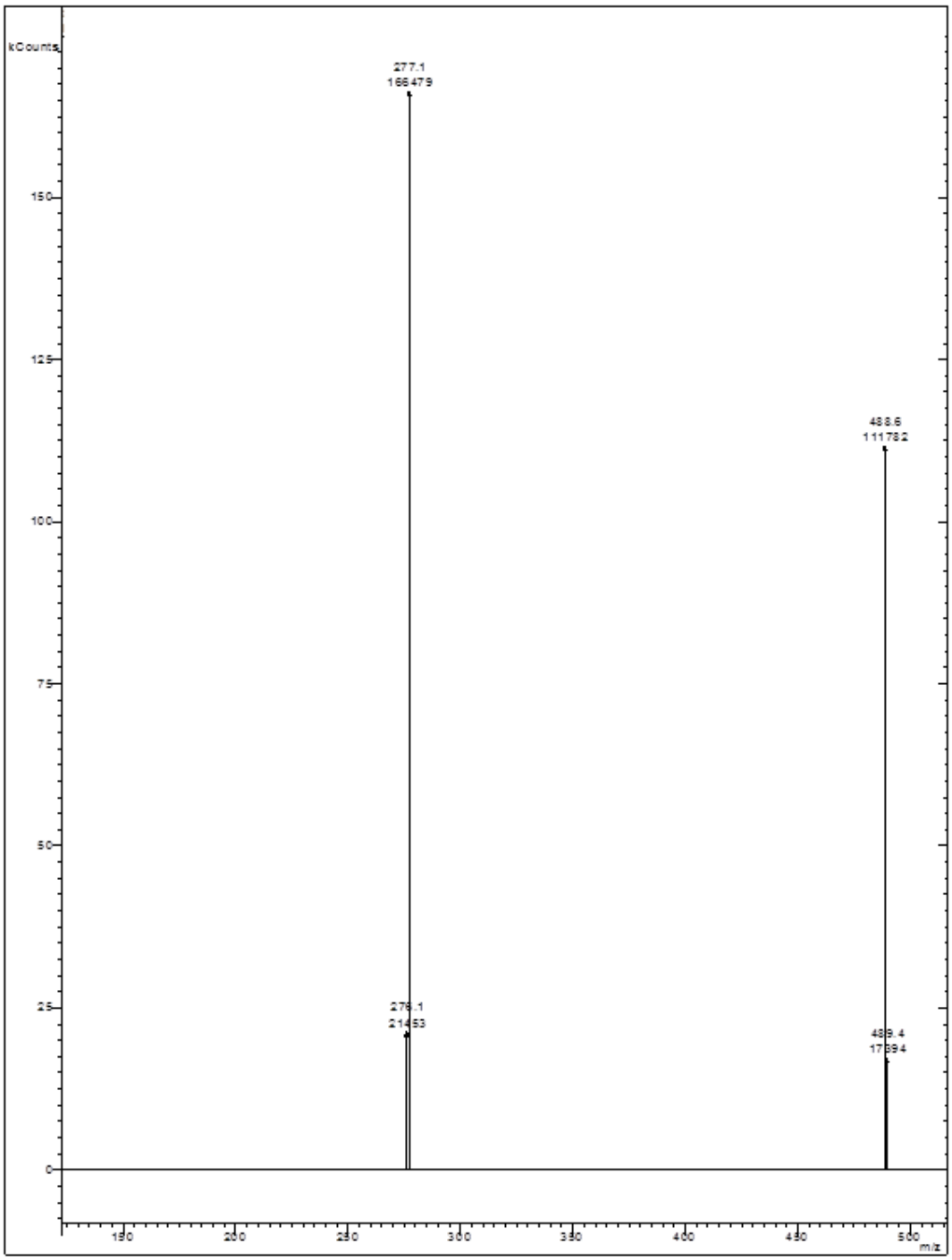
kCounts
277.1
166479
488.6
111782
278.1
21453
489.4
17394
150
125
100
75
50
25
0
190
200
250
300
350
400
450
500
m/z

ESI MS for 4

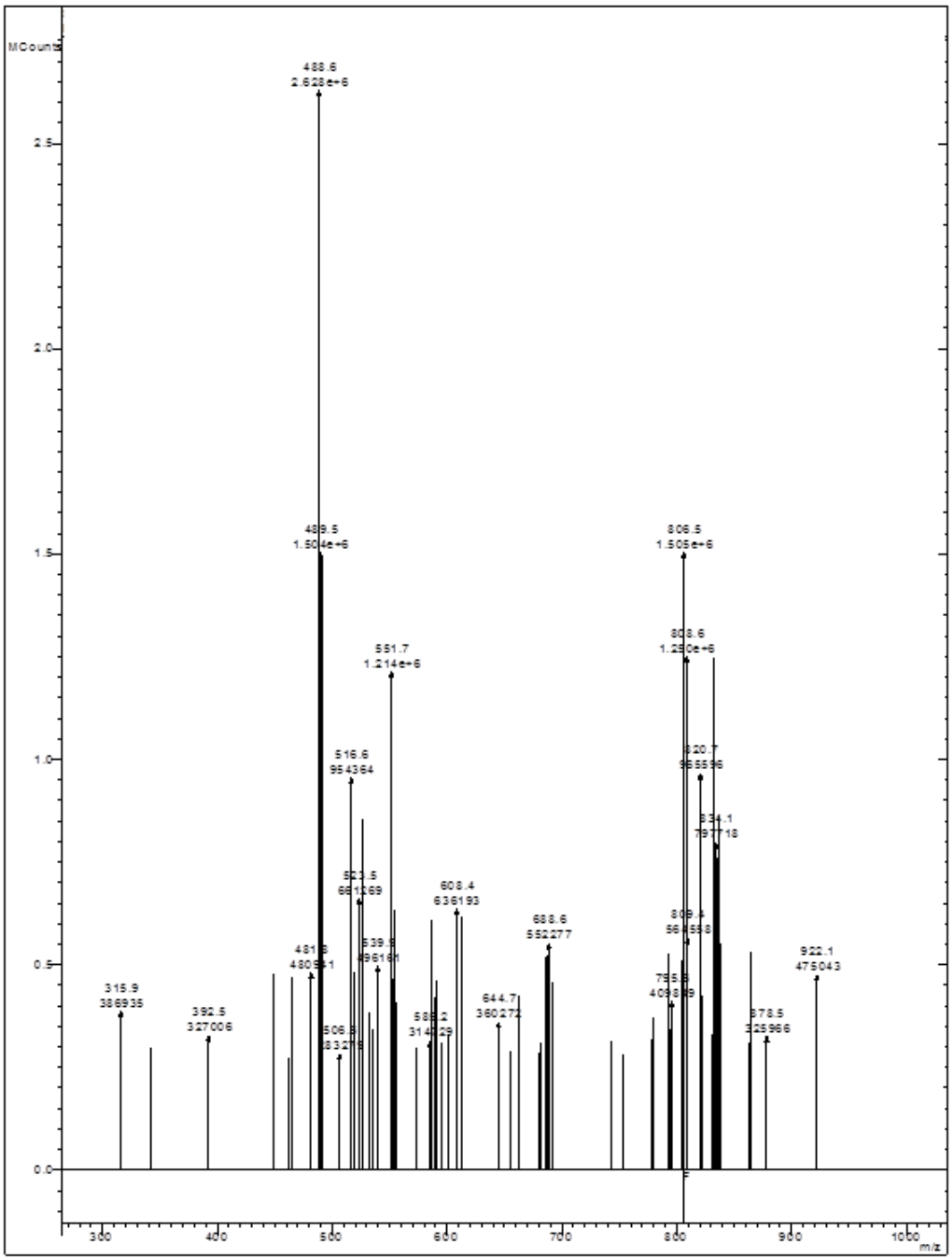
MCounts
488.6
2.628e+6
489.5
1.504e+6
806.5
1.505e+6
551.7
1.214e+6
516.6
954364
608.4
636193
688.6
552277
922.1
475043
315.9
386935
392.5
327006
644.7
360272
878.5
325966
300
400
500
600
700
800
900
1000
m/z

ESI MS for 6

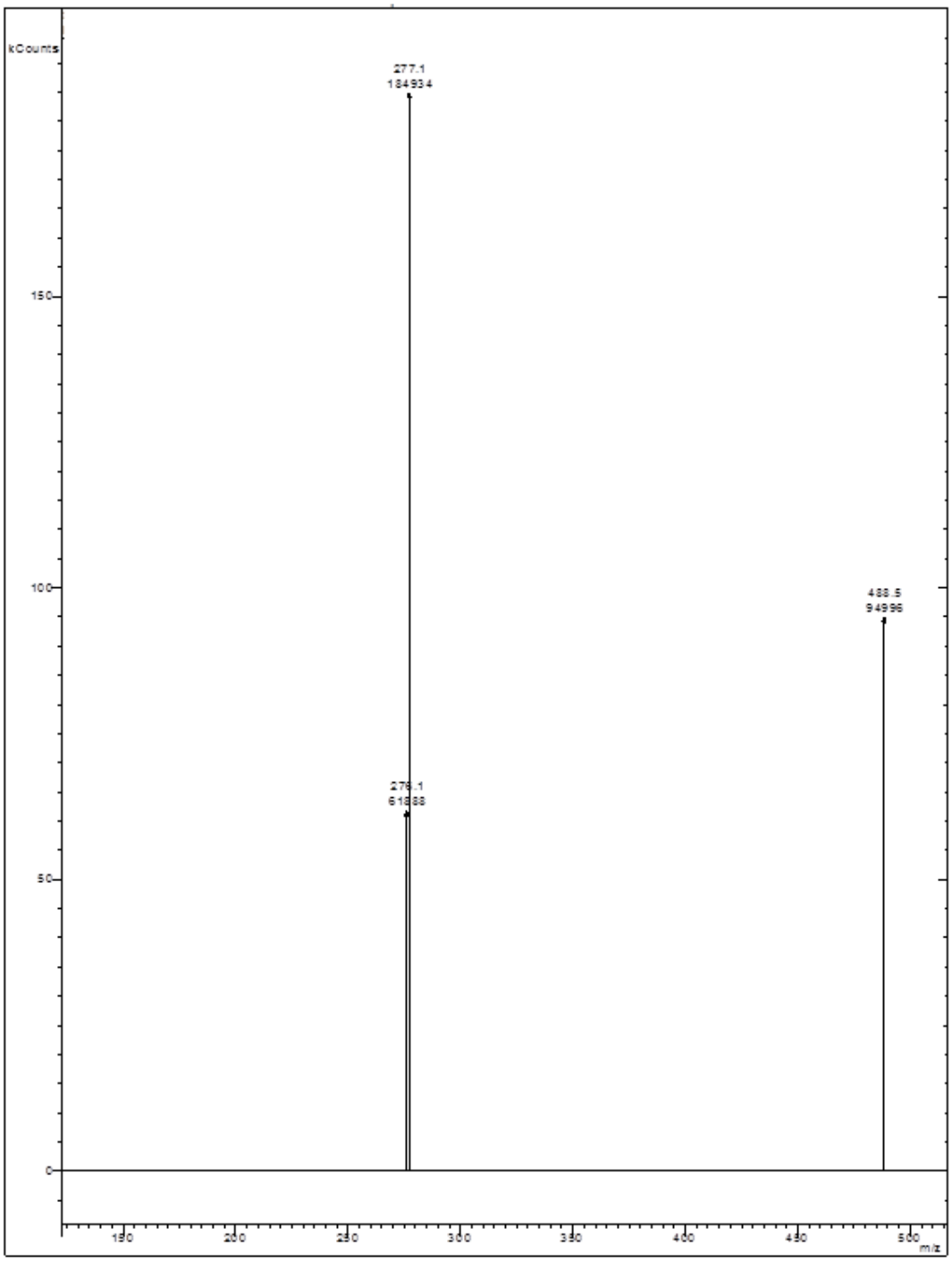
kCounts
277.1
184934
276.1
61688
488.5
94996
150
100
50
0
150
200
250
300
350
400
450
500
m/z

ESI MS for 6

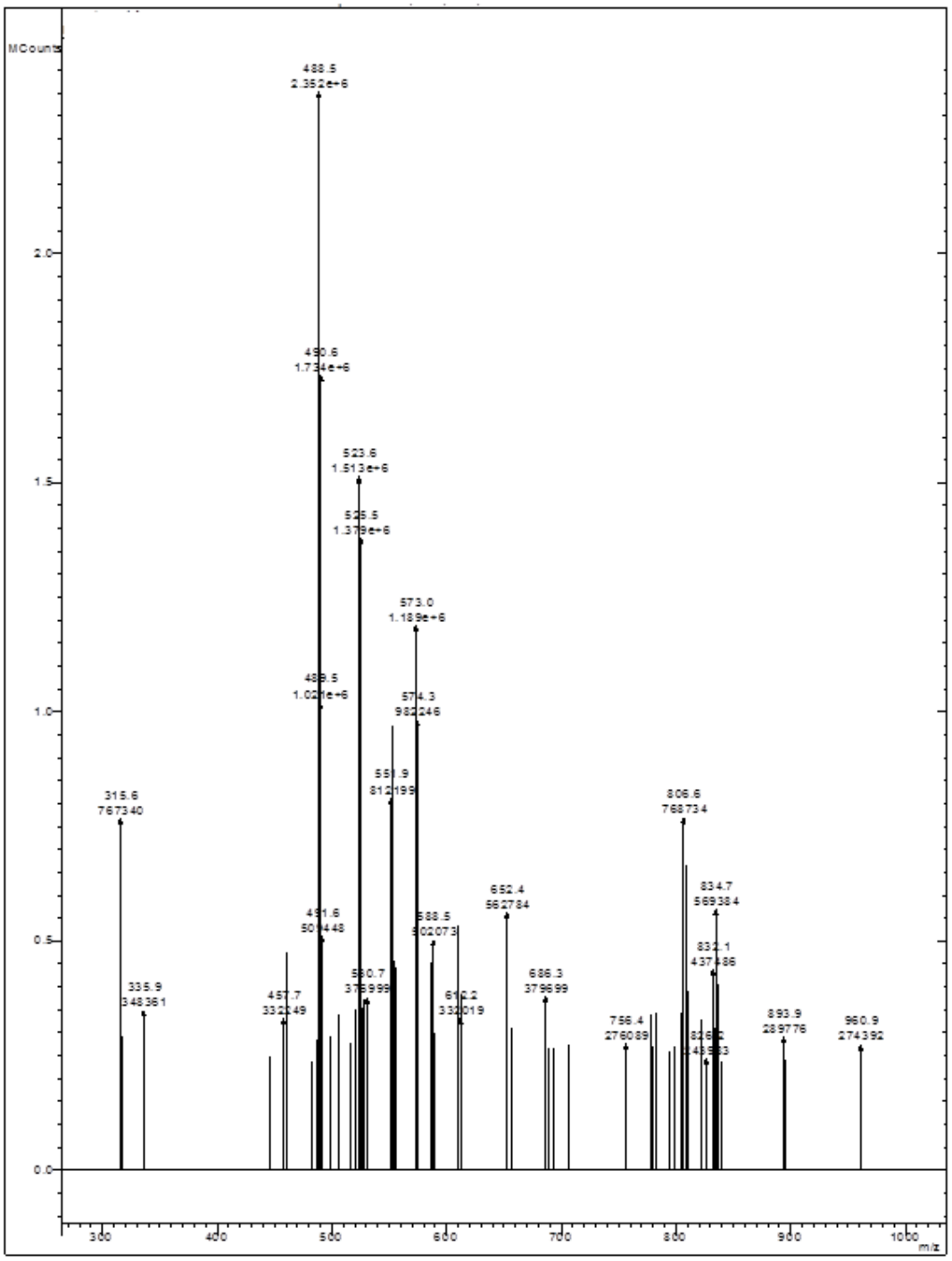
MCounts
488.5
2.352e+6
490.6
1.734e+6
523.6
1.513e+6
525.5
1.379e+6
573.0
1.189e+6
489.5
1.021e+6
574.3
982246
551.9
812199
315.6
767340
806.6
768734
652.4
562784
834.7
569384
491.6
504448
588.5
502073
832.1
437486
335.9
348361
457.7
332149
560.7
376999
614.2
332019
686.3
379699
756.4
276089
893.9
289776
960.9
274392
2.0
1.5
1.0
0.5
0.0
300
400
500
600
700
800
900
1000
m/z

Fig. S2. Absorbance of the solid powder samples of compounds **1** (bottom black curve) and **2** (top red curve) as obtained from the diffuse reflectance spectral measurements.

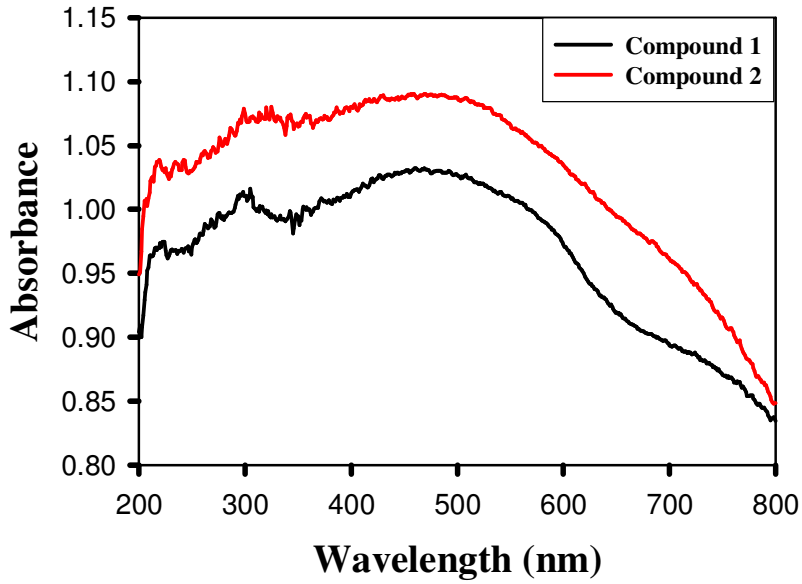

Fig. S3. Electronic spectra of the compounds in the near-IR and visible regions along with their Gaussian analyses: panel A: **1** in CH_3OH [1.27×10^{-3} mol L^{-1}], panel B: **2** in CH_3OH [1.80×10^{-3} mol L^{-1}], panel C: **4** in CH_2Cl_2 [4.8×10^{-4} mol L^{-1}], panel D: **5** in CH_2Cl_2 [2.12×10^{-4} mol L^{-1}]. Top broad curve in each panel is the experimental.

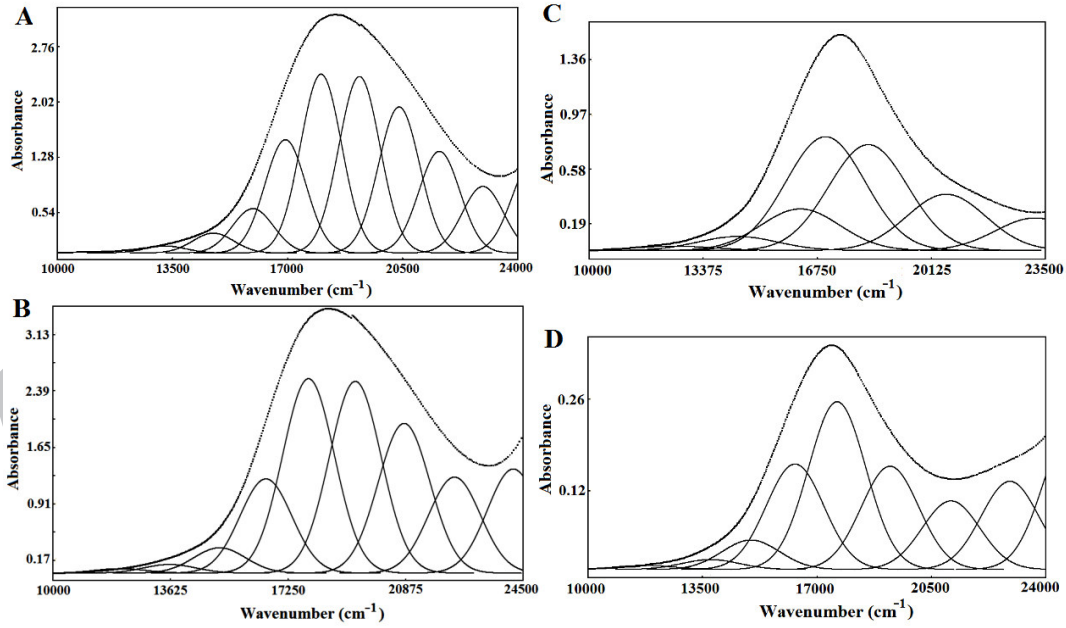

Fig. S4. Ground state optimized structures of the three complexes **1**-**3** used for calculating bond angles and dihedral angles presented in Table 1.

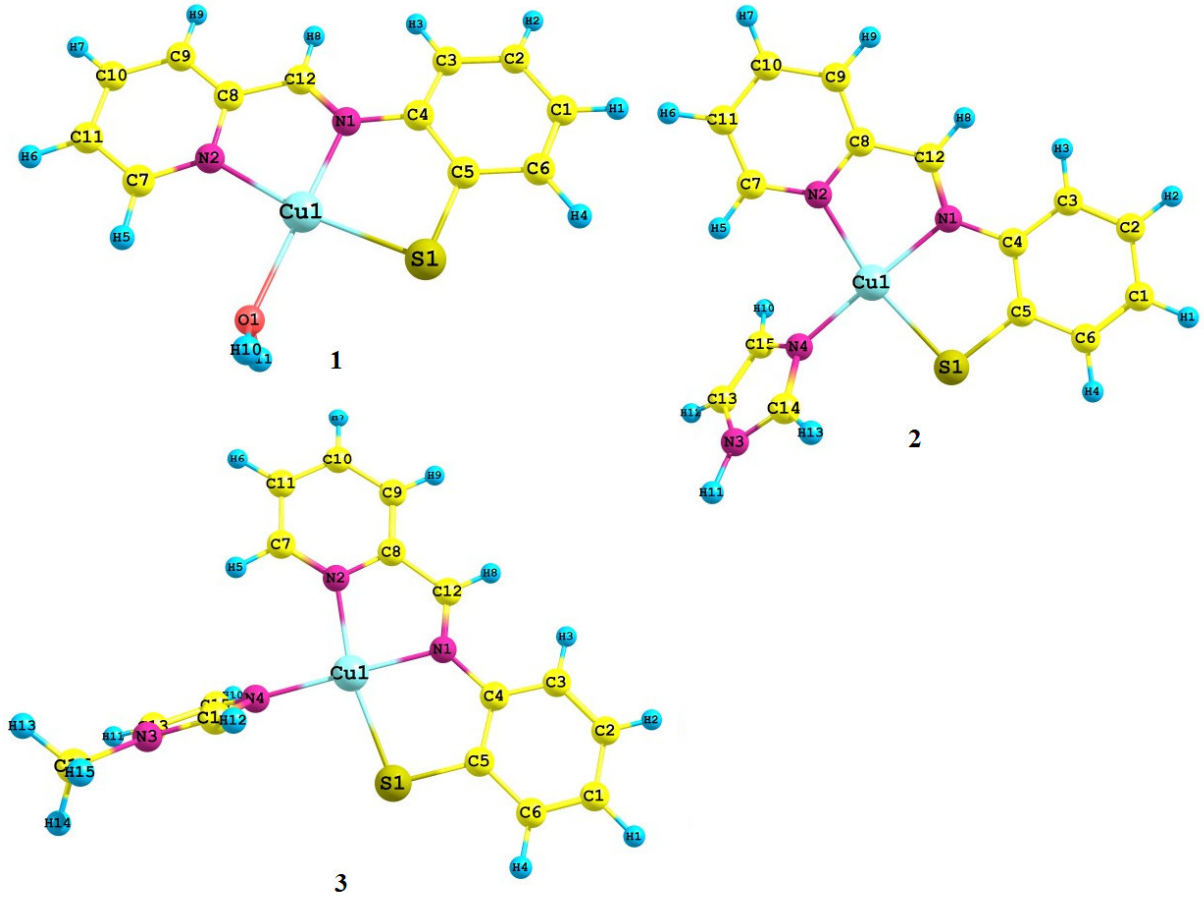

ACCEP

Fig. S5. DNA binding study using electronic spectra: Panel A. (a) **2** in water [0.92×10^{-4} mol L^{-1}]. Then incremental amount of cold plasmid DNA solution [140.5 ng/ul] was added and spectral change was recorded. (b) 10 µL DNA, (c) 20 µL DNA, (d) 30 µL DNA, (e) 40 µL DNA, (f) 50 µL DNA, (g) 60 µL DNA, (h) 70 µL DNA, (i) 80 µL DNA, (j) 90 µL DNA, and (k) 100 µL DNA. (l) DNA in water [10.8 µg/mL]. Panels B-D. Electronic absorption spectra of **1**-**3** upon the titration of ct-DNA (0–40 µM) dissolved in 10 mM Tris–HCl buffer (pH 7.43). Panel B. (a) **1** in water [2×10^{-4} mol L^{-1}]. Panel C. (a) **2** in water [2×10^{-4} mol L^{-1}]. Panel D. (a) **3** in water [1.5×10^{-4} mol L^{-1}]. The arrow shows the decrease in absorbance with respect to an increase in the concentration of ct-DNA. The figure in inset shows the linear fit of $[DNA]/(\varepsilon_a - \varepsilon_f)$ versus [DNA]. The binding constant (K_b) was calculated using the eqn. 2.

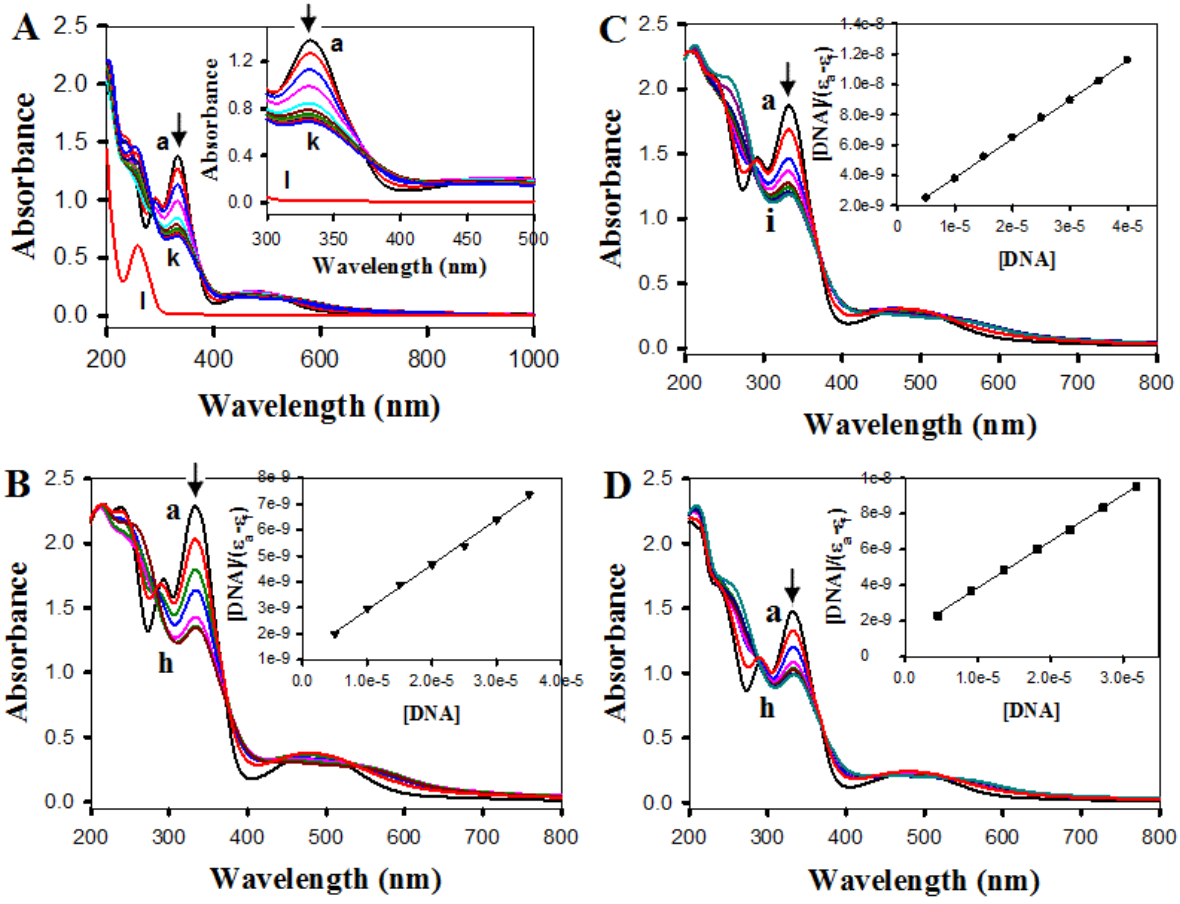

Fig. S6. Panel A. Dependence of the initial rate of oxidation reaction of 3,5-DTBC on the concentration of the substrate 3,5-DTBC catalyzed by complex **1** [1 x 10^{-5} M] in methanol. The reaction was followed at 396 nm. Panel B. Lineweaver–Burk plot for **1**. Panel C. Dependence of the initial rate of oxidation reaction of 3,5-DTBC on the concentration of the substrate 3,5-DTBC catalyzed by complex **2** [2 × 10^{-5}M] in methanol. The reaction was followed at 392 nm. Panel D. Lineweaver–Burk plot for **2**.

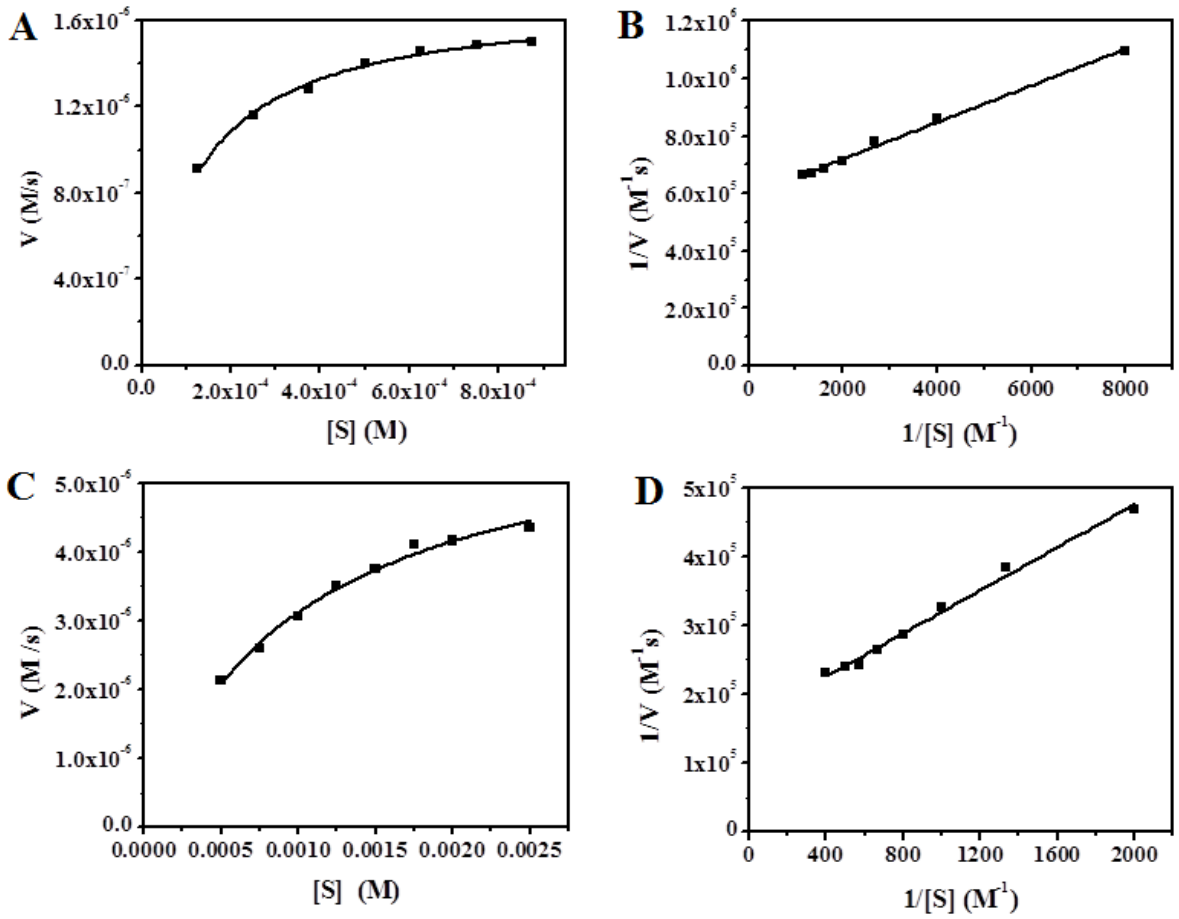

Fig. S7. IR spectra of **1** and **4** in KBr.

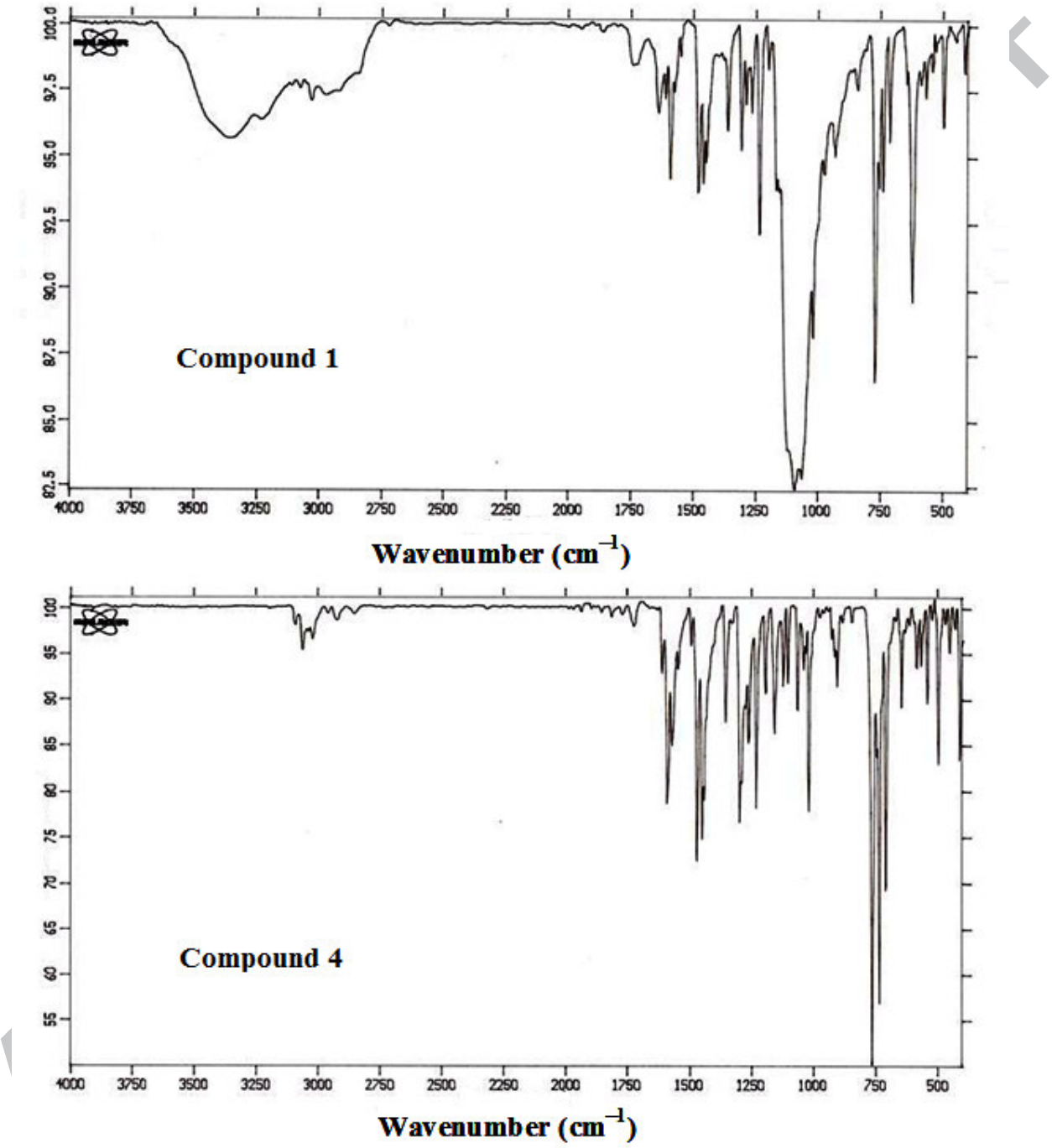

Fig. S8. Far infrared spectra for **1**, **2** and **4** in panels A-C, respectively.

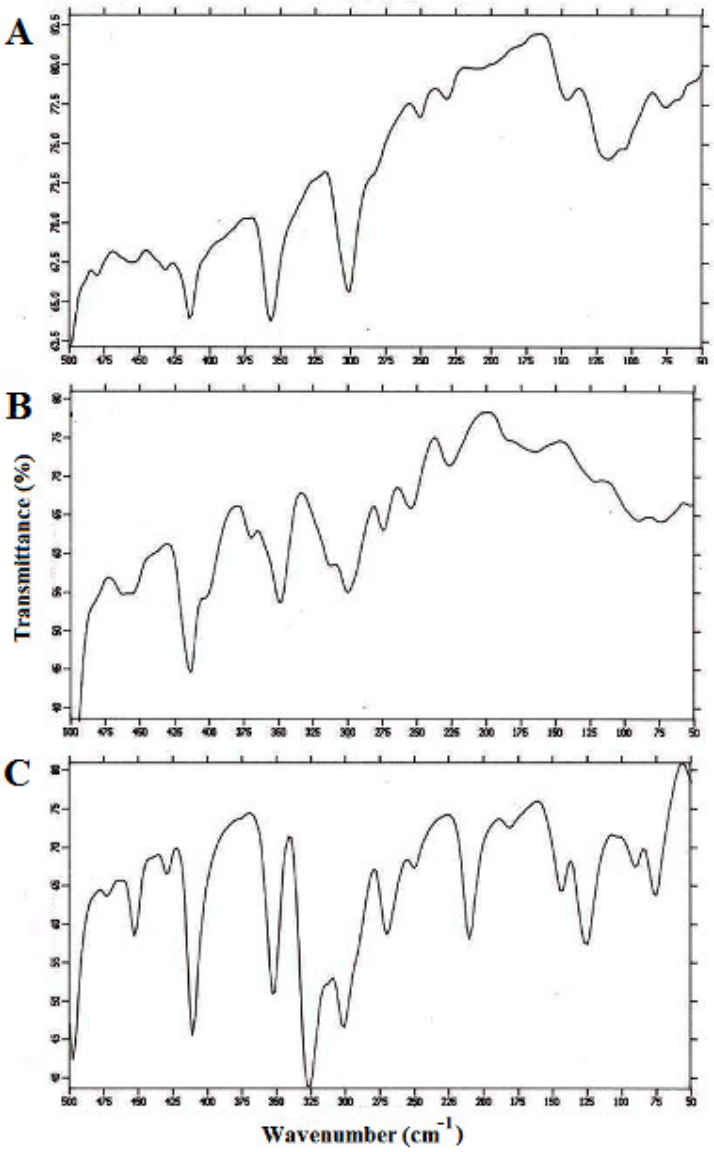

ACCEPTED MANUSCRIPT

Fig. S9. EPR spectra of compound **4** at X-band without DPPH: (A) RT solution in CH_2Cl_2; (B) Frozen glass at LNT in CH_2Cl_2:THF (1 : 1).

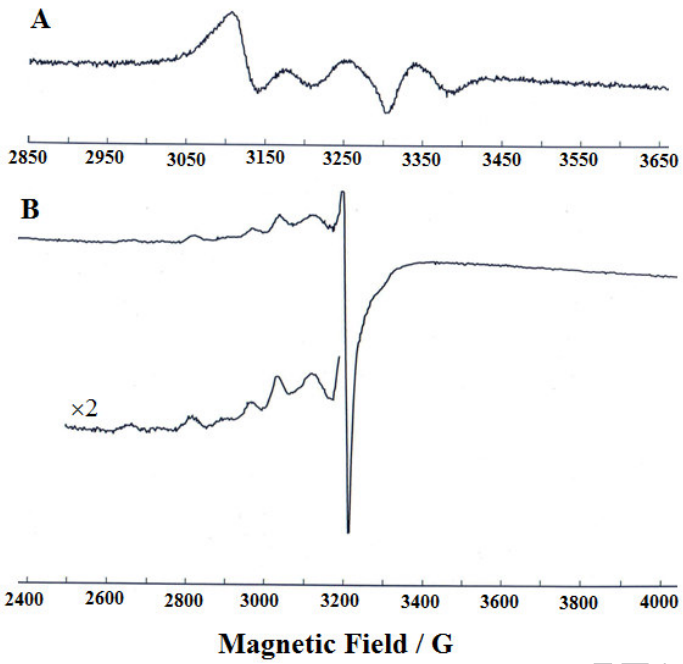

Fig. S10. Packing of the molecules of $Cu(NMe\text{-}Imz)_4(ClO_4)_2$ in the unit cell.

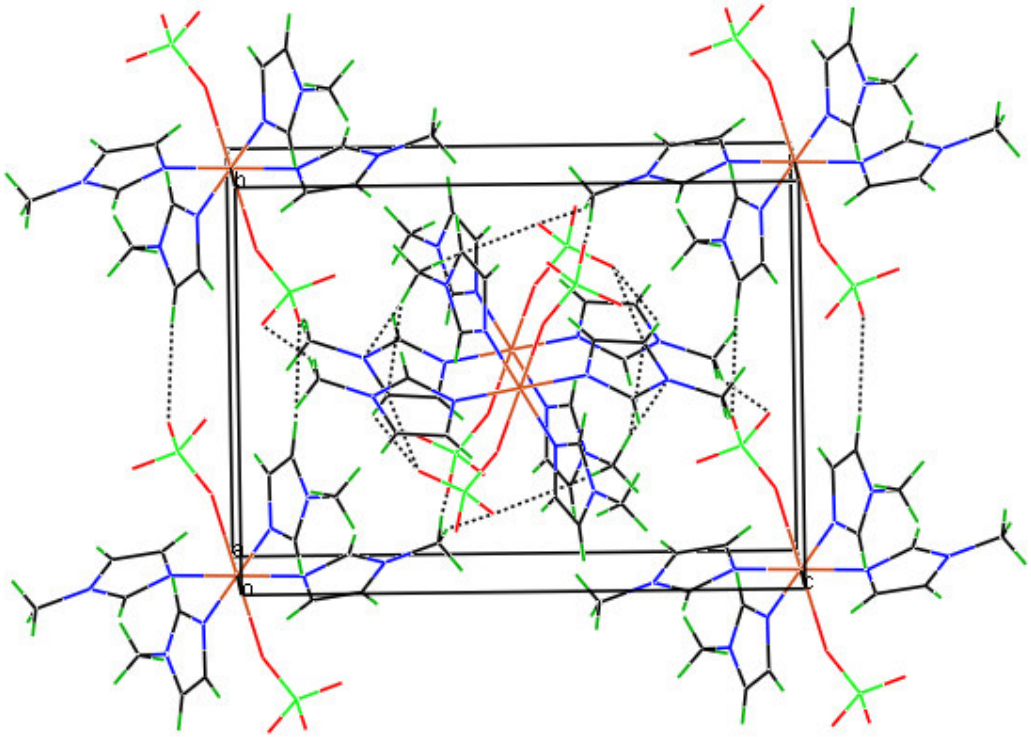

ACCEPTED MANUSCRIPT

Fig. S11. X-band powder EPR spectrum of $Cu(N\text{-}MeImz)_4(ClO_4)_2$ at RT.

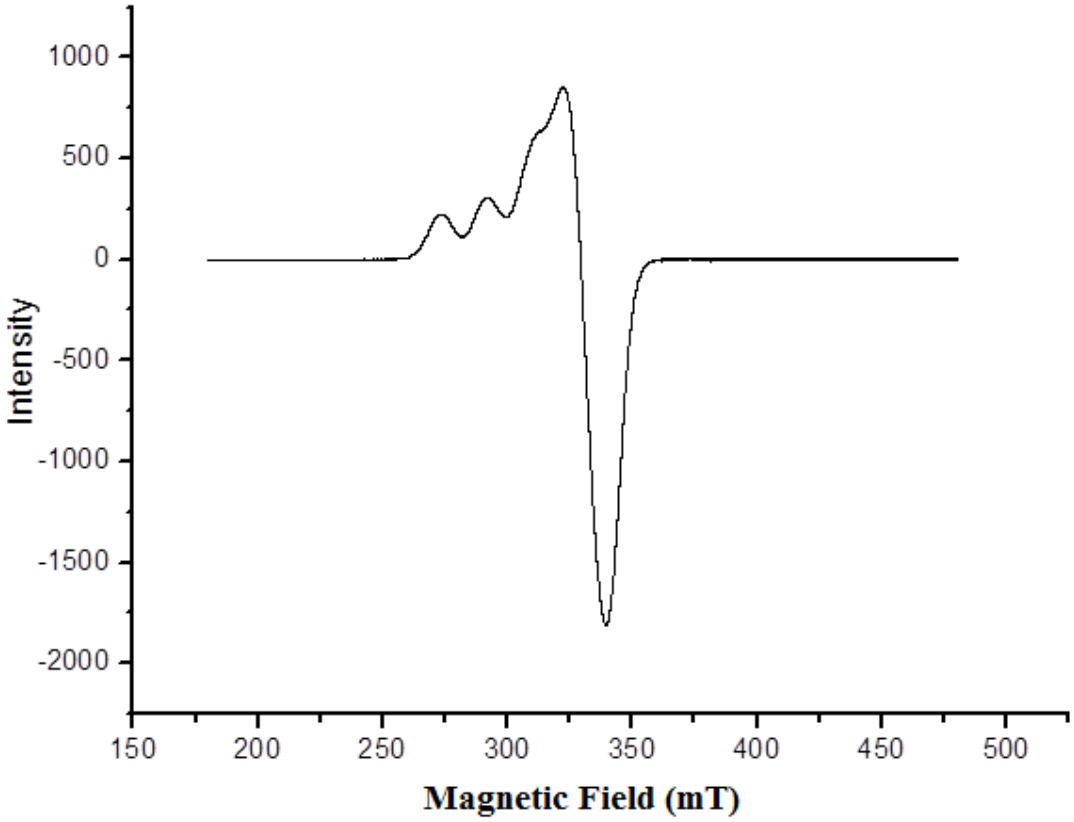

ACCEPTED

ACCEPTED MANUSCRIPT

Table S1. XYZ coordinates of the ground state optimized geometries of complex **1** (with & without solvent), complex **2** (with & without solvent), complex **3** (with & without solvent).

Complex **1** (without solvent)

6	-4.619283000	-0.962571000	-0.000306000
6	-3.877210000	-2.169600000	-0.000236000
6	-2.482854000	-2.125966000	-0.000034000
6	-1.812825000	-0.873188000	0.000074000
6	-2.556814000	0.340548000	-0.000070000
6	-3.966327000	0.278864000	-0.000229000
7	-0.406021000	-0.745440000	0.000239000
16	-1.722483000	1.963748000	-0.000061000
29	0.425269000	1.087326000	0.000124000
6	3.444653000	0.463035000	-0.000614000
7	2.169187000	0.020348000	-0.000051000
6	1.907631000	-1.328423000	0.000370000
6	2.949976000	-2.270631000	0.000349000
6	4.282443000	-1.812045000	-0.000203000
6	4.536335000	-0.428866000	-0.000728000
6	0.488344000	-1.700033000	0.000636000
1	-5.705184000	-0.995853000	-0.000476000
1	-4.392231000	-3.125265000	-0.000330000
1	-1.922407000	-3.056824000	0.000006000
1	-4.542666000	1.198698000	-0.000308000
1	3.586409000	1.538532000	-0.001034000
1	5.549357000	-0.041808000	-0.001233000
1	5.103997000	-2.521754000	-0.000284000
1	0.228141000	-2.756988000	0.001085000

ACCEPTED MANUSCRIPT

ACCEPTED MANUSCRIPT

1	2.725869000	-3.332969000	0.000676000
1	1.176620000	3.512706000	0.806492000
8	1.267451000	2.965532000	0.000277000
1	1.172854000	3.513746000	-0.804808000

Complex **1** (with solvent)

6	-4.633791000	-0.953567000	0.000004000
6	-3.887878000	-2.155607000	0.000158000
6	-2.489822000	-2.105576000	0.000205000
6	-1.823362000	-0.854145000	0.000073000
6	-2.568439000	0.357470000	-0.000140000
6	-3.979460000	0.289063000	-0.000147000
7	-0.409510000	-0.726746000	0.000107000
16	-1.729106000	1.983480000	-0.000248000
29	0.436756000	1.098722000	-0.000081000
6	3.428438000	0.450658000	-0.000376000
7	2.155816000	0.007898000	-0.000133000
6	1.890725000	-1.338294000	0.000175000
6	2.925429000	-2.285863000	0.000309000
6	4.260019000	-1.829326000	0.000085000
6	4.516762000	-0.447868000	-0.000312000
6	0.468120000	-1.694069000	0.000316000
1	-5.719834000	-0.988056000	-0.000027000
1	-4.395834000	-3.115235000	0.000271000
1	-1.926486000	-3.033683000	0.000346000
1	-4.558643000	1.207683000	-0.000276000
1	3.570620000	1.525176000	-0.000719000

ACCEPTED MANUSCRIPT

ACCEPTED MANUSCRIPT

1	5.529953000	-0.062681000	-0.000554000
1	5.078931000	-2.541138000	0.000157000
1	0.195780000	-2.746944000	0.000533000
1	2.696591000	-3.346293000	0.000559000
1	1.401158000	3.431328000	0.808271000
8	1.358244000	2.884004000	0.000252000
1	1.396995000	3.433894000	-0.806239000

Complex **2** (without solvent)

6	-5.099766000	-0.671120000	0.054542000
6	-4.946570000	0.737141000	0.109272000
6	-3.668417000	1.294399000	0.105087000
6	-2.523283000	0.453700000	0.046067000
6	-2.674814000	-0.961288000	-0.010790000
6	-3.978070000	-1.508513000	-0.003318000
7	-1.198702000	0.947718000	0.033380000
16	-1.231700000	-2.063522000	-0.080284000
29	0.369321000	-0.334473000	-0.029007000
6	2.774331000	1.667281000	-0.173561000
7	1.443932000	1.457105000	-0.071869000
6	0.590441000	2.528933000	0.005840000
6	1.072800000	3.850319000	-0.001107000
6	2.459961000	4.069430000	-0.098309000
6	3.325117000	2.964203000	-0.190689000
6	-0.836419000	2.204501000	0.067521000
1	-6.094949000	-1.107202000	0.058764000
1	-5.820968000	1.379072000	0.155709000

ACCEPTED MANUSCRIPT

ACCEPTED MANUSCRIPT

1	-3.563991000	2.375038000	0.148025000
1	-4.102667000	-2.586237000	-0.042003000
1	3.404588000	0.787908000	-0.248750000
1	4.398572000	3.093841000	-0.274875000
1	2.855050000	5.080649000	-0.106419000
1	-1.547960000	3.026217000	0.123965000
1	0.379164000	4.683184000	0.062951000
6	3.660070000	-2.843011000	0.712977000
7	3.083308000	-3.445737000	-0.405982000
6	2.008427000	-2.698597000	-0.800448000
7	1.874129000	-1.636883000	0.014353000
6	2.901641000	-1.715960000	0.967341000
1	3.006414000	-0.999553000	1.765815000
1	3.396934000	-4.301944000	-0.847476000
1	4.518337000	-3.251144000	1.220713000
1	1.357028000	-2.947683000	-1.622404000

Complex **2** (with solvent)

6	-5.128041000	-0.723371000	0.020463000
6	-4.979649000	0.683606000	0.018310000
6	-3.698841000	1.246369000	0.014297000
6	-2.552082000	0.411682000	0.012091000
6	-2.695927000	-1.003704000	0.013930000
6	-3.997573000	-1.555718000	0.018564000
7	-1.222835000	0.915306000	0.005693000
16	-1.234305000	-2.099024000	0.009844000

ACCEPTED MANUSCRIPT

29	0.356817000	-0.347726000	0.003032000
6	2.735994000	1.632227000	-0.036969000
7	1.402866000	1.432347000	-0.016880000
6	0.550105000	2.505828000	-0.014810000
6	1.029624000	3.824934000	-0.031154000
6	2.422969000	4.038368000	-0.050614000
6	3.287709000	2.930793000	-0.054067000
6	-0.877096000	2.174656000	-0.000808000
1	-6.120706000	-1.165468000	0.023511000
1	-5.854538000	1.326729000	0.019729000
1	-3.598106000	2.327351000	0.012586000
1	-4.118081000	-2.635132000	0.020265000
1	3.366735000	0.751027000	-0.040701000
1	4.364341000	3.055614000	-0.069913000
1	2.820729000	5.047748000	-0.063677000
1	-1.593804000	2.992878000	0.000846000
1	0.334225000	4.657509000	-0.029817000
6	3.637065000	-2.853263000	0.717932000
7	3.394510000	-3.089148000	-0.634797000
6	2.342563000	-2.316188000	-1.033157000
7	1.899401000	-1.588987000	0.009384000
6	2.700118000	-1.916010000	1.114324000
1	2.549005000	-1.473697000	2.085349000
1	3.910946000	-3.727247000	-1.228988000
1	4.421824000	-3.349554000	1.263497000
1	1.939392000	-2.307187000	-2.031889000

ACCEPTED MANUSCRIPT

ACCEPTED MANUSCRIPT

Complex **3** (without solvent)

6	-4.808454000	-2.175832000	0.023154000
6	-5.131757000	-0.795490000	0.035128000
6	-4.110514000	0.153741000	0.033710000
6	-2.750297000	-0.260432000	0.019980000
6	-2.422874000	-1.646646000	0.005606000
6	-3.471770000	-2.594589000	0.010181000
7	-1.664729000	0.644886000	0.012018000
16	-0.695730000	-2.209740000	-0.006245000
29	0.242119000	-0.045926000	0.017760000
6	1.847394000	2.636580000	-0.176348000
7	0.660058000	2.000269000	-0.078756000
6	-0.501602000	2.729582000	-0.041133000
6	-0.484266000	4.135676000	-0.082813000
6	0.753605000	4.799583000	-0.174682000
6	1.937505000	4.041837000	-0.227782000
6	-1.740874000	1.951103000	0.014188000
6	4.150363000	-1.269451000	0.933978000
7	3.845069000	-2.100406000	-0.146554000
6	2.595323000	-1.768145000	-0.588353000
7	2.089467000	-0.762429000	0.153538000
6	3.057516000	-0.442080000	1.114413000
1	-5.602809000	-2.917191000	0.025255000
1	-6.170283000	-0.478993000	0.046843000
1	-4.370835000	1.208590000	0.043843000
1	-3.231445000	-3.653233000	0.004042000
1	2.733741000	2.013203000	-0.220521000

ACCEPTED MANUSCRIPT

1	2.908588000	4.518084000	-0.307878000
1	0.791684000	5.884077000	-0.209242000
1	-2.685649000	2.491095000	0.038119000
1	-1.415540000	4.692954000	-0.049551000
1	2.899748000	0.313446000	1.867024000
1	5.081143000	-1.338951000	1.473408000
1	2.085428000	-2.265982000	-1.397372000
6	4.713221000	-3.158016000	-0.697883000
1	5.643003000	-2.724476000	-1.078362000
1	4.944160000	-3.894556000	0.077371000
1	4.195138000	-3.661143000	-1.517878000

Complex **3** (with solvent)

6	-4.973736000	-1.932421000	-0.009811000
6	-5.206127000	-0.536993000	-0.034046000
6	-4.121800000	0.346840000	-0.038126000
6	-2.794140000	-0.151844000	-0.017819000
6	-2.554831000	-1.554020000	0.006360000
6	-3.662284000	-2.433015000	0.010655000
7	-1.647851000	0.688408000	-0.021486000
16	-0.853957000	-2.218758000	0.031853000
29	0.211951000	-0.104697000	0.044717000
6	1.975031000	2.437680000	-0.063370000
7	0.743628000	1.889268000	-0.036595000
6	-0.365293000	2.694942000	-0.070929000
6	-0.255569000	4.093299000	-0.126636000

ACCEPTED MANUSCRIPT

6	1.030227000	4.670912000	-0.150768000
6	2.159538000	3.835280000	-0.120979000
6	-1.651897000	1.993787000	-0.058240000
6	4.001994000	-1.539945000	1.076828000
7	3.878177000	-2.031698000	-0.224458000
6	2.673172000	-1.617395000	-0.716324000
7	2.023276000	-0.881352000	0.207952000
6	2.846828000	-0.826451000	1.340135000
1	-5.812513000	-2.623341000	-0.006177000
1	-6.220802000	-0.150654000	-0.048374000
1	-4.312091000	1.415561000	-0.055403000
1	-3.490996000	-3.505347000	0.030018000
1	2.817939000	1.756979000	-0.040257000
1	3.163594000	4.243221000	-0.141286000
1	1.143460000	5.749150000	-0.193953000
1	-2.562152000	2.588409000	-0.086663000
1	-1.147493000	4.710285000	-0.152605000
1	2.561392000	-0.301199000	2.237057000
1	4.870025000	-1.731932000	1.685830000
1	2.308418000	-1.858847000	-1.701037000
6	4.874492000	-2.852786000	-0.936584000
1	5.816322000	-2.304271000	-1.025087000
1	5.046389000	-3.785764000	-0.392659000
1	4.500996000	-3.085487000	-1.935816000

Table S2. Far-infrared spectral band (cm^{-1}) assignments [70] for compounds **1**. **2** and **4**.

Compound	ν(Cu-N)	ν(Cu-N(py))	ν(Cu-N(Im))	ν(Cu-S)	ν(Cu-Cl)
1	414	285	—	357	—
2	413	273.5	311.5	348	—
4	411	270	—	352	327

Graphical abstract

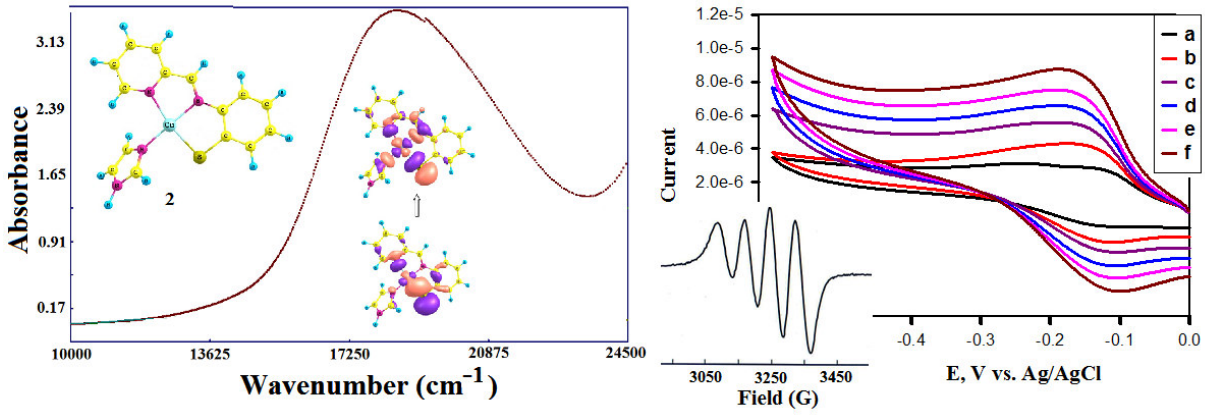

Cu(II) complexes containing a Schiff base N-(2-mercaptophenyl)-2'-pyridylmethylenimine display a four-line EPR pattern as well as strong electronic spectra exhibiting intense S → Cu(II) LMCT bands in the visible region. Nearly reversible or quasi-reversible Cu(II)/Cu(I) couple is observed in the range –0.08 to –0.20 V versus Ag/AgCl. Presence of imidazole group as a coligand enhanced DNA cleavage and cytotoxicity.

ACCEPTED MANUSCRIPT

Figure Captions

Fig. 1. Structures of the ligands.

Fig. 2. Proposed structures of the compounds **1-7** in solution.

Fig. 3. ^{1}H NMR results of compounds **2** and **3** in d_6-DMSO at RT.

Fig. 4. Electronic spectra of the compounds. Panel A. A quantitative comparison of the electronic spectra of **1**-**3** in methanol. Black curve *a* for **1** [1.89 $\times 10^{-4}$ mol L^{-1}], red curve *b* for **2** [2.17 $\times 10^{-4}$ mol L^{-1}] and blue curve *c* for **3** [1.84 $\times 10^{-4}$ mol L^{-1}], respectively. Panel B. Blue curve *a*. **4** in CH_2Cl_2 [6.1 $\times 10^{-4}$ mol L^{-1}]. black curve *b*: **5** in CH_2Cl_2 [2.1 $\times 10^{-4}$ mol L^{-1}], purple curve *c*: **5** in CH_3OH [3.2 $\times 10^{-4}$ mol L^{-1}]. Panel C. black curve *a*: **2** in CH_3OH [2.17 $\times 10^{-4}$ mol L^{-1}], red curve *b*: **2** in water [2.19 $\times 10^{-4}$ mol L^{-1}]. Panel D. Blue curve *a*. **6** in CH_3CN [0.8 $\times 10^{-4}$ mol L^{-1}]. black curve *b*: **7** in CH_3CN [0.6 $\times 10^{-4}$ mol L^{-1}]. Inset of panel D. Blue curve *a*. **6** in CH_3CN [7.0 $\times 10^{-4}$ mol L^{-1}]. black curve *b*: **7** in CH_3CN [2.6 $\times 10^{-4}$ mol L^{-1}].

Fig. 5. Ground state optimized structures of the complexes **1**, **2**, and **3** without and with solvent, respectively. The numbers between the atoms are respective bond distances in Å.

Fig. 6. Orbitals involved in the electronic excitations corresponding to the dominant configurations for compounds **1**, **2**, and **3**, respectively.

Fig. 7. Electronic spectral changes for the reactions of the compounds. Panel A. Reaction of **2** with imidazole. Black curve *a*. **2** in CH_3CN [2.17 $\times 10^{-4}$ mol L^{-1}], red curve *b*: within 5 min after

ACCEPTED MANUSCRIPT

addition of 2-fold excess of solid imidazole, and blue curve *c*: after 20 min. Panel B. Reaction of **6** with imidazole. Black curve *a*. **6** in CH_3CN [5.50×10^{-4} mol L^{-1}], blue curve *b*: immediately after adding 2-fold excess of solid imidazole, curve *d*: recorded after 15 min, and curve *e*: recorded after 20 min. Curves *d* and *e* are identical indicating the steady state reached within 15 min. Panel C. Plot of absorbance change at 546 nm with time for the spectral data presented in panel B. The solid line represents the fitting of the experimental points (circles) using the model $\Delta A_t = c + a(1 - e^{-k\,t})$.

Fig. 8. Panel A. Electronic spectra (a) compound **1** in water [1.51×10^{-4} mol L^{-1}], (b) compound **1** in water [1.51×10^{-4} mol L^{-1}] + 10.8 µg/mL plasmid DNA, and (c) plasmid DNA in water [10.8 µg/mL]. Panel B. Electronic spectra (a) compound **2** in water [0.92×10^{-4} mol L^{-1}], (b) compound **2** in water [0.92×10^{-4} mol L^{-1}] + 10.8 µg/mL plasmid DNA, and (c) plasmid DNA in water [10.8 µg/mL].

Fig. 9. The catalytic activity of compounds **1** and **2** were performed by treating 1×10^{-4} mol L^{-1} complex solutions with 1×10^{-2} mol L^{-1} of 3,5-di-*tert*-butyl catechol (3,5-DTBC) as model substrate in methanol at RT. Panel A and B show the electronic spectral change for the formation of 3,5-DTBQ from the catalytic oxidation of 3,5-DTBC with compounds **1** and **2**, respectively, in methanol at RT. Panel C shows the plot of absorbance change at 401 nm with time showing the relative rate of formation of 3,5-DTBQ. The solid line represents the fitting of the experimental points (circles) using the model $\Delta A_t = c + a_1(1 - e^{-k_1 t}) + a_2(1 - e^{-k_2 t})$.

Fig. 10. X-band powder EPR spectra for **1-7** at RT. (A) **1** with DPPH; (B) **2** with DPPH; (C) **4** with DPPH; (D) **3** without DPPH, (E) **5** without DPPH, (F) **6** without DPPH, and (G) **7** without DPPH.

ACCEPTED MANUSCRIPT

Fig. 11. X-band solution EPR spectra of **1**-**7** at RT. (A) **1** in CH_3CN:CH_2Cl_2 (2 : 1), (B) **2** in CH_3CN:CH_2Cl_2 (2 : 1); (C) **3** in CH_3CN, (D) **4** in DMF; (E) **1** in CH_3OH; (F) **2** in CH_3OH; (G) **5** in CH_3CN; (H) **6** in DMF; (I) **6** in CH_3CN; and (J) **7** in CH_3CN.

Fig. 12. Frozen glass EPR spectra of the compounds at LNT without DPPH. (A) **2** in CH_3OH. (B) **5** in CH_3CN. (C) **6** in DMF, and (D) **7** in CH_3CN.

Fig. 13. Plate with *Escherichia coli* lawn showing the effect of sample discs (labels are for compounds **1**, **2**, **4**-**6**). The control disc with just DMSO is in the center.

Fig. 14. 1% agarose gel depicting effects of treatment of 5 µL plasmid DNA with copper compounds. The loading volume is 10 µL in each lane. A = compound **1**, B = compound **4**, C = compound **2**, D = compound **7**, E = compound **6**, and F = compound **5**. Final concentration: [1.69×10^{-4} mol L^{-1}] for **1**, [1.50×10^{-4} mol L^{-1}] for **2**, [2.13×10^{-4} mol L^{-1}] for **4**, [2.13×10^{-4} mol L^{-1}] for **5**, [1.18×10^{-4} mol L^{-1}] for **6**, [1.18×10^{-4} mol L^{-1}] for **7**, and [0.1 mol L^{-1}] for DMSO.

Fig. 15**.** Effect on DNA. 1% agarose gel depicting effects of treatment of 5 µL plasmid DNA with copper compounds. Left panel. Lane 1: Control Plasmid DNA, lane 2: Plasmid DNA + DMSO, lane 3: Plasmid DNA + **2** in DMSO, lane 4: Plasmid DNA + **3** in DMSO, lane 5: Plasmid DNA + $Cu(NMe\text{-}Imz)_4(ClO_4)_2$ in DMSO, respectively. Right panel. Lane 1: Control Plasmid DNA, lane 2: Plasmid DNA + **2** in water, lane 3: Plasmid DNA + **3** in water, lane 4: Plasmid DNA + **2** in sodium phosphate buffer (pH 7.00), lane 5 Plasmid DNA + **3** in sodium phosphate buffer (pH 7.00), respectively. Final concentration: [1.69×10^{-4} mol L^{-1}] for **1**, [1.50×10^{-4} mol L^{-1}] for **2**, [1.45×10^{-4} mol L^{-1}] for **3**, [1.13×10^{-4} mol L^{-1}] for $Cu(NMe\text{-}Imz)_4(ClO_4)_2$ and [0.1 mol L^{-1}] for DMSO.

ACCEPTED MANUSCRIPT

Fig. 16. Effect of metal complexes **1**, **2**, and **3** on the cell viability of cultured HeLa cells (A) and C6 glioma cells (B) using the 3-[4,5-dimethylthiazol-2-yl]2,5-diphenyl-tetraazolium bromide (MTT) assay. The two different cell lines were treated with different doses (10, 20, 50 and 100 μM) of the compounds **1**, **2**, and **3** for 24 h and 48 h incubation times. Results are expressed as percentage of viable cells as means of three experiments. *Mean values of the groups are significantly ($p < 0.0001$) decreased from the control of compounds **1**, **2**, and **3**, respectively at both time points 24h and 48h ; [a] Mean values of the groups are significantly ($p < 0.01$) decreased from the control of compound **2** at dose 10 μM and time point 48 h. [NS] Non significant.

Fig. 17. Plot of cell viability versus concentrations of the compounds **1**, **2**, and **3**. Panel A. HeLa cell line. Panel B. C6 glioma cell line.

Fig. 18. Cyclic voltammogram of **1** (1.5×10^{-3} mol L^{-1}) in CH_3CN containing 0.1 M $[N(n\text{-}Bu)_4]ClO_4$ at a scan rate of 100 mV s^{-1}.

Fig. 19. Cyclic voltammogram of **2** (1.15×10^{-3} mol L^{-1}) in CH_3CN containing 0.1 M $[N(n\text{-}Bu)_4]ClO_4$: Panel A. reduction at different scan rates: (a) 50, (b) 100, (c) 200, (d) 300, (e) 400, and (f) 500 mV s^{-1}, respectively. Panel B. oxidation at different scan rates: (a) 50, (b) 100, (c) 250, (d) 300, and (e) 400 mV s^{-1}, respectively.

Fig. 20. Panel A. Cyclic voltammogram of **3** (1.25×10^{-3} mol L^{-1}) in CH_3CN containing 0.1 M $[N(n\text{-}Bu)_4]ClO_4$ at a scan rate of 100 mV s^{-1}. Panel B. Reduction of **3** (1.25×10^{-3} mol L^{-1}) in CH_3CN containing 0.1 M $[N(n\text{-}Bu)_4]ClO_4$ at different scan rates: (a) 50, (b) 100, (c) 200, (d) 300, (e) 400, and (f) 500 mV s^{-1}.

ACCEPTED MANUSCRIPT

Fig. 21. Cyclic voltammograms of **6** (2.05×10^{-3} mol L^{-1}) (panel A) and **7** (1.25×10^{-3} mol L^{-1}) (panel B) in CH_3CN containing 0.1 M $[N(n\text{-}Bu)_4]PF_6$ at a scan rate of 100 mV s^{-1}.

Fig. 22. Cyclic voltammograms of **6** (2.05×10^{-3} mol L^{-1}) (panel A) and **7** (1.25×10^{-3} mol L^{-1}) (panel B) in CH_3CN containing 0.1 M $[N(n\text{-}Bu)_4]PF_6$. Panel A. Reduction of **6** at different scan rates: (a) 20, (b) 50, (c) 100, (d) 200, (e) 400, and (f) 600 mV s^{-1}, respectively. Panel B. Reduction of **7** at different scan rates: (a) 20, (b) 50, (c) 100, (d) 200, (e) 400, and (f) 600 mV s^{-1}, respectively.

Fig. 23. Optimised structure for the one-electron reduced Cu^+ species of **2**.

Fig. 24. ORTEP diagram of compound $Cu(NMe\text{-}Imz)_4(ClO_4)_2$. Selected bond lengths (Å) and angles (^{o}): N(2)-Cu(1), 1.981(2) Å; N(3)-Cu(1), 2.026(2) Å; Cu(1)-N(2′), 1.981(2) Å; Cu(1)-N(3′), 2.026(2) Å; Cu(1) –O(1), 2.734(5) Å; N(2′)-Cu(1)-N(2), 180.0°; N(3)-Cu(1)-N(3′), 180.0°; N(2′)-Cu(1)-N(3), 90.00(9)°; N(2)-Cu(1)-N(3), 90.00(9)°; N(2′)-Cu(1)-N(3′), 90.00(9)°; N(2)-Cu(1)-N(3′), 90.00(9)°.

ACCEPTED MANUSCRIPT

ACCEPTED MANUSCRIPT

Highlights

- Mononuclear copper(II) complexes exhibit rich electronic spectra.
- Some of them show DNA binding and its complete cleavage.
- Possess catechol oxidation activity.
- Show cytotoxicity for the cervical cancer HeLa cell line.
- Also show cytotoxicity against C6 glioma cell line.

ACCEPTED MANUSCRIPT

Graphical abstract

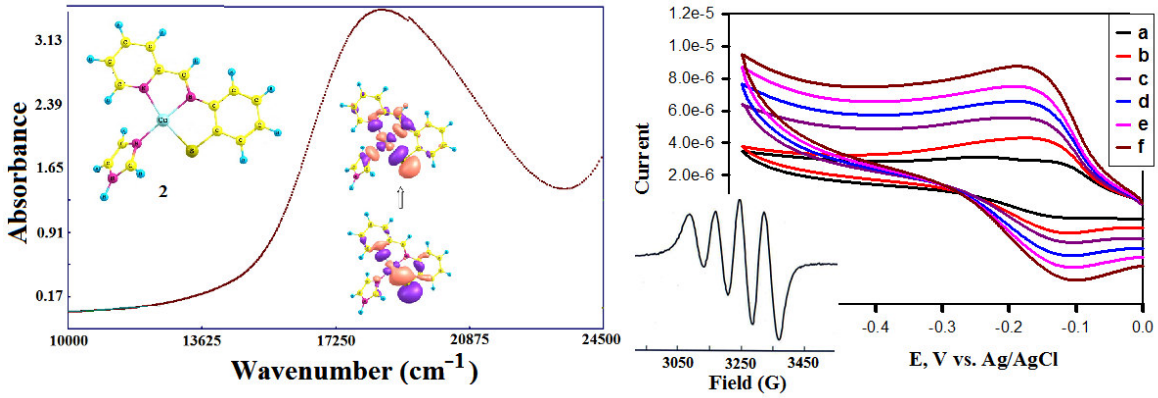

Cu(II) complexes containing a Schiff base N-(2-mercaptophenyl)-2'-pyridylmethylenimine display a four-line EPR pattern as well as strong electronic spectra exhibiting intense S → Cu(II) LMCT bands in the visible region. Nearly reversible or quasi-reversible Cu(II)/Cu(I) couple is observed in the range −0.08 to −0.20 V versus Ag/AgCl. Presence of imidazole group as a coligand enhanced DNA cleavage and cytotoxicity.

ACCEPTED MANUSCRIPT